STIMULATED RAMAN SCATTERING IN MONOMODE OPTICAL FIBRES

A Thesis

Submitted to the Faculty of Engineering

of the University of Glasgow

for the degree of

Doctor of Philosophy

by

William Paul Urquhart

October, 1984

ProQuest LLC.
789 East Eisenhower Parkway
P.O. Box 1346
Ann Arbor, MI 48106 – 1346

ACKNOWLEDGEMENTS

I wish to thank Dr. Peter Laybourn for helpful and understanding supervision, Mr. Ray Hutchins for moral support and Professor John Lamb for the provision of Departmental facilities.

I am most indebted to Miss Anne MacKinnon for her cheerful and patient advice on all aspects of computing.

The manuscript was skilfully typed by Mrs. Joyce Wink.

The project was financed by the U.K. Science and Engineering Research Council.

SUMMARY

A theoretical investigation of stimulated Raman scattering in step-index, monomode optical fibres is presented. The regime of validity of existing mathematical analyses has been extended to account in greater detail than previously reported for the spectral characteristics of optical fibres in which stimulated Raman scattering is occurring.

The variation of fibre loss and transverse modal confinement over the range of frequencies, which are subject to Raman amplification, is considered. It is shown that the growth of total power generated by stimulated Raman scattering with the corresponding depletion of laser input power can be modelled by only two coupled differential equations. In order to do so it has been necessary to develop the concepts of an effective Stokes loss and a weighted Raman line-shape function. The coupled pair of equations has been solved analytically in the special cases where all losses are zero and where all losses are a wavelength independent constant. Numerical solutions and a quantitative discussion of the mechanism of power transfer from pump to Stokes wavelengths are offered for circumstances of inequality of pump and Stokes losses.

As a result of this work is is possible to predict with greater accuracy the length of communications fibre which is free from cross-talk due to stimulated Raman scattering. A method of designing a source, fibre and detector system which is free of threshold stimulated Raman scattering has been developed. Finally, it has been shown that the mathematical model developed here agrees well with published experimental data.

TABLE OF CONTENTS

CHAPTER ONE

INTRODUCTION

1.1 The study of stimulated Raman scattering in optical fibres

When a low power light source is coupled into an optical fibre it is found that the power at the output end of the fibre, at the transmitting wavelength, is directly proportional to the power at the input end. When a high power laser is used, this proportionality breaks down.[1] One or more nonlinear optical effects occur and give rise to a shift in wavelength of the light in the fibre. The wavelength shifting effect to be studied in this thesis is called stimulated Raman scattering.

Stimulated Raman scattering (S.R.S.) was first reported in a Bulk Optical Medium in 1962[2] and in Optical Fibres in 1970[3,4]. Like nearly all other nonlinear phenomena, S.R.S. is usually associated with high power lasers. However, recently it has been possible to observe S.R.S. in optical fibres at power levels down to a few milliwatts.[5] This would appear surprising when it is realised that glass, of which optical fibres are composed, is not a type of medium noted for its tendency towards nonlinear effects.[6] The reasons why such low onset powers for S.R.S. in optical fibres are possible are: (a) the large interaction length, (b) the high degree of power confinement in the fibre core and (c) the low losses available in modern fibres.

The study of S.R.S. in optical fibres is of interest for two reasons. First, as a physical phenomenon upon which devices are constructed, of which the single and multiple pass "fibre Raman laser" is of particular interest.[7] Second, as an unwanted phenomenon which could lead to signal distortion in optical fibre telecommunications.[8]

There are four developments in optical communications which could increase the tendency for S.R.S. and hence justify detailed investigations

into Raman threshold power levels: (a) coherent transmission,[9] (b) wavelength division multiplexing,[10] (c) ultra low-loss mid-infrared fibres[11] and (d) higher power sources.[12] Coherent transmission is the use of analogue signals to give high receiver sensitivity. S.R.S. thresholds are likely to be lower in analogue than in digital systems because digital (pulsed) S.R.S. is sensitive to temporal separation of the laser and Raman-shifted wavelengths caused by fibre dispersion. Wavelength division multiplexing could lower S.R.S. thresholds if the wavelength of one channel coincided with the Raman shifted wavelength of another. Mid-IR fibres could offer exceedingly low losses and, depending upon materials, high Raman gains, both of which lower the S.R.S. threshold. High power sources, such as quantum-well lasers reduce the length of fibre which is free from S.R.S.

Since 1970 there have been numerous papers on S.R.S. in optical fibres[7,13], the overwhelming majority of which are experimental. The purpose of this thesis is to widen the range of validity of the existing theoretical framework[14,15,16,17,18] and to develop a method of design of a source, fibre and detector system which is free from stimulated Raman scattering.

1.2 The layout of the thesis

In the theory presented in this thesis, as in any physical theory, it is necessary to make assumptions and approximations. The assumptions made in the existing, literature are stated in section 1.3. Chapters 2 to 6 are designed to progressively reduce the number of assumptions required; in other words to widen the range of validity of the subject matter. It is then possible to develop a method of designing systems so that they are free of S.R.S. (chapter 7) and to compare theory with

published experimental data (chapter 8).

Chapter 2 establishes the basic theoretical framework upon which the model is built, giving a qualitative discussion of light scattering in general and S.R.S. in glasses in particular. An empirical mathematical representation of the Raman gain profile of pure silica is found.

An existing model[15] of S.R.S. in wavelength-independent loss fibres, where the pump depletion is accounted for, is re-derived in chapter 3 in a dimensionless coordinate scheme. (Mathematical details are in appendix 2.) Analytical expressions are found for pump and Stokes power evolution, spontaneously scattered power, threshold length and the maximum loss and minimum length for which threshold can occur. The power evolution and threshold length is derived for the special case of zero loss in appendix 1.

The level of complexity is increased in chapter 4. A "two-wavelength" model for unequal losses at the pump and Stokes wavelengths is solved numerically. It is assumed that there is some "effective Stokes loss" which can represent the variation of losses over the range of Stokes wavelengths. The evolution of pump and Stokes power along the length of a fibre, power coupling and the relationship between pump and Stokes output with pump input powers are discussed. It has been found that there is no obvious analytic solution. Three unsuccessful approaches are outlined in appendix 3.

The spectrum of Stokes wavelengths in the fibre is investigated by use of the "multiwavelength model" in chapter 5. It is thus possible to find a general expression for the effective Stokes loss. The equivalence of the multiwavelength model and the two wavelength model are shown. The effective Stokes loss is derived for the specific case of a linear Stokes loss profile.

Basic fibre waveguiding properties are discussed in chapter 6. The concept of effective core area is derived from the multiwavelength model. The multiwavelength model can be reduced to a two wavelength model if the appropriate value of the effective core area is used together with a spontaneous Stokes power calculated from a weighted lineshape function.

A method for designing source-fibre-detector systems which are free of S.R.S. is given in chapter 7. The cases of equal and unequal pump and Stokes losses are discussed.

Chapter 8 is a comparison of the theoretical ideas in the previous chapters with results from published literature. The main conclusions of the text, together with suggestions for further research appear in chapter 9.

The analytical and numerical solutions throughout are illustrated by examples involving plausible parameters for monomode fibres (section 3.5). No single set of data is likely to be simultaneously applicable to fibre Raman lasers and telecommunication fibres in which S.R.S. is undesirable. The data chosen are principally aimed at transmitting fibres in which S.R.S. is a parasitic effect, having signal distorting potential. Fibre Raman lasers are thus mainly treated by implication.

The propagation of pump and Stokes power in the fibre is derived throughout in terms of a dimensionless coordinate scheme, first introduced in section 3.2. Although less intuitively obvious than the physical units, which would be measured in a laboratory, a considerable reduction in the number of constants in equations is achieved. A major advantage of the dimensionless units is found in chapter 7 in which general graphs relating to the design of optical fibres are plotted. In those parts of the text where physical quantities are referred to, S.I. units are used.

The wavenumber, or cm^{-1}, commonly used in spectroscopic work and the dB/km are exceptions. Conversions are given by:

$$1\ cm^{-1} \equiv 3 \times 10^{10}\ Hz.$$

$$1\ dB/km \equiv 2.3026 \times 10^{-4}\ m^{-1}.$$

1.3 Assumptions employed in the thesis

A soluble model requires resorting to approximations. Those used here are listed below:

(a) Stimulated Raman scattering is the only nonlinear effect occurring.[19]

(b) Only the first order forward-propagating[20,21] Raman Stokes spectrum is considered (see section 2.2).

(c) The laser input is approximately continuous wave and monochromatic.

(d) The guided waves make only a single transit through the fibre. There is no reverberation between fibre ends nor reflections from splices. (See section 8.4)

(e) The fibre is LP_{01}-transverse mode at all wavelengths, (see section 6.2).

(f) The fibre is step-index, cylindrical and "weakly-guiding" (see section 6.2).

(g) The Raman gain, the parameter which dictates the strength of frequency conversion, is the same for the fibre cladding and core.

(h) There is no mutual coupling between Stokes modes (see section 3.2).

(i) The effective core area is independent of length (see section 6.7).

(j) The only input photons at the Stokes wavelengths arise from spontaneous scattering (see section 3.4).

(k) The fibre absorption is not so high as to give rise to either material damage or a thermal variation of refractive index with a high power laser input (see section 8.3).

The following assumptions have been employed in the literature. It is the purpose of chapters 4, 5 and 6 to examine what happens when they are violated.

(l) The effective core area is constant for all pump-longitudinal Stokes modes interactions and is given by the self-interaction approximation (see section 6.5).

And either:

(m) The losses at all propagating wavelengths are equal.[15]

Or:

(n) Small signal theory: the only significant attenuating influence upon the pump power is fibre loss.[14]

If (n) is assumed it is also required that:

(o) There is some single value of Stokes loss which is equivalent to the entire loss profile. Thus the Stokes power evolution can be described by one equation (see section 5.4).

References

1. Sasaki, Y., Ohmori, Y., Kawachi, M., Edahiro, T., "C.W. Single-pass Raman generation in optical fibres", Electron. Lett. 17, 315, (1981).

2. Woodburry, E.J. and Ng, W.K., "Ruby laser operation in the near I.R.", Proc. I.R.E. 50, 2367 (1962).

3. Ippen, E.P., "Low-power quasi-CW Raman oscillator", Appl. Phys. Lett., 16, 303 (1970).

4. Stolen, R.H., Ippen, E.P., Tynes, A.R., "Raman oscillation in glass optical waveguides", Appl. Phys. Lett. 20, 62 (1972).

5. Tomita, A., "Cross talk caused by stimulated Raman scattering in single-mode wavelength-division multiplexed systems", Optics. Lett., 8, 412, (1983).

6. Heiman, D., Hellwarth, R.W., Hamilton, D.S., "Raman scattering and nonlinear refractive index measurements of optical galsses", J. Non Crystalline Solids, 34, 63 (1979).

7. Stolen, R.H., "Fibre Raman lasers", in "Fibre and Integrated Optics", D.B. Ostrowsky (Ed.) Plenum Press, New York, 1979.

8. Nakamura, K., Kimura, M., Yoshida, S., Hidaka, T., Mitsuhashi, Y., "Raman amplification of 1.50μm laser diode light in a low fibre loss region", J. Lightwave Technology, LT-2, 379 (1984).

9. Yamamoto, Y. Kimura, T., "Coherent optical fibre transmission systems", I.E.E.E. J. Quantum Electron. QE-17, 919 (1981).

10. Mahlein, H.F., "Crosstalk due to stimulated Raman scattering in single-mode fibres for optical communication in wavelength division multiplex systems", Optical and Quantum Electron., 16, 409 (1984).

11. Miyashita, T., Toyotaka, T., "Infrared optical fibres", I.E.E.E. J. Quantum Electron., QE-18, 1432 (1982).

12. Holonyak, N., Kolbas, R.M., Dupuis, R.D., Dapkus, P.D., Quantum-well heterostructure lasers", I.E.E.E. J. Quantum Electron., QE-16, 170, (1980).

13. Stolen, R.H., "Nonlinear properties of optical fibres", in "Optical fibre telecommunications", Miller, S.E. and Chynoweth, A.G. (Eds.) Academic Press, New York (1979).

14. Smith, R.G., "Critical power handling capacity of low loss optical fibres as determined by stimulated Raman and Brillouin scattering", Appl. Optics, 11, 2489 (1972).

15. Au Yeung, J. and Yariv, A., "Spontaneous and stimulated Raman scattering in long low-loss fibres", I.E.E.E. J. Quantum Electron., QE-14, 347, (1978).

16. Au Yeung, J. and Yariv, A., "Theory of C.W. Raman oscillation in optical fibres", J. Opt. Soc. Am., 69, 803, (1979).

17. Crosignani, B. and Di Porto, P., "Influence of guiding structures on spontaneous and stimulated emission: Raman scattering in optical fibres", Phys. Rev. A., 21, 594 (1980).

18. Capasso, F. and Di Porto, P., "Coupled-mode theory of Raman amplification in lossless optical fibres", J. Appl. Phys., 47, 1472, (1976).

19. Koepf, G.A., Kalen, D.M., Greene, K.H., "Raman amplification at 1.118μm in single mode fibre and its limitation by Brillouin scattering", Electron. Lett., 18, 942 (1982).

20. Lin, C-H., Marshall, B.R., Nelson, M.A. and Theobald, J.K., "Backward stimulated Raman scattering in multimode fibre., Appl. Optics, 16, 2486 (1978).

21. Nakazawa, M., Tokuda, M., Negishi, Y., Uchida, N., "Active transmission line: light amplification by backward-stimulated Raman scattering in polarisation maintaining optical fibres", J. Opt. Soc. Am., B1, 80 (1984).

CHAPTER TWO

STIMULATED RAMAN SCATTERING IN GLASS

2.1 Introduction

There are several comprehensive reviews of stimulated Raman scattering in the literature,[1,2,3,4] including rigorous quantum mechanical treatments.[5] The account contained here is mainly qualitative and is classical in scope.

Section 2.2 is an outline of the optical scattering processes which occur in matter, which are of relevance to optical fibres. Section 2.3 discusses the particular case of stimulated Raman scattering and states the appropriate photon number and power equations. Section 2.4 deals with Raman gain for various media applicable to optical fibre fabrication, whilst section 2.5 concentrates on simple mathematical models for Raman gain in silica.

2.2 A review of spontaneous and stimulated light scattering processes

In all spontaneous light scattering processes an incident photon, $h\nu_\ell$ is inelastically scattered by an optical scattering centre, which may be initially in the ground state (vibrational, rotational or electronic) or in one of the excited quantum levels. If the interaction is with a ground state scattering centre, the outgoing photon has been down shifted to energy $h\nu_s$, whilst the difference in energy, $h(\nu_\ell - \nu_s) = h\Delta\nu$ is absorbed by the centre. This is referred to as a Stokes process, hence the subscript s. If, on the other hand, the scattering centre is initially in an excited state the outgoing photon is raised in energy with respect to the incident photon to $h\nu_a$. The material centre donates the packet of energy, $h\Delta\nu$. This is an anti-Stokes interaction. See Fig. 2-1(a) and (b).

A very simple fact can be deduced about the relative strengths of the Stokes and anti-Stokes interactions. The Bose-Einstein energy distribution requires that for room temperature the excited states will be less heavily populated than the ground states:

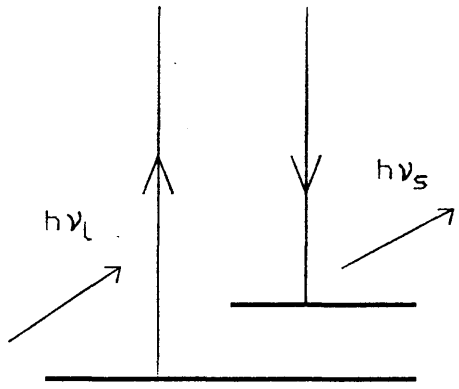

(A) SPONTANEOUS
STOKES SCATTERING

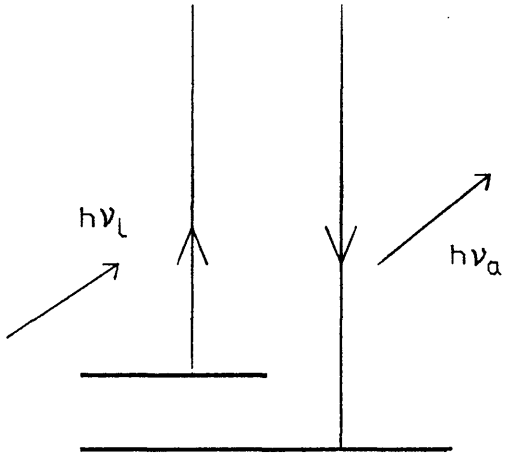

(B) SPONTANEOUS
ANTISTOKES SCATTERING

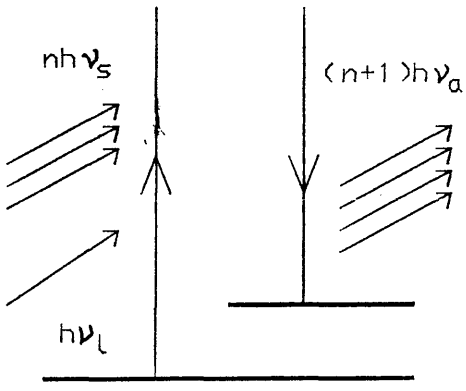

(C) STIMULATED
STOKES SCATTERING

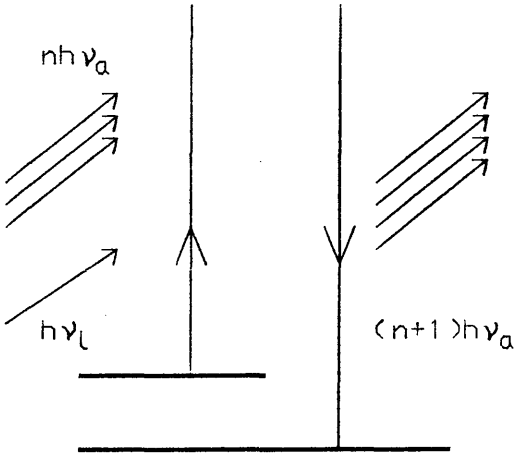

(D) STIMULATED
ANTISTOKES SCATTERING

FIG. 2-1 ENERGY LEVEL DIAGRAMS ILLUSTRATING
SPONTANEOUS AND STIMULATED LIGHT SCATTERING.

$$N(\text{excited state}) = N(\text{ground state})/(\exp(\frac{h\Delta\nu}{k_B T})-1) \qquad (2.1)$$

T is temperature, k_B is the Boltzman constant (1.381×10^{23} $J.K^{-1}$) and N represents the occupation densities for the ground and excited quantised energy levels. The consequence of Eq. (2.1) is that the anti-Stokes interactions are much less probable than the corresponding Stokes interactions. At absolute zero no anti-Stokes processes can occur.

The processes so far described are "Spontaneous" Stokes and anti-Stokes scattering. When a photon of frequency, ν_s is simultaneously incident at the scattering centre with a photon of energy $h\nu_\ell$ one gets "stimulated" Stokes scattering. There is a corresponding stimulated anti-Stokes process (see Fig. 2.1(c) and (d)). Note the similarity with spontaneous and stimulated emission between two energy levels. In both stimulated scattering and stimulated emission there is optical amplification to give a coherent output.

As far as optical fibres are concerned (or indeed, in most laboratory applications) the photons of frequency ν_s (or ν_a) simultaneously incident with photons of ν_ℓ in stimulated scattering come from previous spontaneous events. In other words, light of frequency ν_ℓ initially incident on the medium is first spontaneously scattered to ν_s (or ν_a). These Stokes (or anti-Stokes) photons together with further laser photons, $h\nu_\ell$ subsequently partake in a stimulated scattering event. Therefore if the spontaneous anti-Stokes process was improbable in the first place it will be doubly unlikely in the stimulated form. Gain at the Stokes frequency corresponds to absorption at the anti-Stokes frequency.

The scattering processes are designated "Raman" scattering if the quantised energy levels correspond to optical branch phonons and "Brillouin" if to acoustic branch phonons. Typical frequency shifts,

$\Delta\nu_R$ for Raman scattering are 100 to 5000 cm^{-1}. Frequency shifts, $\Delta\nu_B$ for Brillouin scattering are in the order of 0.01 to 5 cm^{-1}. (Note: 1 cm^{-1} = 3×10^{10} Hz.) Both Brillouin and Raman scattering can be Stokes or anti-Stokes, spontaneous or stimulated, but are subject to the principle that stimulated anti-Stokes scattering is very unlikely indeed.

Stimulated Raman scattering can be regarded as a molecular vibration (or electronic transition) modulating the refractive index at $\Delta\nu_R$. This leads to a phase modulation of any field present so creating side bands separated by $\Delta\nu_R$ from the pump at ν_ℓ. Stimulated Brillouin scattering can be visualised as arising from an optically driven periodic electrostrictive strain driving an acoustic wave of frequency $\Delta\nu_B$. In Brillouin scattering it is this acoustic wave which phase modulates the laser pump. In most media (including optical fibres) Brillouin gain is greater than Raman gain.

Fig. 2.2 is an example of an idealised spontaneously scattered frequency spectrum for a given detection angle. The general Raman scattering geometry is shown in Fig. 2.3. A narrow bandwidth laser line is scattered by a medium whose energy levels experience only Lorentzian (homogeneous) broadening. As can be seen from this hypothetical medium the Stokes lines are more intense than their anti-Stokes counterparts, the Brillouin lines are more intense than the Raman lines, and the Raman linewidths are greater than the Brillouin linewidths. The Rayleigh scattering and Rayleigh wing scattering are centred on the narrow laser line.

Rayleigh scattering is due to interactions with non-propagating entropy fluctuations. Rayleigh-wing scattering is from orientation fluctuations in isotropic molecules.[1] Rayleigh scattering in its spontaneous form is important to optical fibre technology as a loss-mechanism. Even if all atoms absorbing at the propagation wavelength

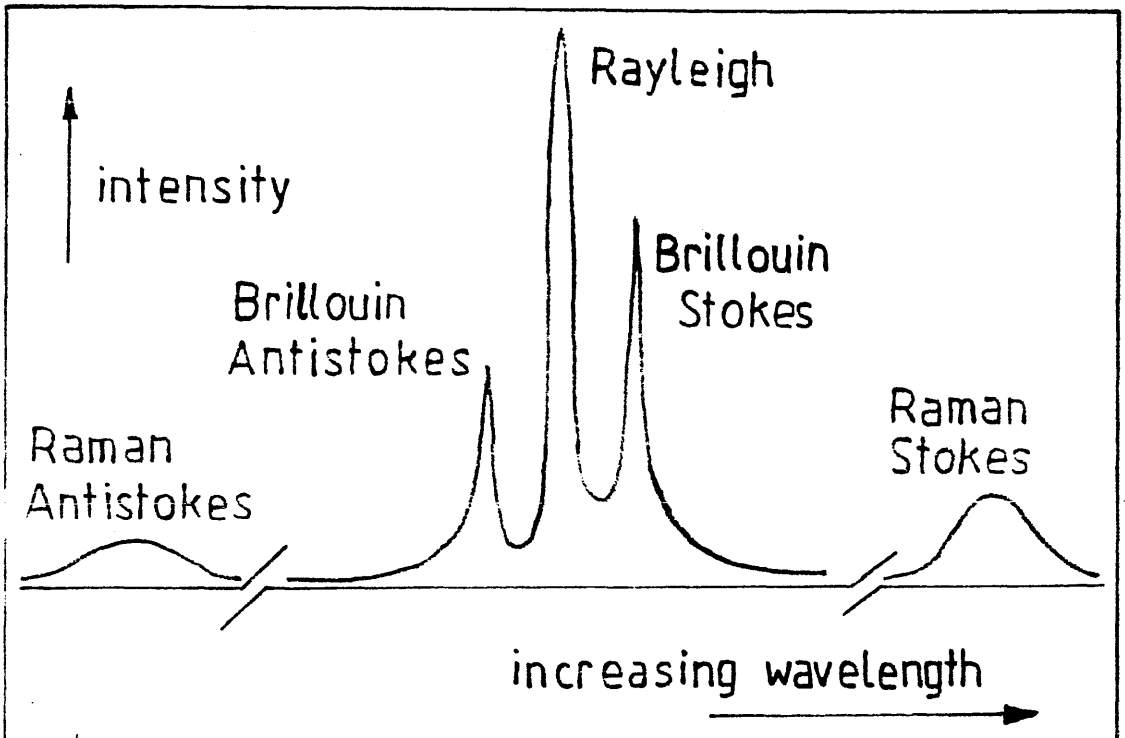

Fig 2-2 spontaneous light scattering processes

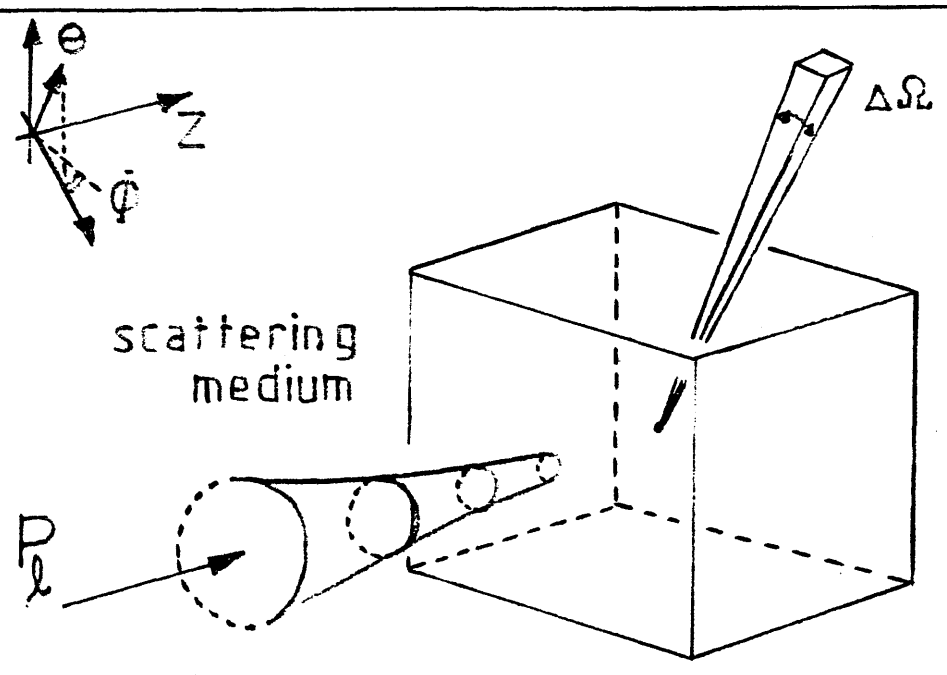

Fig 2-3

Raman scattering geometry

could be removed from the fibre, Rayleigh scattering would impose a lower limit to loss performance. As with all the scattering mechanisms discussed here the Rayleigh cross section varies as λ^{-4}, therefore it is advantageous to use as long a transmitting wavelength as is practical. The best silica based fibres at 1.55μm cannot exhibit a loss below about 0.15dB/km no matter how low the absorption.[6] Lower losses than this could only possibly be achieved at longer wavelengths.

Stimulated Rayleigh scattering does exist, but it has not been demonstrated in optical fibres. This is either because it is "smothered" by the broad Raman gain spectra (section 2.4) or more likely because the gain is at least an order of magnitude less than that of stimulated Raman or Brillouin scattering.[1]

The spectrum illustrated in Fig. 2.2 is a considerable simplification. In practice there will be multiple Raman and Brillouin active vibrational modes, giving numerous Stokes and anti-Stokes lines, some of which may be overlapping.[4] In the case of stimulated scattering, the spectrum consists of a smaller number of lines and often one of the scattering mechanisms occurs in isolation. When intense stimulated scattering occurs it is quite possible for one of the scattered lines to promote significant light scattering in its own right. The wave generated in this way is the result of second order Raman or Brillouin scattering. Provided that the input laser beam is sufficiently powerful it is quite possible to generate a cascade of multiple Raman or Brillouin orders.

2.3 Stimulated Raman scattering

From now on consider only first order Stokes Raman scattering. The variation of the Stokes photon number, per unit volume, $N_s(\nu)$ with respect to length, z is given by[2] equation (2.2):

$$\frac{dN_s(\nu)}{dz} = N_\ell N_a \left(\frac{\partial(\sigma(\theta,\phi))}{\partial\Omega}\right)\Delta\Omega \qquad (2.2)$$

N_ℓ and N_a are the volume densities of laser photons and scattering centres in the ground state, respectively. $\sigma(\theta,\phi)$ is the scattering cross section for some defined state of polarisation with respect to the coordinate system of Fig. 2.3. $\partial(\sigma(\theta,\phi))/\partial\Omega$ is the differential cross section per unit volume and $\Delta\Omega$ an element of solid angle. ν is frequency. Equation (2.2) can be used as a definition of Raman scattering cross-section.

In spontaneous scattering the density of states is the number of vacuum oscillators per unit volume per unit solid angle, per unit frequency interval, $\nu_s^2 n_s^3/c^3$. ν_s is the frequency of the most prominent feature on the Raman gain curve and n_s is the refractive index at ν_s. c is the speed of light in vacuo. In stimulated scattering one is interested in the density of states in the material as represented by the normalised lineshape function, $\mathcal{L}_N(\nu)$. $\mathcal{L}_N(\nu)$ obeys:

$$\int_{-\infty}^{+\infty} \mathcal{L}_N(\nu)d\nu = 1 \qquad (2.3)$$

For stimulated Raman scattering when the Raman linewidth is narrow:

$$\frac{dN_s(\nu)}{dz} = (N_a - N_b)\left(\frac{\partial\sigma}{d\Omega}\right) N_\ell N_s \left(\frac{c^3}{\nu_s^2 n_s^3}\right)\mathcal{L}_N(\nu) \qquad (2.4)$$

N_b is the number density of scattering centres in state $|b\rangle$. See Fig. 2.1(c). The relationship between N_a and N_b is given by (2.1). It is often more convenient to express (2.4) in terms of a frequency dependent gain per unit area, $G(\nu)$

$$\frac{dN_s(\nu)}{dz} = G(\nu)N_\ell N_s(\nu) \qquad (2.5)$$

where[3]: $G(\nu) \propto (\partial\sigma/d\Omega).(1/\nu_\ell^2).(1-\exp(-h\Delta\nu/k_BT))\mathcal{L}_N(\nu)$ (2.6)

In some texts N_ℓ is incorporated in the definition of gain, but not so here. To convert a Raman scattering spectrum into a gain profile one must scale by the thermal population factor, (2.1) for all frequency shifts, $\Delta\nu$ of interest.

It is desirable to re-express equation (2.5) in terms of power, the parameter measured in experiments:

$$\frac{dP_s(\nu)}{dz} = \frac{g(\nu)}{A}\left(\frac{\nu_s}{\nu_\ell}\right) P_\ell P_s(\nu) \tag{2.7}$$

P_ℓ and $P_s(\nu)$ are the laser and Stokes powers, respectively. The laser is assumed to be monochromatic. The factor (ν_s/ν_ℓ) is required to convert photon number to power. A is the cross sectional area of a beam of light consisting of quasi-planar wavefronts. (Due to diffraction truly planar wavefronts must be of infinite extent.) g is the power gain defined by:

$$g(\nu) = \frac{A\,G(\nu)}{h\nu_\ell} \tag{2.8}$$

Equation (2.7) is an expression of the growth of Stokes power with respect to length. For a given distance of travel along the medium, it can be seen from (2.7) that, Stokes power increases with an increase in gain and decreases with an increase in cross-sectional area. There is a companion equation to (2.7) to represent the depletion of laser pump power:

$$\frac{dP_\ell}{dz} = -\frac{g(\nu)}{A} P_\ell P_s(\nu) \tag{2.9}$$

The negative sign in (2.9) expresses the fact that power is being drained from the pump beam.

It can be seen from (2.6) and (2.8) that $g(\nu)$ varies as ν_ℓ^{-3}

multiplied by the frequency variation of the cross section. As with Rayleigh scattering, the cross-section is proportional to ν_ℓ^4. Consequently, Raman power gain is directly proportional to the laser frequency. As far as optical fibres are concerned, attempts to increase the wavelength of operation to reduce Rayleigh scattering loss will result in a decreased Raman gain. If a Raman gain is determined experimentally at a known wavelength it can be calculated for operation at any other wavelength by scaling linearly.

Extended versions of equations (2.7) and (2.9) form the basis of the work described in this thesis. In section 3.2 equations (2.7) and (2.9) are converted to dimensionless coordinates. They are solved subject to appropriate boundary conditions in appendix 1. One of the features of that solution is an exponential dependence on gain. Consequently, those frequency shift values for which there is high Raman gain will experience considerably greater amplification than those for which there is low Raman gain. The result is line narrowing: the Stokes spectrum from simulated Raman scattering is narrower than that from spontaneous Raman scattering. This point will be returned to in sections 3.4 and 5.3.

2.4 Raman gain profiles

There have been numerous Raman spectroscopic studies of both crystalline and amorphous dielectrics, virtually all of which have been for structure determination for use by chemists and solid state physicists. See for example Barker and Sievers[7] and references therein. Consequently, there is little interest in determining absolute values of Raman scattering cross-sections. It is standard practice for the vertical axis of a Raman spectrum to be calibrated in normalised coordinates, ranging from zero to unity at the most prominent feature. It is important to realise that for the quantitative evaluation of power levels at which S.R.S. will become problematical for optical communications absolute cross section

and hence gain, values must be known. For a discussion of experimental techniques, including laser types, in Raman spectroscopy see Mooradian.[4]

Glasses are amorphous dielectrics, usually associated with the idea of an absorption "window" at some range of frequencies. The molecular arrangement is thought of as being a sort of disordered periodicity[7]. Valence is locally satisfied, but bond lengths and angles are randomly arranged. Consequently X-ray diffraction photographs lack sharp rings and spots, but instead have broad haloes. This criterion can even constitute a working definition of an amorphous system.

In general there is no unique amorphous state, each example being thermodynamically unstable or metastable. The thermal history will determine its micro-structure, and which in turn will dictate the bulk physical properties, including the Raman scattering spectrum.

The absence of true periodicity of glass molecular structure allows many modes of the system to be both infrared-absorption-active and Raman-spectroscopically-active. Quantum mechanical selection rules, which usually apply to other media, are not obeyed.

Gain profiles for silica (SiO_2) and germania (GeO_2) are depicted on Figs. 2.4 and 2.5, respectively. These broad curves can, to a first approximation, be thought of as being made up of many Lorentzians superposed at slightly different frequency shifts. Raman gain profiles for glasses reflect the total density of states, displaying generally broad plateaux and in some cases narrow peaks at high frequency shifts. Unfortunately the calculation of the density of states is a considerable task, and there is a scarcity of theoretical results. Curves representing the Raman scattering cross sections of other glasses have been reported[8,9,10]. Scale using (2.1) to give the shapes of the equivalent gain profiles.

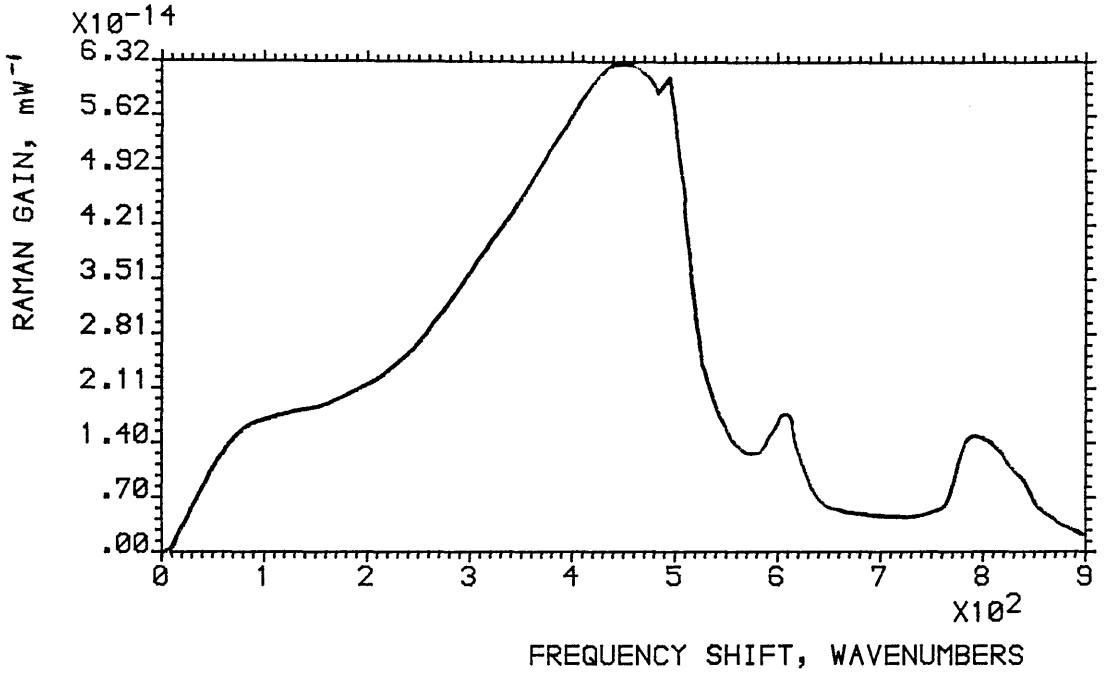

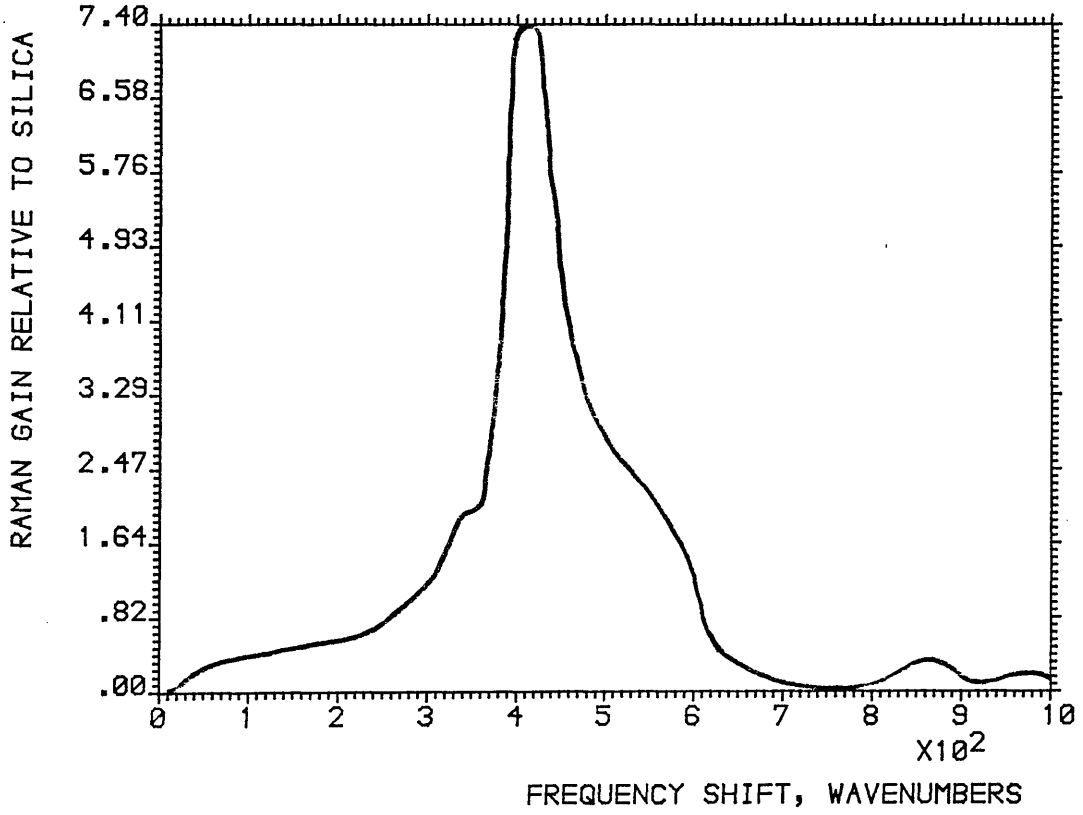

TOP: FIG 2-4; RAMAN GAIN PROFILE OF SILICA[10]. THE CALIBRATION IS FOR 1.55 um OPERATION.

BOTTOM: FIG 2-5; RAMAN GAIN PROFILE OF GERMANIA[10]. THE CALIBRATION IS RELATIVE TO THAT OF SILICA.

The broad feature centred at 440cm^{-1} on the silica gain profile is attributed to out-of-plane rocking of the oxygen atom bridging two silicon atoms[9]. The 420cm^{-1} mode of germania has an intensity 7.4 times that of silica and is due to a similar mechanism. Heiman et al[8] have measured the scattering cross section for berylium fluoride (BeF_2), a potential material for future generations of ultra-low loss mid-infrared optical fibre communications. BeF_2 has an exceptionally low peak Raman gain.

It has not been possible to locate published literature on the Raman gain of doped silica. It would be of special interest to ascertain the variation of the gain profile, and peak gain in particular, of silica as the percentage of germania doping is increased. In chapter 8 one calculation is based on the possibility that the peak Raman gain varies linearly with the percentage of GeO_2 doping. This is purely speculative.

2.5 Functional representation of the Raman gain profile

In section 3.4 the power arising from spontaneous Raman scattering will be calculated. In order to do so it is necessary to represent the gain profile of silica by some simple mathematical function. Two have been suggested in the literature: a Lorentzian which has been approximated by a parabola[11] and a triangle[12]. Whatever function is used to represent the profile it is important to realise that is must be truncated at frequency shifts representing the zero frequency shift and the maximum measurable frequency shift.

A Lorentzian gain profile is given by:

$$g(\nu) = g_o(\nu) = g_o\left[1 + \left(\frac{\nu-\nu_s}{\delta\nu/2}\right)^2\right]^{-1} \quad ; \quad \nu_o^- < \nu < \nu_o^+ \qquad (2.10)$$

$$= 0 \text{ elsewhere}$$

ν is the frequency, g_o the peak gain at $\nu = \nu_s$ and $\delta\nu$ the full with at half maximum (FWHM).

Expand equation (2.10) by the binomial theorem and retain only the first two terms to give:

$$g(\nu) = g_o[1 - (\frac{\nu - \nu_s}{\delta\nu/2})^2] \qquad (2.11)$$

(2.11) has been used by Smith[11] as an approximation to a Lorentzian for the purpose of calculating spontaneously scattered power. It is a parabola with maximum value g_o at frequency ν_s. The intersects with the frequency axis are at $\nu_s \pm (\delta\nu/2)$.

The use of a right angled triangle as a model for Raman gain profiles is as a result of work done on cross-talk due to S.R.S. in wavelength-division multiplexed optical fibre transmission systems.[12] The gain profile is given by (2.12).

$$g(\nu) = g_o(1 + \frac{\nu_s' - \nu}{\nu_s' - \nu_\ell}); \quad \nu_\ell \leq \nu \leq \nu_s' \qquad (2.12)$$

$$0 \quad \text{elsewhere}$$

ν_ℓ is the laser frequency and ν_s' is the peak frequency of the triangle. The gradient of the hypotenuse of the triangle is g_o/ν_s'.

The three mathematical approximations for the experimental gain profile of silica will now be considered. The constants ν_s and $\delta\nu/2$ or ν_s' as appropriate are to be adjusted so as to give the best model. It will be argued that a Lorentzian having $\nu_s = 440\ cm^{-1}$ and $\delta\nu/2 = 120\ cm^{-1}$ is the most realistic choice.

Fig. 2.6 shows curves (B), (C) and (D) corresponding to equations (2.10), (2.11) and (2.12), respectively, superposed on silica gain profiles labelled (A). The values $\nu_s = 440\ cm^{-1}$ and $\delta\nu/2 = 120\ cm^{-1}$ were used in computing (B) and (C) and $\nu_s' = 522\ cm^{-1}$ in computing (D). The silica

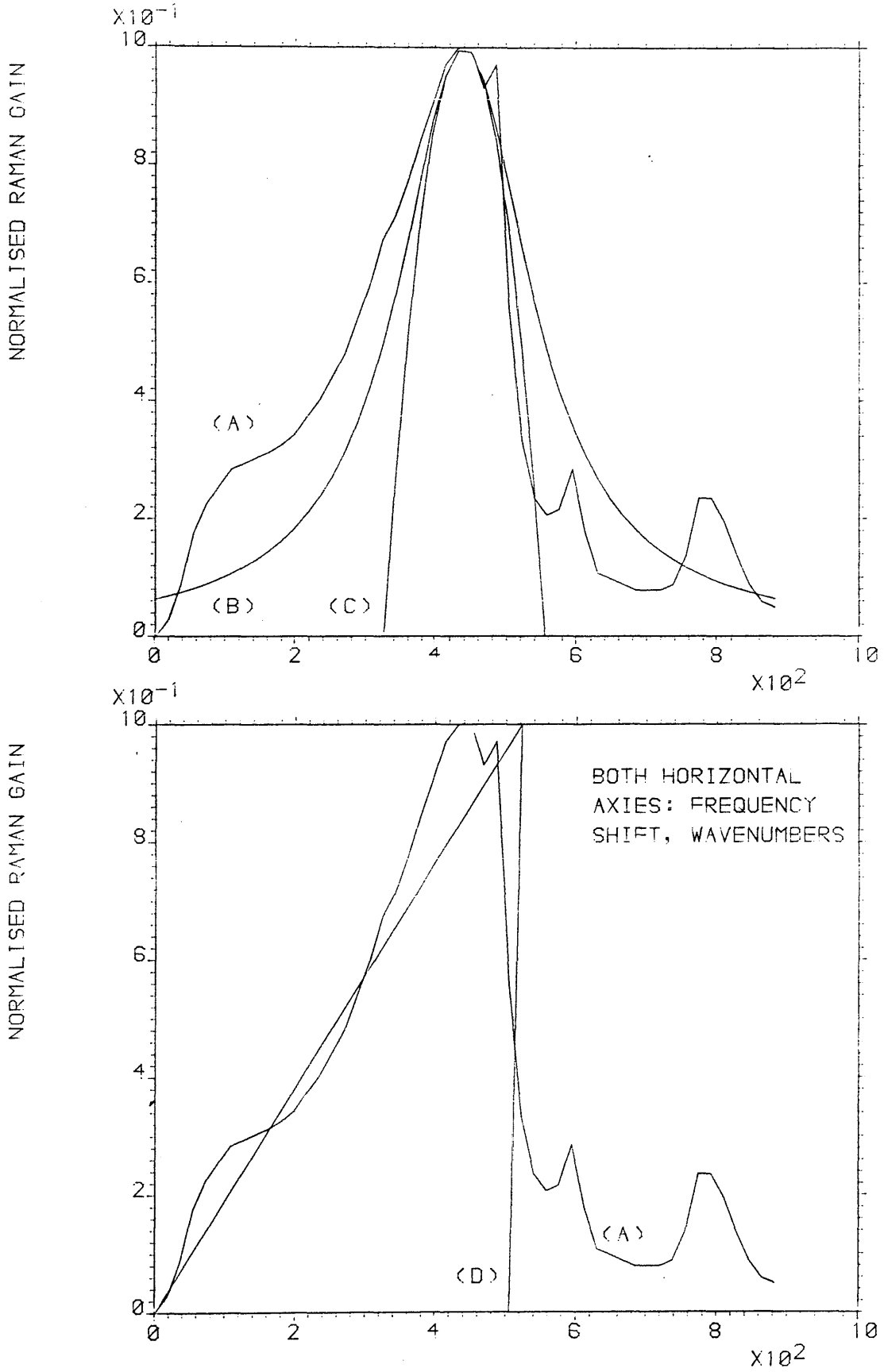

FIG 2-6 : COMPARISON OF (A) THE RAMAN GAIN PROFILE OF SILICA WITH (B) LORENTZIAN, (C) PARABOLA & (D) TRIANGLE.

profile was taken from Stolen et al[10]. The gain was digitised at 18 cm^{-1} intervals from 0 to 900 cm^{-1} and stored in a 51 element array (including an element for 0 cm^{-1} shift) in the program which produced the graphics for Fig. 2.6.

There are various techniques in the numerical analysis literature for the comparison of functions and the adjustment of constants to obtain the closest match. See for example the optimisation routines in the NAG library[13] and references therein. Had there been a larger number of published Raman gain profiles for optical fibre glasses it would be worth giving considerable attention to finding empirical models for the evolution of the profile with dopant concentrations. However, given the lack of published data there is little to be gained in using a method more subtle than finding the minimum value of the sum of squares of differences between the experimental and theoretical lineshape functions.

Define:
$$\text{diff} = \sum_{i=1}^{51} (\mathcal{L}_i^e - \mathcal{L}_i^t)^2 \qquad (2.13)$$

$\mathcal{L}_i^e$ and $\mathcal{L}_i^t$ are the i^{th} components of the experimental and theoretical lineshape functions, respectively. There is a perfect fit when diff is zero. It should be noted that the accuracy is dependent upon the error in the experimental data.

In the case of the Lorentzian and parabolic lineshape functions ν_s was held constant at 440 cm^{-1}, the same peak shift as the experimental curve, and diff calculated for a range of $\delta\nu$ values. See curves (B1) and (C), respectively of Fig. 2.7. diff is measured on the vertical axis. It can be seen that diff is minimised for the Lorentzian with $\delta\nu$ = 240 cm^{-1} and the parabola with $\delta\nu$ = 780 cm^{-1}. For no value of $\delta\nu$ is the parabola as good a fit as the Lorentzian. In fact it has been shown that even if ν_s is allowed to vary a parabola will never give a value of diff as low as that obtainable from a Lorentzian. On these grounds

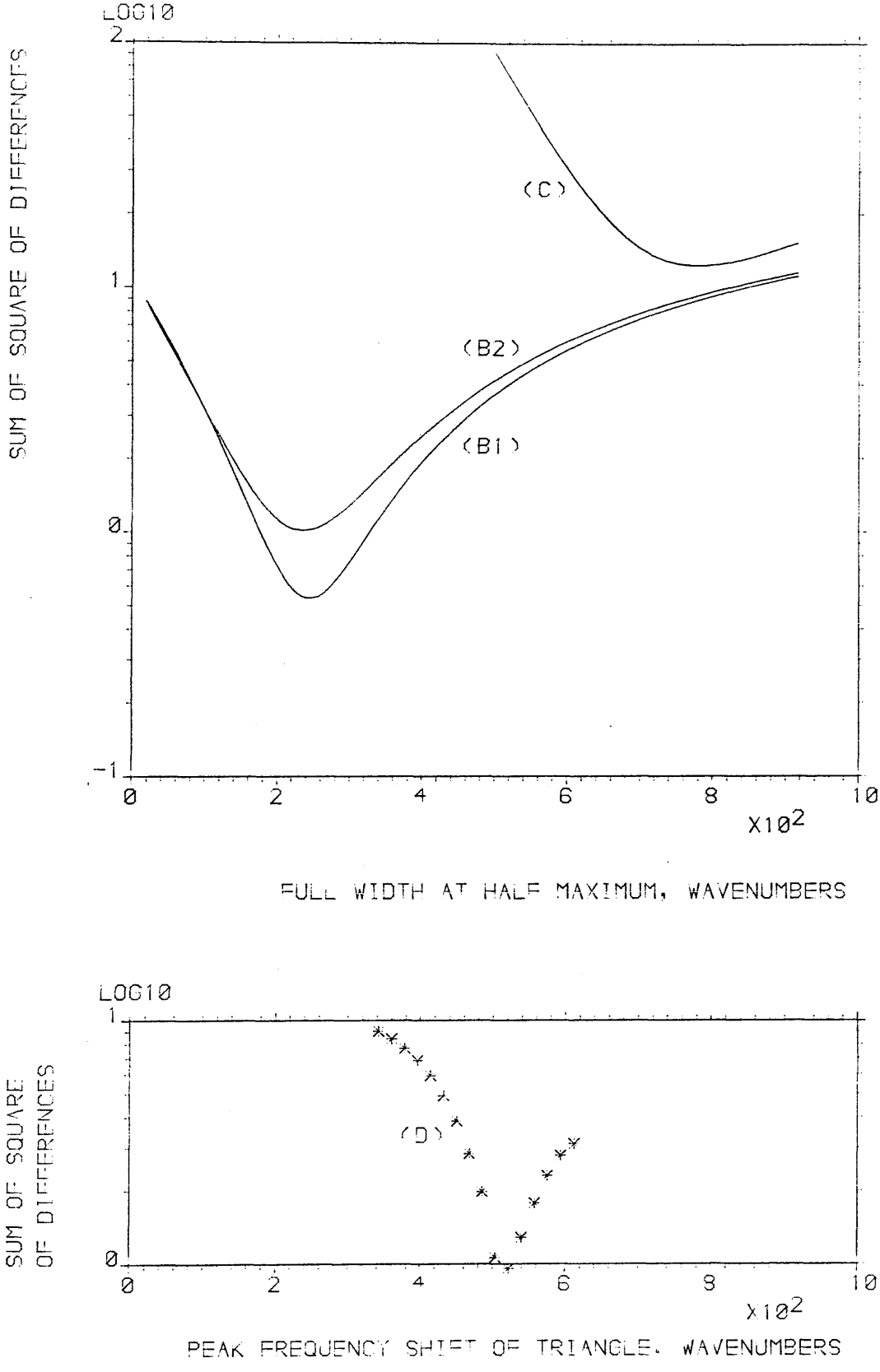

FIG. 2-7 LEAST SQUARES PLOTS. TOP: (B1) & (B2) LORENTZIANS WITH PEAK SHIFTS AT 440 & 405 WAVENUMBERS, RESPECTIVELY AND (C) PARABOLA. BOTTOM: (D) TRIANGLE.

alone a parabola is eliminated as the best functional representation for the silica gain profile.

In the case of the triangle the only constant which can be adjusted is the frequency shift ν_s' (equation 2.12). From curve (D) of Fig. 2.7 it can be seen that diff is minimised at $\nu_s' = 520\ cm^{-1}$. Curve (D) is marked as asterisks to emphasise the fact that the 51-element digitisation constrains the positioning of the vertex of the triangle. It can be seen that from the actual values of diff that:

$$\text{diff(Lorentzian; } \nu_s=440cm^{-1};\ \delta\nu=240cm^{-1})=\text{diff(triangle; } \nu_s'=522cm^{-1})=1.0$$

It has been found by trial and error that a lower value of diff can be obtained if the freedom to choose a Lorentzian with $\nu_s = 405\ cm^{-1}$ is assumed. See curve (B1) of Fig. 2.7.

The problem with choosing functions with a peak frequency shift different from $440\ cm^{-1}$ is that one is distorting the physically measurable fact that maximum amplification of Stokes photons occurs at $440\ cm^{-1}$. If the mathematical models presented in this thesis were to be extended to include higher order Stokes scattering any falsification of ν_s would increase with the number of Stokes orders. A triangle with $\nu_s' = 440\ cm^{-1}$ gives diff = 4.5, significantly worse than the Lorentzian of curve (B1) at $440\ cm^{-1}$.

There are two further disadvantages with a triangle. Firstly, there is a large discontinuity at $\nu = \nu_s'$ with a rather artificially sharp peak. Secondly, the Lorentzian form is much closer to the gain profile of pure germania (Fig. 2.5). In fact there is liable to be a larger number of materials to which a Lorentzian model and hence the analysis in the rest of the text can be applied. The most realistic model of Raman gain in silica is, thus, the Lorentzian with ν in cm^{-1}:

$$g(\nu) = g_o\mathcal{L}(\nu) = g_o\left[1 + \left(\frac{\nu - 440}{(240/2)}\right)^2\right]^{-1} \qquad (2.14)$$

References

1. Kaiser, W. and Mayer, M., Stimulated Rayleigh, Brillouin and Raman spectroscopy in Laser Handbook. Arecchi, F.T. and Schulz-Du Bois, E.O.; North Holland (1972).

2. Bloembergen, N. The stimulated Raman Effect. Am. J. Phys. 35, 989, (1967).

3. Yariv, A. Quantum Electronics, 2nd Edition, Willey, 1975 (Section 18.2).

4. Mooradian, A. Raman Spectroscopy of Solids in Laser Handbook, Arecchi, F.T. and Schulz-Du Bois (Editors); North Holland (1972).

5. Wang, C.-S. "The Stimulated Raman Process" in Quantum Electronics Vol.1 Part AI (Nonlinear Optics). H. Rabin and C.L. Tang (Editors).

6. Garrett, I. and Todd, C.J. "Components and Systems for Long Wavelength Monomode Fibre Transmission". Optical and Quantum Electronics 14. 95 (1982).

7. Barker, A.S., and Sievers, A.J. "Optical Studies of the Vibrational Properties of Disordered Solids." Rev. Mod. Phys. 47 (Supplement No. 2) S1 (1975).

8. Heiman, D., Hellwarth, R.W., and Hamilton, D.S. "Raman Scattering and Nonlinear Refractive Index Measurements of Optical Glasses." J. Non-Crystalline Solids 34, 63 (1979).

9. Galeener, F.L., Mikkelsen, J.C., Geils, R.H. and Mosby, W.J. "The Relative Raman Cross-Sections of Vitreous SiO_2; GeO_2; B_2O_3 and P_2O_5." Appl. Phys. Lett. 32, 34 (1978).

10. Stolen, R.H., Ippen, E.P. and Tynes, A.R. "Raman Oscillation in Glass Optical Waveguides." Appl. Phys. Lett., 20, 62 (1972), and Stolen, R.H., Fibre Raman Lasers in Fibre and Integrated Optics Vol. 3; Ostrowsky, D.B. (Ed.), Plenum, (1980).

11. Smith, R.G. "Critical Power Handling Capacity of Low Loss Optical Fibres as Determined by Stimulated Raman and Brillouin Scattering." Appl. Optics, 11, 2489 (1972).

12. Chraplyvy, A.R. "Optical Power Limits in Multichannel Wavelength-Division Multiplexed Systems due to Stimulated Raman Scattering." Electron. Lett., 20, 58 (1984).

13. Numerical Algorithms Group (N.A.G.) Fortran Program Library Mark 10, Vol.3. See, for example, E04ABF.

CHAPTER THREE

THE THEORY OF STIMULATED RAMAN SCATTERING IN OPTICAL FIBRES WITH CONSTANT LOSSES

3.1 Introduction

Equations (2.7) and (2.9) concerning the variation of power with respect to length at the pump and Stokes wavelengths are stated in terms of physical units which can be measured in a laboratory. The use of these familiar quantities is sacrificed in favour of the less intuitively-obvious dimensionless units, which are introduced in section 3.2. The reasons for doing so were given in section 1.2. The normalisation procedure is a simple modification of that of von der Linde et al[1]. In section 3.3 the theory of S.R.S. in optical fibres due to Au Yeung and Yariv[2] is rederived* in terms of the dimensionless coordinate system. The mathematical details are in section A2.1.

---

* It is believed that equation (A5) of their paper is in error. The mistake is compensated for by the approximation for large Z in obtaining their equation (18). One further minor algebraic error occurs in converting their equations (16) and (18), which are in photon number form, to (22) and (23), which are in power form. The term

$$\frac{g_s P_o}{\alpha A}$$

inside the exponentials of (22) and (23) should become

$$\left(\frac{g_s P_o}{\alpha A}\right)\left(\frac{\nu_p}{\nu_s}\right)$$

The first two mistakes cancel each other out and the third gives rise to a very small numerical deviation. There are two typographical errors in the equation following equation (27). p' on the left hand side should be P' and γ_o in the denominator of the right hand side should be g_s. p' in equations (28) and (30) should be P'. The mistakes in this paper also occur in the Ph.D. thesis of Au Yeung[2].

A complete specification of the dynamics requires an evaluation of the power from spontaneous Raman scattering in terms of macroscopic parameters. This is done in section 3.4,where it is also shown that spontaneous power is dependent upon the Raman gain profile. The spontaneous power arising from triangular, parabolic and Lorentzian gain profiles is considered. The computational details are in section A2.2.

In order to illustrate the theoretical work of sections 3.2 to 3.4 some possible values of the necessary constants are established in section 3.5. There is a listing in table 3.1. These numbers are used in section 3.6 to give computed graphs of pump and Stokes power evolution. The analytic solution of section 3.3 is compared to a numerical one.

In section 3.7 expressions are derived for threshold length and power for stimulated Raman scattering. There is the first discussion in the text of what is actually meant by threshold. Finally the optimal length for the most efficient conversion in a single pass fibre Raman laser is derived in section 3.8.

3.2 The propagation equations in dimensionless units

Consider a monomode, TEM_{oo} laser beam, such as that illustrated in Fig. 3.1, being coupled into a monomode optical fibre by the use of suitable lenses. The fibre has a length coordinate z, ranging from $z = 0$ to $z = L$. Power, P_o is successfully coupled into the fibre at $z = 0$. The laser is assumed to be monochromatic, having wavelength λ_ℓ.

The Stokes wave generated in the fibre grows from amplified spontaneous scattering.One accounts for the spontaneous Stokes wave[3] by assuming the fictitious injection at $z = 0$ of one photon for each of the longitudinal modes in the fibre. There is only one Stokes mode in the transverse direction in a monomode fibre. The fictitious injection

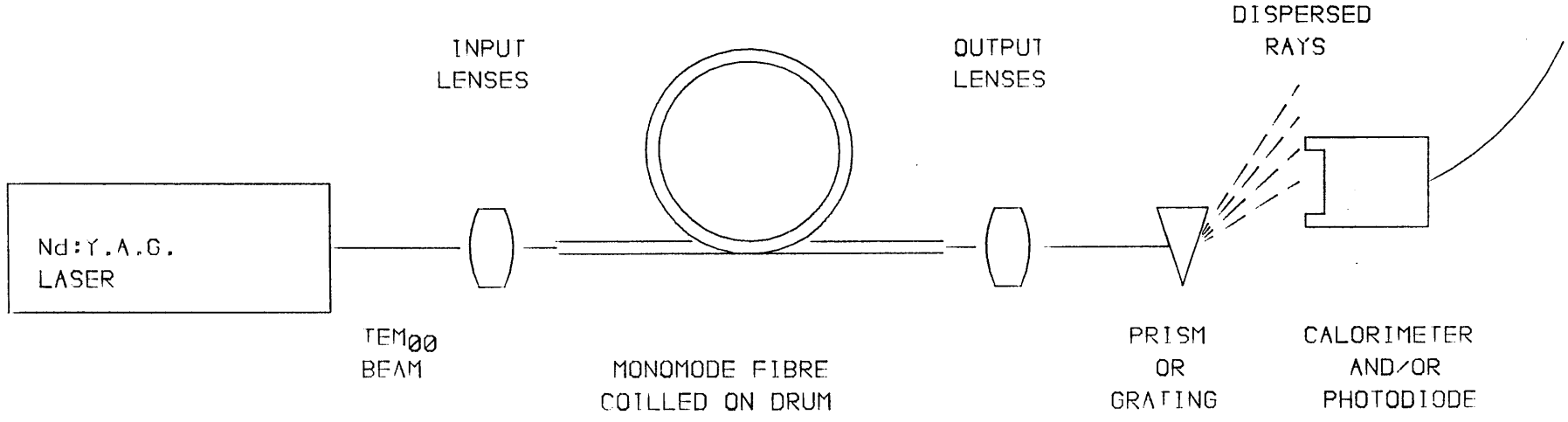

FIG. 3-1 EXPERIMENTAL APPARATUS FOR THE PRODUCTION AND DETECTION OF STIMULATED RAMAN SCATTERING IN OPTICAL FIBRES.

of these spontaneous Stokes photons has been shown by Smith[3] to be equivalent to the amplification of all of the spontaneous emission along the length of the fibre. The power of the i^{th} Stokes mode is:

$$p_i = \frac{d}{dt}(h\nu_{si}) = \frac{hc\nu_{si}}{n_e L} \tag{3.1}$$

n_e is the effective core refractive index[4], so that the group velocity in the fibre is c/n_e, n_e is approximately equal to the core refractive index.

The laser pump power, P_ℓ is depleted by linear optical loss mechanisms as well as nonlinear optical Raman conversion. The fibre loss at all the laser wavelengths corresponding to the Stokes modes is α, a constant. The equations dictating the evolution of the pump wave power is an extended version of (2.9). There is a total of q Stokes modes, each with power p_{si}.

Thus:

$$\frac{dP_\ell}{dz} + \alpha P_\ell = -\frac{1}{A}P_\ell(g_1(P_{si} + p_1) + g_2(P_{s2} + p_2) + \ldots + g_q(P_{sq} + p_q)) \tag{3.2}$$

The corresponding equation for the i^{th} Stokes mode, i=1, 2, ...q is:

$$\frac{dP_{si}}{dz} + \alpha P_{si} = +(\frac{\lambda_\ell}{\lambda_{si}})(\frac{g_i}{A})P_\ell(P_{si} + p_{si}) \tag{3.3}$$

λ_ℓ and λ_{si} are the wavelengths of the laser and the i^{th} Stokes modes, respectively. See equation (2.7). The total Stokes power is therefore given by:

$$P_s = \sum_{i=1}^{q} P_{si} \text{ and } p = \frac{1}{q}\sum_{i=1}^{q} p_{si} \tag{3.4}$$

The gain, g_i is that of the i^{th} mode supported under the broad gain profile appropriate to the fibre core material.

For each of the i equations represented by (3.3) the Stokes power, P_{si} is coupled to the laser power. It is an assumption used throughout this thesis that any mutual coupling that may exist between different Stokes modes is negligible. Mutual coupling between Stokes modes has been considered theoretically by Capasso and Di Porto[5], who show that the powers, P_{si} of the q modes are mutually independent when there is weak coupling. They show that strong coupling between the Stokes modes gives rise to equipartitioning of the Stokes modes. In that case the Raman gain over all the modes is uniform, being equal to the average of the individual gain values g_i. Stolen et al[6] have shown both theoretically and experimentally how mutual coupling gives rise to a transfer of power within the range of frequencies covered by the Raman gain profile. However, it is shown[6] that although mutual mode coupling alters the frequency distribution of the output power, the evolution of the Raman spectrum can be satisfactorily explained by the broad Raman gain profile without mutual coupling.

The terms in equations (3.2) and (3.3) are summed using (3.4) to give:

$$\frac{dP_\ell}{dz} + \alpha P_\ell = -\left(\frac{g_o}{A}\right) P_\ell (P_s + pq) \qquad (3.5)$$

$$\frac{dP_s}{dz} + \alpha P_s = \left(\frac{\lambda_\ell}{\lambda_s}\right)\left(\frac{g_o}{A}\right) P_\ell (P_s + pq) \qquad (3.6)$$

Note that in (3.5) and (3.6) the gain increments, g_i are replaced by a single gain, g_o. The reason why this can be done is discussed in section 3.4. The area, A is the effective core area, the subject matter of chapter 6. At this stage it is necessary to assume only that A is similar in value to the actual fibre core area and that it is constant for all Stokes modes.

Equations (3.5) and (3.6) are subject to the initial conditions:

$$P_\ell(z = 0) = P_o \tag{3.7}$$

$$P_s(z = 0) = q\left(\frac{h\nu_s c}{n_e L}\right) = pq \tag{3.8}$$

(3.7) is simply a statement that power, P_o is coupled into the input end of the fibre. (3.8) is based upon the assertion that the Stokes signal grows from a spontaneous background which is equivalent to the fictitious injection of 1 photon for each of the q Stokes modes. See section 3.4.

The pump and Stokes powers can now be normalised and the other quantities rendered dimensionless. As the pump and Stokes guided waves travel along the fibre one would not expect P_ℓ, P_s or $P_\ell + P_s$ to exceed P_o because of the one-way direction of power coupling: from pump wave to Stokes wave. It will be shown in section 3.4 that qp is of miniscule magnitude. Consequently the pump and Stokes powers will lie within the range zero to unity if devided by P_o. Introduce the quantities:

$$R_\ell = P_\ell/P_o \tag{3.9}$$

$$R_s = P_s/P_o \tag{3.10}$$

qp is also a power term and is divided by P_o to give

$$Q = \frac{qp}{P_o} \tag{3.11}$$

The fibre loss, α and the fibre length coordinate, z are weighted so as to remove g_o and A from (3.5) and (3.6):

$$Z = \frac{zP_o g_o}{A} \tag{3.12}$$

and

$$\beta = \frac{\alpha A}{g_o P_o} \tag{3.13}$$

and, finally introduce:

$$\Lambda = \frac{\lambda_\ell}{\lambda_s} \tag{3.14}$$

The form of the propagation equations which will be used in the remainder of the chapter are given by (3.15) and (3.16):

$$\frac{dR_\ell}{dZ} + \beta R_\ell = - R_\ell (R_s + Q) \tag{3.15}$$

$$\frac{dR_s}{dZ} + \beta R_s = + \Lambda R_\ell (R_s + Q) \tag{3.16}$$

The initial conditions now become:

$$R_\ell (Z = 0) = 1 \tag{3.17}$$

$$R_s (Z = 0) = Q \tag{3.18}$$

In the S.I. system of units z, λ_ℓ and λ_s are in metres, P_ℓ, P_s, pq and P_o are in watts, α is in reciprocal metres, A in square metres and g_o is in metres per watt. It can be checked from equations (3.9) to (3.14) that all of the quantities in (3.15) and (3.16) are dimensionless. The quantities which constitute equations (3.15) and (3.16) are not familiar. To give some idea of their magnitude some typical values applying to monomode fibres are given:

$$0.9 \leq \Lambda < 1.0$$

$$5 \times 10^{-3} < \beta < 10^{-1}$$

$$10^{-9} < Q < 10^{-6}$$

Z explores the range 0 to 100 and R_ℓ and R_s explore the range zero to unity.

By using the above data in conjunction with equations (3.17) and (3.18) it can be seen that $R_\ell(Z = 0) >> R_s(Z = 0)$.

3.3 Pump and Stokes power evolution

Equations (3.15) and (3.16) are coupled nonlinear first order ordinary differential equations. There are two dependent variables, R_ℓ and R_s, varying with respect to the independent variable Z. By adding the product of equation (3.15) and Λ to (3.16) one obtains (3.19):

$$\frac{d}{dZ}(\Lambda R_\ell + R_s) + \beta(\Lambda R_\ell + R_s) = 0 \qquad (3.19)$$

Solve equation (3.19) for $\Lambda R_\ell + R_s$ by the method of separation of variables and use the initial conditions (3.17) and (3.18) to evaluate the arbitrary constant, which arises, to give:

$$\Lambda R_\ell + R_s = (\Lambda + Q)\exp(-\beta Z)$$

$$\doteqdot \Lambda\exp(-\beta Z) \qquad (3.20)$$

Equation (3.20) is a conservation statement. $\Lambda R_\ell + R_s$ is directly proportional to the total number of photons in the fibre at any value of Z. Photons are lost only by the mechanism of linear loss. The nonlinear components in equations (3.15) and (3.16) represent the conversion from photons of wavelength λ_ℓ to wavelength λ_s. As appendix 1 discusses, in the case where $\beta = 0$, no photons are lost by the system.

Now substitute (3.20) into (3.15) and (3.16) to give:

$$\frac{dR_\ell}{dZ} + R_\ell(\beta + Q + \Lambda\exp(-\beta Z)) = \Lambda R_\ell^2 \qquad (3.21)$$

$$\frac{dR_s}{dZ} + R_s(\beta + Q - \Lambda\exp(-\beta Z)) = +\Lambda Q\exp(-\beta Z) - R_s^2 \qquad (3.22)$$

Equations (3.21) and (3.22) are de-coupled equations describing the evolution of pump and Stokes power, respectively. They are solved in section A2.1 to give:

$$R_\ell = \frac{\exp(-\beta Z)}{1 + \eta} \qquad (3.23)$$

$$R_s = \frac{\Lambda\eta\exp(-\beta Z)}{1 + \eta} \qquad (3.24)$$

Where:

$$\eta = (\frac{Q}{\beta})\exp[-(\frac{\Lambda}{\beta})\exp(-\beta Z)]\{\mathrm{Mei}(\frac{\Lambda}{\beta}) - \mathrm{Mei}(\frac{\Lambda}{\beta}\exp(-\beta Z))\} \qquad (3.25)$$

The function Mei is a special function which is designated for the purpose of this work as the "modified exponential integral" and is evaluated as:

$$\mathrm{Mei}(u) = \sum_{n=0}^{\infty} \frac{u^{n+1}}{(n+1).(n+1)!}$$

Further details are given in section A2.1.

It is also shown in section A2.1 that in the case where $\beta << 1$, the low loss case:

$$\eta(Z) = (\frac{Q}{\Lambda})\exp[(\frac{\Lambda}{\beta})(1 - \exp(-\beta Z))] \qquad (3.26)$$

In practice, in nearly all cases of interest, one can use the approximate form (3.26). When β is large $\exp(-\beta Z)$ rapidly deviates from unity, even for small Z-values. Consequently, as Z increases a significant difference in the arguments of the exponential integrals in (3.25) rapidly develops. For all except the smallest Z-values, the terms $\mathrm{Mei}(\Lambda/\beta)$ dominates. When β is large both expressions, (3.25) and (3.26) for η are considerably less than unity for all Z and the exponential term on the numerator of R_ℓ and R_s dominates.

Equation (3.26), together with (3.23) and (3.24) give the final result of Au Yeung and Yariv[2] to within a factor of Λ. It can be seen from (3.24) that a binomial series gives:

$$R_s(Z) = \frac{Q}{\Lambda}\exp(-\beta Z + \frac{\Lambda}{\beta}(1 - \exp(-\beta Z))[1 - (\frac{Q}{\Lambda})\exp(\frac{\Lambda}{\beta}(1 - \exp(-\beta Z)))]$$

$$+ (\frac{Q}{\Lambda})^2\exp(\frac{2\Lambda}{\beta}(1 - \exp(-\beta Z)))- \ldots\ldots]$$

For $\beta \ll 1$ and large Z:

$$R_s(Z) \doteq \frac{Q}{\Lambda}\exp(-\beta Z + \frac{\Lambda}{\beta}(1 - \exp(-\beta Z))) \qquad (3.27)$$

So

$$R_s(Z) \doteq \frac{Q}{\Lambda}\exp(-\beta Z + \frac{\Lambda}{\beta}) \qquad (3.28)$$

Equations (3.27) and (3.28) are the results of the calculations of Stokes power arising from small signal analysis[3].

Consider the i^{th} Stokes mode:

$$R_{si} \doteq \frac{1}{\Lambda P_o}\exp(-\beta Z + \frac{\Lambda}{\beta}(1 - \exp(-\beta Z))) \qquad (3.29)$$

Thus

$$R_{si} = \frac{1}{\Lambda P_o}\exp(-\beta Z + \frac{\Lambda}{\beta}) \qquad (3.30)$$

Equations (3.29) and (3.30) are of importance in evaluating the spontaneous power in section (3.4).

3.4 The power contribution from spontaneous Raman scattering

Having established the relationship between R_ℓ, R_s and Z, it is now necessary to evaluate the only remaining unknown, the spontaneous power, Q. The exact procedure to determine the Stokes power evolution

as equations (3.2) and (3.3) suggest, would be to assign a gain $g_i = g(\nu_i)$ to each of the q Stokes modes. i = 1, 2, ... q. $R_\ell(Z)$ and $R_s(Z)$ were derived in section 3.3 with the aid of the assignment[3] of a constant value of gain, $g_i = g_o$ for all i. The gain is equal to g_o over a range of frequencies known as the effective bandwidth, B_{eff}, and is zero elsewhere. It is important to realise that B_{eff} is dependent upon the nature of the gain profile. As will be seen, from a knowledge of B_{eff} it is a simple matter to determine q, the spontaneous photon number and hence Q, the dimensionless spontaneous Stokes power.

The effective bandwidth will be evaluated for the three Raman gain profiles discussed in section 2.5: a right angled triangle, a parabola and a truncated Lorentzian. Obviously any number of mathematical functions could be taken to represent the profiles arising from the various Raman-active media which could constitute the core and cladding of an optical fibre. As well as being of use in their own right, the three profiles chosen here illustrate how computation of B_{eff} is to be performed in general. The mathematical details of the computations are in section A2.2.

The q longitudinal fibre modes are supported within the Raman gain profile, which is represented as:

$$g(\nu) = g_o \mathfrak{L}(\nu) \tag{3.31}$$

$\mathfrak{L}(\nu)$ is the lineshape function. See Fig. 2.7. One now makes the assumption that the modes are so closely separated in the frequency domain that any summation over all q such modes can be represented by an integral.

The dimensionless Stokes power, R_s is evaluated when Z is large, that is, one wants to find the bandwidth when the Stokes conversion process is largely complete. To do so one sums over the power contributions from each amplified Stokes mode as represented by equation (3.29).

From (3.12) and (3.13) it can be seen that the frequency dependent versions of Z and β are given by

$$Z(\nu) = \frac{zP_o g_o \mathcal{L}(\nu)}{A_{eff}} \tag{3.32}$$

$$\beta(\nu) = \frac{\alpha A_{eff}}{P_o g_o \mathcal{L}(\nu)} \tag{3.33}$$

The product of $Z(\nu)$ and $\beta(\nu)$ is frequency independent. Thus the total Stokes power is

$$R_s(Z) = \int_{\nu_s}^{\nu_\ell} \frac{h\nu}{\Delta P_\phi} \exp\{-\beta Z + \frac{\Lambda \mathcal{L}(\nu)}{\beta}\} d\nu \ , \tag{3.34}$$

where h is Planck's constant.

In section A2.2 the integral (3.34) is solved for $\mathcal{L}(\nu)$ satisfying equations (2.10), (2.11). The results are as follows:

Triangular gain profile: $B_{eff} = (\beta\Delta\nu)/\Lambda$ (3.35)

Parabolic gain profile: $B_{eff} = (\frac{\pi\beta}{4\Lambda})^{\frac{1}{2}} \delta\nu$ (3.36)

Consider, now the Lorentzian profile as specified by equation (2.12). It is easy to show that the full width at the 1/x maximum (FW 1/xM) of an exponentially amplified Lorentzian is approximately equal to the FW1/xM of an exponentially amplified parabola as follows:

For a parabola with $u = (\frac{\nu - \nu_s}{\delta\nu/2})$:

$$\mathcal{L}(u) = \frac{\Lambda}{\beta}(1 - u^2)$$

Thus at FW1/xM

$$\exp\{\frac{\Lambda}{\beta}(1 - u^2)\} = \frac{1}{x}\exp(\frac{\Lambda}{\beta})$$

Giving $$u = \pm [(\beta/\Lambda)\mathrm{Ln}(x)]^{\frac{1}{2}}$$

and $$\mathrm{FW1/xM} = 2[(\beta/\Lambda)\mathrm{Ln}(x)]^{\frac{1}{2}} \qquad (3.37)$$

Similarly for a Lorentzian at FW1/xM:

$$\exp\{\frac{\Lambda/\beta}{1 + u^2}\} = \frac{1}{x}\exp(\frac{\Lambda}{\beta})$$

so $$\mathrm{FW1/xM} = 2[\frac{(\beta/\Lambda)\mathrm{Ln}(x)}{1-(\beta/\Lambda)\mathrm{Ln}(x)}]^{\frac{1}{2}} \qquad (3.38)$$

It can be seen that for $\beta << 1$ and all except the largest values of x that after exponential amplification according to equation (3.30) FW1/xM (parabola) $\doteq$ FW1/xM (Lorentzian). The consequence is that the integrand in equation (3.34) is very similar for both Lorentzian and parabolic gain profiles, despite the fact that the Lorentzian and parabola of Fig. 2.7 were markedly different in appearance. Thus the effective bandwidth of a Lorentzian gain profile is given by equation (3.36) to a good approximation.

The variation of effective bandwidth with respect to length within the limitations of the small signal theory can be obtained by starting the above analysis with equation (3.29) instead of (3.30). The term $-\beta Z$ is independent of ν and thus it can easily be seen that the effective bandwidths are given by (3.39) and (3.40).

Triangular gain profile:

$$B_{eff} = \frac{(\beta/\Lambda)\Delta\nu}{(1 - \exp(-\beta Z))} \tag{3.39}$$

Parabolic and Lorentzian gain profiles:

$$B_{eff} = \delta\nu\{\frac{\pi\beta}{4\Lambda(1-\exp(-\beta Z))}\}^{\frac{1}{2}} \tag{3.40}$$

It is now possible to evaluate the total number of spontaneously scattered photons and thus the spontaneous power. The spontaneously scattered photon number for a single transverse mode optical fibre is the reciprocal transit time multiplied by the effective bandwidth:

$$q = n_{eff} \frac{L}{c} B_{eff} \tag{3.41}$$

and hence by (3.8) and (3.11) the normalised spontaneous power is:

$$Q = \frac{h\nu_s B_{eff}}{P_o} \tag{3.42}$$

Equations (3.35) to (3.40) are substituted as appropriate into (3.42).

When (3.42) is used in conjunction with (3.15) and (3.16) the pump and Stokes power can be fully evaluated in terms of known parameters. It can be seen that the evolution of pump and Stokes power is dependent upon the nature of the Raman gain profile. The degree of the dependence will be estimated in section 3.6.

3.5 Values of constants for numerical examples

The various results and conclusions arrived at throughout this thesis will be illustrated with graphs computed from a common set of data which appears in table 3.1. The values presented, with the possible exception of the laser input power, apply to a 1.55μm telecommunications system rather than a single-pass fibre Raman laser. They are thus more in keeping with one of the declared aims of section

Transmitting wavelength, λ_ℓ	Peak Stokes wavelength, λ_s	Ratio of wavelengths, Λ	Input power, P_o	Fibre length, L	Core radius, a	V-value at λ_ℓ	V-value at λ_s
1.55μm	1.656μm	0.936	8W	1.2×10^{4}m	2.25μm	1.50	1.41

Cut-off wavelength, λ_c	Effective core area, A	Gain, $g_o/2$ at λ_ℓ=1.55μm	Peak frequency shift, $\Delta\nu$	F.W.H.M. of gain profile, $\delta\nu$	Fibre loss at pump wavelength (physical units), α_ℓ
0.967μm	$4.79\times10^{-11}m^2$	3.16×10^{-14} $m.W^{-1}$	440 cm^{-1}	240 cm^{-1}	0.2dB/km

Fibre loss at pump wavelength (dimensionless units), β_ℓ
8.73×10^{-3}

TABLE 3.1 Values of constants for examples used throughout the thesis. See sections 2.5, 3.5 and 6.6 for explanation. The gain profile is assumed to be a Lorentzian, except where stated to the contrary.

1.2; that the thesis should be biased towards Raman-free design, rather than Raman-prone design. To avoid duplication of results, Raman-prone conditions are treated by implication.

Table 3.1 applies to a fibre having a Lorentzian gain profile which exists for frequency shifts between 0 and 880 cm^{-1} from the 1.55μm laser pump. The peak shift of the profile is 440 cm^{-1} and the full width at half maximum is 240 cm^{-1}. The peak Stokes wavelength is thus at 1.65μm. The cut-off wavelength[4] of the second transverse mode in the fibre is at 1.0μm.

Due to the fact that little has been published on the Raman gains of doped silica glasses it is possible to assume only that the fibre is a silica-based material of unspecified core and cladding dopants and unspecified fabrication process. However, two requirements are made of the fibre fabrication: firstly, the materials of the core and cladding are capable of being purified to give very low losses and secondly, the process is sufficiently well controlled to give good core and cladding refractive index definition.

Most optical fibres tend to randomise the state of polarisation of a plane polarised pump after a short distance[7] due to inherent birefringence caused by defects, strains, bending, twisting, mounting, temperature gradients, etc. By using the gain value g_o up until now it has been implicity assumed that both pump and Stokes waves maintain the same state of polarisation during their progress along the fibre.

Stolen[8] has used a polarisation length, ℓ_p to determine whether or not polarisation scrambling occurs:

$$\ell_p = \frac{c}{\Delta n \Delta \nu} \qquad \text{(S.I. units)} \qquad (3.43)$$

Δn is the fibre birefringence, the difference of refractive indices experienced by the two polarisation states. If fibre length, $L < \ell_p$ it can be assumed that no polarisation scrambling will take place and thus gain will be those values given on the vertical axies of Fig. 2.5. If $L >> \ell_p$ the interaction between the pump and Stokes modes becomes decoupled. In this case the pump and Stokes waves will spend as much time polarised parallel as perpendicular with respect to each other. There is at least an order of magnitude[9] difference in scattering intensity between the parallel and perpendicular cases. Consequently, one would anticipate that the averaged gain is close to half of the value for parallel pump and Stokes polarisations.

If, as in silica $\Delta\nu = 440\ cm^{-1}$ ($=1.32 \times 10^{13}$Hz) then the polarisation length, where $\Delta n = 5 \times 10^{-6}$, is 4.5 metres. Only in the very shortest of telecommunications fibres with very high power lasers could one anticipate having to use g_o. In all other cases substitute $g_o/2$. The value of gain in table 3.1 is the peak value of the gain profile of silica (see Fig. 2.5), scaled for operation at 1.55μm in accordance with section 2.3, and divided by two to account for polarisation scrambling. So g_o is used as it appears in table 3.1 for 1.55μm operation.

The input power in table 3.1 is 8 watts. Although higher than that appropriate to a telecommunications system, the value is chosen because an 8 watts input gives a clear illustration of efficient stimulated Raman scattering in medium length fibres. The effective core area in table 3.1 is close in value to the actual core area. The justification for the value chosen, together with the V-values from which it is calculated is left until section 6.6.

3.6 A numerical example of pump and Stokes power evolution

The analysis of the power evolution is now illustrated by the use of the values of the constants contained in table 3.1. The analytic solution is compared with a numerical computer solution to equations (3.15) and (3.16), subject to the initial conditions (3.17) and (3.18). The method by which the computer solution was carried out is described in appendix 4.

Fig. 3.2 and 3.3 illustrate the high and low conversion efficiency cases, respectively. The higher the loss, β the smaller the Stokes wave generated. In Fig. 3.2 $R_\ell(Z)$ and $R_s(Z)$ are plotted for a low value of β. Assuming no bending or fibre imperfection losses, α is about the lowest loss[10] that one would expect from a silica fibre at 1.55μm. Equation (3.13) is used in conjunction with table 3.1 to give $\beta = 8.73 \times 10^{-3}$, which is considerably less than unity. Consequently, equations (3.23), (3.24) and (3.26) were used to compute the solid lines in Fig. 3.2.

By equation (3.17), the input pump power, $R_\ell(Z = 0)$ is unity. It can be seen from Fig. 3.2 that at no value of Z greater than zero do either R_ℓ or R_s equal or exceed unity. The gradient of R_ℓ is negative everywhere, which is consistent with the requirements of equation (3.15). The input Stokes power, Q (see (3.18)) is so small on the scale of Fig. 3.2 that it appears to be zero. R_s changes gradient from positive, through zero, to negative, reaching its maximum when Z = 27.5. The maximum fibre length considered is 12km, corresponding to Z = 63.3

Fig. 3.3 represents a much higher loss case (α = 1.2 dB/km; $\beta = 5.24 \times 10^{-2}$), displaying very low conversion efficiency.
As with Fig. 3.2, equation (3.26) was used in conjunction with (3.23)

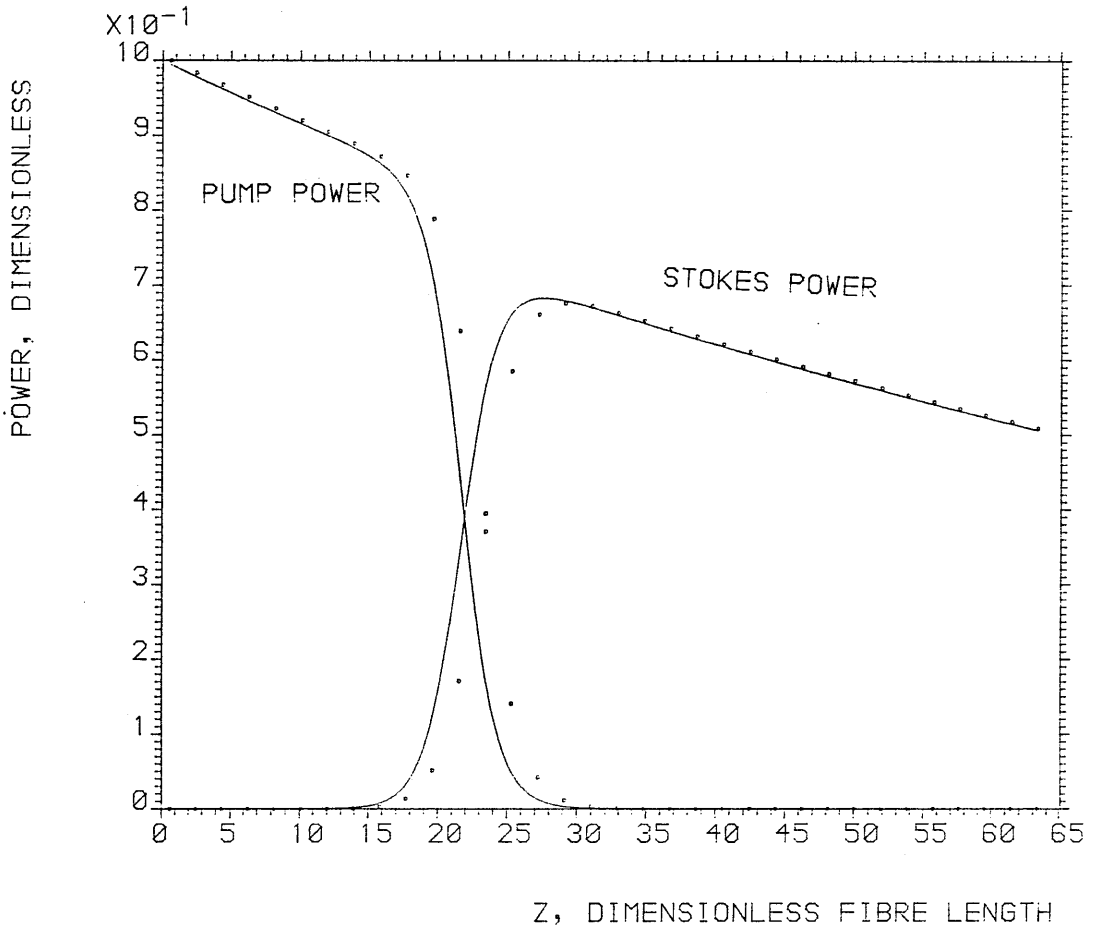

FIG. 3-2 STIMULATED RAMAN SCATTERING IN A STEP-INDEX MONOMODE OPTICAL FIBRE. COMPARISON OF SOLUTIONS: ANALYTICAL (SOLID LINE) AND NUMERICAL (BROKEN LINE). THE EQUATIONS REPRESENT THE EVOLUTION OF THE PUMP AND STOKES POWER IN THE CASE WHERE THE LOSSES AT THE PUMP AND STOKES WAVELENGTHS ARE EQUAL.
FIBRE LOSS = .2 DB/KM.
OTHER DATA USED IN COMPUTATIONS ARE GIVEN IN TABLE 3-1.

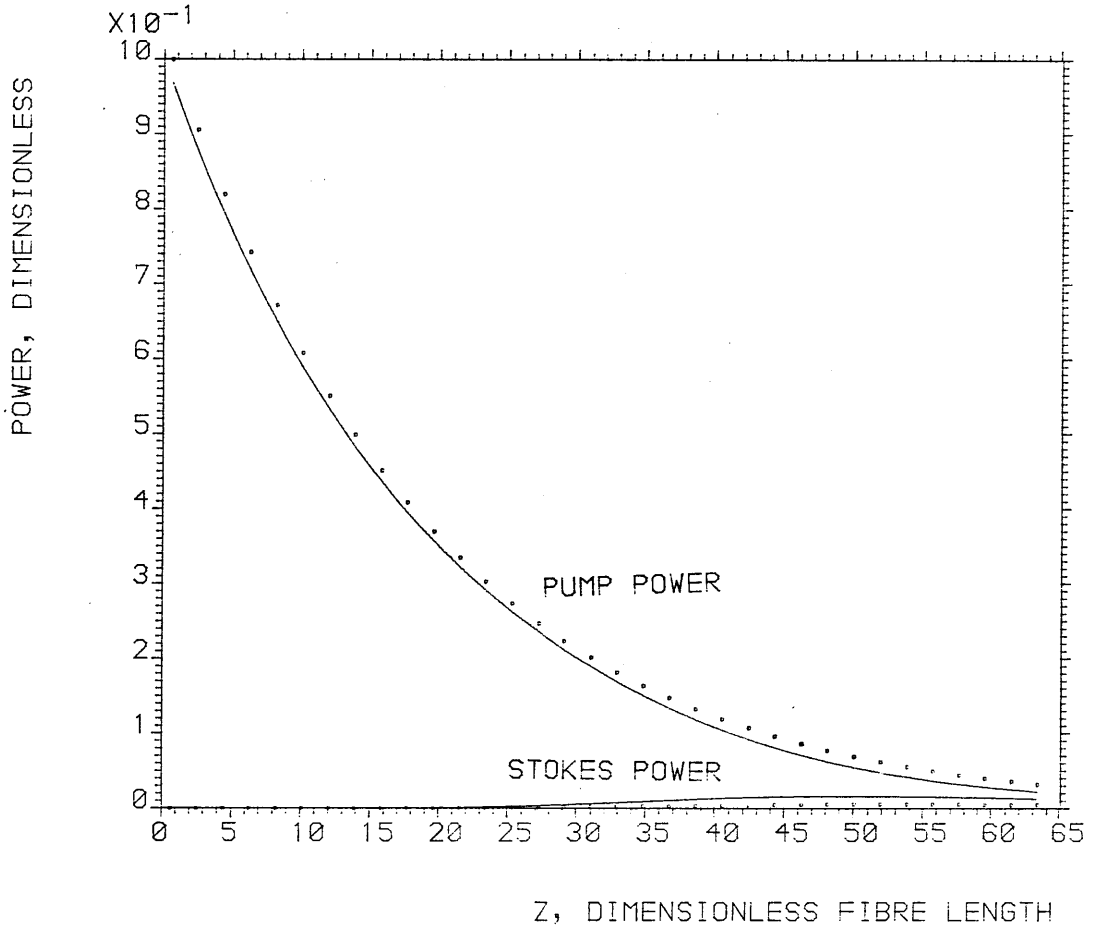

FIG. 3-3 STIMULATED RAMAN SCATTERING IN A STEP-INDEX MONOMODE OPTICAL FIBRE. COMPARISON OF SOLUTIONS: ANALYTICAL (SOLID LINE) AND NUMERICAL (BROKEN LINE). THE EQUATIONS REPRESENT THE EVOLUTION OF THE PUMP AND STOKES POWER IN THE CASE WHERE THE LOSSES AT THE PUMP AND STOKES WAVELENGTHS ARE EQUAL.
FIBRE LOSS = 1.2 DB/KM.
OTHER DATA USED IN COMPUTATIONS ARE GIVEN IN TABLE 3-1.

and (3.24) in computing R_ℓ and R_s, note that for nearly all Z, $\eta << 1$. The exponential term in the numerator of (3.23) for $R_\ell(z)$ dominates. $R_s(z)$ displays minimal growth.

The dotted lines on Fig. 3.2 and 3.3 represent numerical solutions to equations (3.5) and (3.6) by the method used in chapter 4. It can be seen that the analysis of section 3.5 compares well with an alternative procedure.

Fig. 3.4 contains two isometric projections representing how the Stokes and pump waves grow and decline, respectively, when the loss is varied between 0.1 and 2.1dB/km. At high losses (Y-axis, right) the pump power experiences almost exponential decay whilst the Stokes wave hardly grows at all, the effect of the loss being greater than that of the nonlinear conversion. At low losses (Y-axis, left) the nonlinear process is dominant.

3.7 Threshold stimulated Raman scattering

The design of a source, fibre and detector system which is Raman free, (to be discussed in chapter 7) requires the designation of some value of fibre length as threshold length, Z_{th}. At fibre lengths greater than Z_{th} the stimulated Raman wavelength conversion process is occurring to a significant extent.

The problem arising from the previous analysis is that with the model used there is no unique starting point other than Z = 0 for the onset of stimulated Raman scattering. R_ℓ, R_s and their derivatives are continuous everywhere, one, therefore, has to choose a criterion for threshold and evaluate Z_{th} according to whether or not the criterion is satisfied. The criterion is arbitrary and in practice one would choose it to suit the situation to which it would be applied.

(A) PUMP POWER

X-AXIS: DIMENSIONLESS Z-COORDINATE
Y-AXIS: DIMENSIONLESS FIBRE LOSS
Z-AXIS: NORMALISED POWER

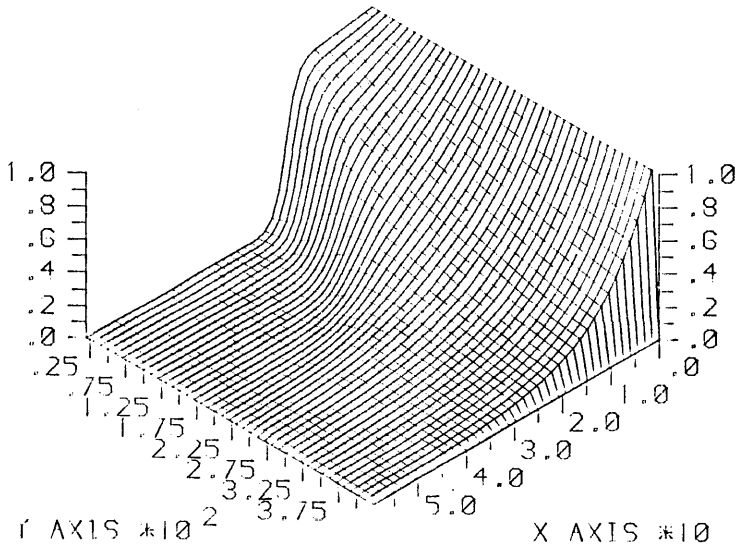

(B) STOKES POWER

X-AXIS: DIMENSIONLESS Z-COORDINATE
Y-AXIS: DIMENSIONLESS FIBRE LOSS
Z-AXIS: NORMALISED POWER

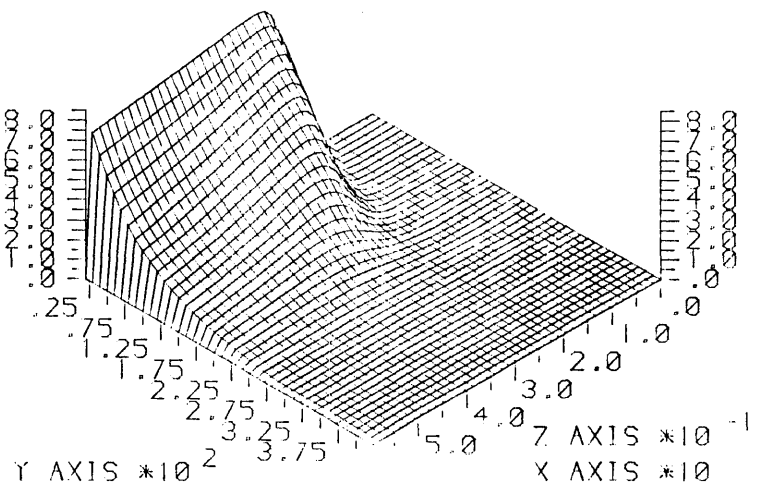

FIG.3-4 ISOMETRIC PROJECTIONS REPRESENTING THE EVOLUTION OF (A) PUMP AND (B) STOKES POWER ALONG THE LENGTH OF A MONOMODE STEP-INDEX OPTICAL FIBRE. SEE TABLE 3-1 FOR DATA.

From Fig.s 3.2 and 3.3 a possible criterion could be that threshold occurs at length Z_{th} such that the Stokes power has grown in magnitude until it is equal to the pump power. Then:

$$R_{\ell} = R_{s} \tag{3.44}$$

In fact, a slightly more mathematically convenient criterion is:

$$\Lambda R_{\ell} = R_{s} \tag{3.45}$$

Equation (3.45) is an expression of the equality of pump and Stokes photon number. A generalisation is to consider when the Stokes photon number grows to 1/y times the pump photon number. In that case:

$$\Lambda R_{\ell} = yR_{s} \tag{3.46}$$

In equation (3.46) y may be less than, equal to or greater than unity, as required. When the appropriate condition (3.44), (3.45) or (3.46) is satisfied $Z = Z_T$. When $Z \geq Z_T$, one observes threshold S.R.S. Another way of looking at the same problem is to enquire what value β must have, for a given value of Z, such that condition (3.44), (3.45) or (3.46), as appropriate, holds. In that case $\beta = \beta_T$. When $\beta \leq \beta_T$ S.R.S is observed.

Condition (3.46) is considered because it is more general than (3.44) or (3.45). Specification in terms of equality of photon number rather than power leads to a slight mathematical simplification. By using (3.23), (3.24) and (3.26) it can be seen that:

$$y\eta = (\frac{yQ}{\Lambda}) \exp\{\frac{\Lambda}{\beta}[1-\exp(-\beta Z)]\} = 1 \tag{3.47}$$

Equation (3.47) is the general expression for threshold length. The value of Z which satisfies (3.47) is Z_T.

The dimensionless spontaneous power, Q depends upon the mathematical model used to represent the gain profile (see section 3.4). Thus the

threshold length depends upon the model used. Equations (3.47) and (3.42) employ expressions (3.39) and (3.40), respectively for the effective bandwidth.

For a triangular profile:

$$\frac{yH\beta\Delta\nu}{\Lambda}\exp[\frac{\Lambda}{\beta}(1-\exp(-\beta Z))] = [1-\exp(-\beta Z)] \qquad (3.48)$$

For a Lorentzian profile:

$$yH(\frac{\pi\beta}{4\Lambda})^{\frac{1}{2}}\delta\nu\ \exp[\frac{\Lambda}{\beta}(1-\exp(-\beta Z))] = [1-\exp(-\beta Z)]^{\frac{1}{2}} \qquad (3.49)$$

Where
$$H = h\nu_s/(P_o\Lambda) \qquad (3.50)$$

(3.48) and (3.49) can be converted to physical units using (3.9) to (3.14), inclusive. The physical units version closely resembles the result of Au Yeung and Yariv[2] (with y = 1 and corrected for their slight algebriac error in λ_ℓ/λ_s).

It is now possible to calculate and draw some interesting conclusions about the maximum loss and minimum length at which threshold stimulated Raman scattering will occur.

Consider when βZ is large: $\beta = \beta_{max}$, and so from (3.47):

$$\beta_{max} = \frac{\Lambda}{\mathrm{Ln}[\frac{\Lambda}{yQ}]} \qquad (3.51)$$

β_{max} is the maximum value of loss for which threshold stimulated Raman scattering will occur when (3.47) is used.

When βZ is small $Z = Z_{min}$, and so:

$$Z_{min} = \frac{1}{\Lambda}\mathrm{Ln}[\frac{\Lambda}{yQ}] \qquad (3.52)$$

Z_{min} is the minimum dimensionless length of fibre required for (3.47)

to be satisfied. (3.52) should be compared with the threshold length in the zero loss limit, (A1-17).

It can be seen from (3.51) and (3.52) that

$$\beta_{max} Z_{min} = 1 \tag{3.53}$$

Equation (3.53) was derived by Au Yeung and Yariv[2] in physical, rather than dimensionless coordinates. In their work the result was shown for the specific case of a parabolic approximation to a Lorentzian gain profile. If one accepts the approximations in obtaining the results of section 3.3, it can be seen that (3.53) holds for all gain profiles. It can also be seen that (3.53) is independent of the value of y. Note the close approximation between (3.52) and the threshold length in the zero loss limit. See equation (A1.17). The small discrepancy is due to the algebraic approximations employed in section A2.1.

Now use the results of the effective bandwidths for the triangular and Lorentzian gain models to give equations (3.54) to (3.57):

Triangular gain:

$$Z_{min} = \frac{1}{\Lambda} \text{Ln}\left[\frac{\Lambda Z_{min}}{yH\Delta\nu}\right] \tag{3.54}$$

$$\beta_{max} = \Lambda\left[\text{Ln}\left(\frac{\Lambda}{y\beta_{max} H\Delta\nu}\right)\right]^{-1} \tag{3.55}$$

Lorentzian gain:

$$Z_{min} = \frac{1}{\Lambda} \text{Ln}\left[\frac{\delta\nu}{yH}\left(\frac{4\Lambda Z_{min}}{\pi}\right)^{\frac{1}{2}}\right] \tag{3.56}$$

$$\beta_{max} = \Lambda\left[\text{Ln}\left[\frac{1}{yH\delta\nu}\left(\frac{4\Lambda}{\pi\beta_{max}}\right)^{\frac{1}{2}}\right]\right]^{-1} \tag{3.57}$$

where H is given by (3.50).

The equations (3.48), (3.49) and (3.54) to (3.57) cannot be rearranged so that any of the quantities appear exclusively on the left hand side. One must use numerical methods, such as the Newton-Raphson iteration formula to solve for the desired quantity. It has been found that (3.54) to (3.57) can be quickly solved by trial and error with the aid of a pocket calculator.

Table 3.2 gives values of the dimensionless quantities β_{max} and Z_{min} with their physical counterparts, α_{max} and z_{min} for triangular and Lorentzian gain profiles. Results are quoted for the cases where $y = 1$ and $y = 10$.

3.8 Optimal conversion

When considering single-pass Raman lasers it would be useful to know the length of fibre which would produce the largest Stokes wave for a given input power. In this way one can make the most efficient use of the laser pump available. It can be seen from Figs. 3.2 and 3.3 that there is some length, Z_{opt} such that the first order Stokes output is optimised. When $Z < Z_{opt}$ the Stokes conversion process is incomplete. When $Z > Z_{opt}$ the attenuation due to fibre loss dominates over amplification due to Raman gain.

From Figs. 3.2 and 3.3 it can be seen that in all cases of practical interest:

$$R_s(Z_{opt}) >> Q$$

From equation (3.15)

$$\frac{dR_s(Z_{opt})}{dZ} = 0 \quad \text{thus} \quad R_\ell(Z_{opt}) = \beta/\Lambda \tag{3.58}$$

From (3.20):

$$R_s(Z_{opt}) = \Lambda\exp(-\beta Z_{opt})-\beta \tag{3.59}$$

Profile type and y-value	Σ_{min}	β_{max}	z_{min} (in metres)	α_{max} (dB/km)
Triangle, $\Delta\nu = 522\ cm^{-1}$ $y = 1$	19.35	5.17×10^{-2}	3667	1.18
Triangle, $\Delta\nu = 522\ cm^{-1}$ $y = 10$	15.77	6.34×10^{-2}	2988	1.45
Lorentzian, $\delta\nu = 240\ cm^{-1}$ $y = 1$	16.34	6.12×10^{-2}	3096	1.40
Lorentzian, $\delta\nu = 240\ cm^{-1}$ $y = 10$	14.11	7.09×10^{-2}	2674	1.62

Table 3.2 Values of minimum length and maximum loss which permit Raman thresholds with $y = 1$ and $y = 10$ to be achieved. Triangle and Lorentzian profiles are considered. See equations (3.53) to (3.57), inclusive.

One can thus calculate optimal fibre length for Stokes conversion from equations (3.59) and (3.24).

$$\Lambda\exp(-\beta Z_{opt}) = \beta(1 + \eta(Z_{opt})) \qquad (3.60)$$

$\eta(Z_{opt})$ is given by (3.26) in the case where $Z = Z_{opt}$.

References

1. von der Linde, D., Maier, M., and Kaiser, W. "Quantitative investigations of the stimulated Raman effect using subnanosecond light pulses", Phys. Rev. 178, 11, (1969).

2. Au Yeung, J. and Yariv, A., "Spontaneous and stimulated Raman scattering in long low loss fibres", I.E.E.E. J. Quantum Electron., QE-14, 347, (1978).

and Au Yeung, J.C-W., Ph.D. Thesis, "Phase conjugate optics and nonlinear optical phenomena in optical fibres", California Institute of Technology, (1979).

3. Smith, R.G., "Critical power handling capacity of low-loss optical fibres as determined by stimulated Raman and Brillouin scattering", Appl. Optics, 11, 2489, (1972).

4. Gloge, D., "Weakly guiding fibres", Appl. Opt., 10, 2252, (1971).

5. Capasso, F. and Di Porto, P., "Coupled-mode theory of Raman amplification in lossless optical fibres", J. Appl. Phys., 47, 1472, (1976).

6. Stolen, R.H., Lee, C., Jain, R.K., "Development of the stimulated Raman spectrum in single mode silica fibres", J. Opt. Soc. Am., B1, 652, (1984).

7. Rashleigh, S.C., "Origins and control of polarisation effects in single-mode fibres", I.E.E.E. J. Lightwave Technol. LT-1, 312, (1983).

8. Stolen, R.H., "Polarisation effects in fibre Raman and Brillouin lasers", I.E.E.E. J. Quantum Electron. QE-15, 1157, (1979).

9. Heiman, D., Hellwarth, R.W., Hamilton, D.S., "Raman scattering and nonlinear refractive index measurements of optical glasses", J. Non Crystalline Solids, 34, 63, (1979).

10. Garrett, I., Todd, C.J., "Components and systems for long-wavelength monomode fibre transmission", Opt. and Quantum Electron., 14, 95, (1982).

CHAPTER FOUR

THE TWO WAVELENGTH MODEL OF STIMULATED RAMAN SCATTERING IN OPTICAL FIBRES WITH NON-CONSTANT LOSSES

4.1 Introduction

The considerations of chapter 3 are now extended to include the case where the Stokes wave experiences a fibre loss different from that of the pump wave and numerically computed solutions are obtained. The theory of Smith[1] shows how an exact analytic solution can be derived when it is assumed that the only attenuating influence upon the pump wave is the fibre loss. It has not been possible to find a satisfactory analytic solution for the situation where the pump wave depletion, due to Raman conversion, is also taken into account. Nevertheless, it has been possible to draw some interesting conclusions about how the energy conversion process in the fibre is affected by the two different losses. Three unsuccessful attempts to find analytical solutions are described in Appendix 3. A brief description of the numerical methods used can be found in Appendix 4.

The differential equations governing pump and Stokes power evolution are stated, which together with a discussion of spontaneous Stokes power, constitute section 4.2. In section 4.3 the relative magnitudes of the pump and Stokes power for various ratios of the two fibre losses are discussed and comparison with the equal loss case is made. It is important to consider how energy is transferred from the pump to the Stokes wave and simultaneously attenuated by the two fibre losses. In section 4.4, mathematical properties connected with the concept of power transfer are derived.

The most important practical situation is where a laser input of variable power is launched into a fixed length of fibre coilled on a drum as in Fig. 3.1. In the final section, 4.5, the relationship between pump and Stokes input and output powers is investigated.

In all except for one of the graphical examples in this chapter the

Stokes loss has been taken to be greater than the pump loss. There are two reasons why. Firstly, the situation is generally more appropriate to one of the declared aims of the whole thesis: to give preferential consideration to stimulated Raman scattering as an undesirable phenomenon in telecommunications. Stokes loss, being greater than pump loss, could result from selective doping to suppress stimulated Raman scattering. Secondly, an interesting phenomenon arises when there is a high ratio of Stokes to pump loss, which casts doubt on the previously accepted definition of threshold. However, the mathematical treatment that is given in this chapter applies equally well to the case of Stokes loss greater than the pump loss or vice-versa.

4.2 The equations for unequal loss propagation

Consider equations (3.2), (3.3) and (3.4): a pump wave of frequency ν_ℓ generates a multifrequency Stokes spectrum, consisting of modes, P_{si}; i = 1,2, ...q. The loss experienced by the laser pump and all of the Stokes modes is taken to be α. In a real fibre one would not expect the losses experienced by the Stokes modes to be equal to that of the pump wave nor equal to each other. The loss at the pump frequency is α_ℓ. Each Stokes mode has its own individual loss term, α_{si}. The discrete loss values, α_{si} follow the loss spectrum of the fibre for that range of frequencies which are enveloped by the Raman gain profile.

It is the purpose of this chapter to assume that the total Stokes power due to Raman generation over a whole series of Stokes losses is identically equivalent to a single Stokes component experiencing the loss α_s. The proof that this is so, together with the derivation of the single loss value, α_s which can represent one possible loss spectrum is left until chapter 5.

The term two wevelength model is used to describe the coupled differential equations:

$$\frac{dP_\ell}{dz} + \alpha_\ell P_\ell = -\left(\frac{g_o}{A}\right)P_\ell(P_s + pq) \tag{4.1}$$

$$\frac{dP_s}{dz} + \alpha_s P_s = \left(\frac{\lambda_\ell}{\lambda_s}\right)\left(\frac{g_o}{A}\right)P_\ell(P_s + pq) \tag{4.2}$$

The normalisation equations (3.9) to (3.12) and (3.14) are used. The normalised losses β_ℓ and β_s are given by (4.3) and (4.4):

$$\beta_\ell = \frac{\alpha_\ell A}{P_o g_o} \tag{4.3}$$

$$\beta_s = \frac{\alpha_s A}{P_o g_o} \tag{4.4}$$

Equations (4.1) and (4.2) can be restated in normalised form:

$$\frac{dR_\ell}{dZ} + \beta_\ell R_\ell = -R_\ell(R_s + Q) \tag{4.5}$$

$$\frac{dR_s}{dZ} + \beta_s R_s = \Lambda R_\ell(R_s + Q) \tag{4.6}$$

The solutions to equations (4.5) and (4.6) from the subject matter of this chapter. The initial conditions are again (3.17) and (3.18).

As far as the normalised spontaneous power, Q is concerned, it is assumed that in the limit as the length becomes large, the Stokes wave can be represented by the small signal result derived by Smith[1]. The same procedure as in section 3.4 is followed in order to calculate the effective bandwidth, B_{eff} and hence Q. The starting equation for calculating B_{eff} is:

$$R_s \doteq \frac{h}{\Lambda}\exp(-\beta_s Z)\int_{\nu_o^-}^{\nu_o^+} \nu\exp\left\{\frac{\Lambda \ell(\nu)}{\beta_\ell}\right\} d\nu \tag{4.7}$$

The result of calculating B_{eff} from (4.7) is the same as that from (3.34), provided that β_ℓ is substituted into the final expression in place of β. The effective Stokes bandwidth is, therefore, independent of the Stokes loss. In all the calculations that follow the gain profile is taken to be Lorentzian.

4.3 The propagation of pump and Stokes waves when β_s is not equal to β_ℓ

Equations (4.5) and (4.6) have been solved numerically for the initial conditions (3.17) and (3.18) by the method outlined in appendix 4. Fig. 4.1 depicts the situation where $\beta_\ell \leq \beta_s$. The values for the physical constants are in table 3.1 and Q was calculated from Lorentzian gain profile theory (see equation (3.36)). In all four cases illustrated in Fig. 4.1 the loss at the pump wavelength is 0.2dB/km, giving $\beta_\ell = 8.73 \times 10^{-3}$. Z covers the same range of values as in Fig. 3.2. Note that in each case the normalised pump power is unity at Z = 0 and the Stokes power has a very small value at Z = 0.

The lines labelled (A) are plots for the same values of Q and β as in Fig. 3.2. For (A) $\beta_\ell = \beta_s = \beta$. (B) corresponds to a Stokes loss 20 times that of the pump. The pump wave is depleted to a considerable extent in both cases. However, in (B) the onset of the zone of rapid depletion of the pump has been delayed by about 5 units along the horizontal axis. The most marked effect is on the Stokes wave, R_s, the growth of which, has become considerably "stunted". The point of maximum Stokes power occurs at a longer length of fibre. R_s is maximised at Z = 28 in (A) and Z = 29 in (B). The cross over point (where $R_\ell = R_s$) is also at a greater fibre length. $R_\ell = R_s$ at Z = 22 in (A) and Z = 29 in (B), from about Z = 50 onwards R_s is of negligible magnitude in (B), whilst it is quite significant in (A).

Consider what happens when there are yet higher Stokes losses. In the pairs of curves labelled (C) and (D), β_s is increased to $30\beta_\ell$ and $40\beta_\ell$,

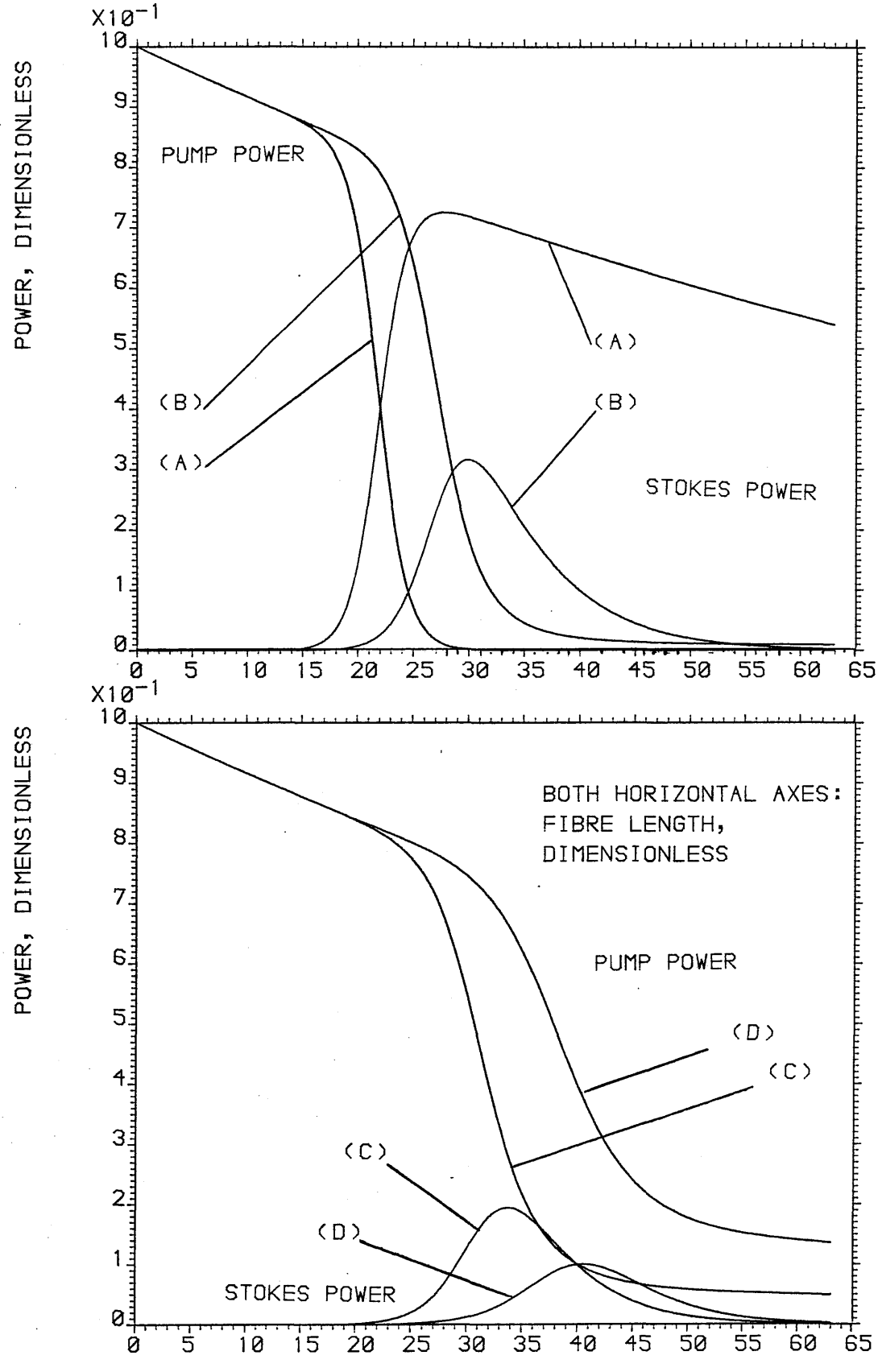

FIG. 4-1 GROWTH OF THE STOKES POWER AND THE CORRESPONDING DEPLETION OF PUMP POWER.
RATIO OF LOSSES; STOKES TO PUMP:
(A) 1.0, (B) 20.0, (C) 30.0, (D) 40.0 .

respectively. The Stokes wave becomes increasingly stunted with the increase of β_s. The peak Stokes power is shifted to even greater fibre lengths. Despite the small magnitude of R_s at all Z values, there is significant depletion of the pump wave which is not attributable to the influence of β_ℓ alone. It is of special importance to note that in (D) R_s never grows to be as large as R_ℓ, despite the fact that R_ℓ is depleted considerably. Whether one chooses $R_\ell = R_s$ or $\Lambda R_\ell = R_s$ to be the threshold criterion, threshold stimulated Raman scattering does not occur in curve (D). In curve (C) there are two values of Z for which $R_\ell = R_s$: Z = 36.5 and Z = 40.

A qualitative explanation is now given for the above behaviour. As soon as photons are converted from wavelength λ_ℓ to λ_s they are rapidly attenuated if $\beta_s > \beta_\ell$. There is thus a lower Stokes power level. The power squared terms on the right hand side of equations (4.5) and (4.6) mean that the rate of Raman conversion is proportional to the magnitude of the Stokes wave that is already present at a given point on the fibre. Due to the relatively high absorption at λ_s the Raman conversion slows down more quickly. Consequently, as in (B) both the cross-over threshold point and the optimal conversion point are shifted to greater fibre lengths.

When the Stokes loss becomes very large, as in (C) and (D), there is only a small Stokes wave generated, however, the pump wave is attenuated to an extent which cannot be explained by β_ℓ alone. In (C) and (D) there is minimal growth of Stokes power, despite considerable pump attenuation. There are two important consequences. Firstly, one must reconsider the criteria of threshold, $R_\ell = R_s$ and $\Lambda R_\ell = yR_s$ (see section 3.6). Secondly, there is an important limitation on the extent to which one can hope to selectively dope a fibre with a highly absorbing material, with the aim of suppressing stimulated Raman scattering. An other reason for questioning the threshold definition of equality of

pump and Stokes power comes from curve (C) at Z = 40. There is a second cross-over point. The result is an ambiguity in the threshold length.

In Fig. 4.2 the pump and Stokes power evolution graphs are redrawn for the case where the Stokes loss is less than the pump loss. In order to avoid the use of excessively low values of the Stokes loss, the pump loss is increased to α_ℓ = 1dB/km, so that $\beta_\ell = 8.73 \times 10^{-2}$. By reducing β_s from being equal to β_ℓ to $0.2\beta_\ell$ there is a noticeable, though not particularly significant effect upon the Stokes wave. As β_s decreases the cross-over point decreases, the length for optimal Stokes power decreases and $R_s(Z)$ becomes more horizontal after the optimal conversion length. A Stokes loss which is less than the pump loss would be of some small benefit in a single pass Raman laser, but rather undesirable in a telecommunications system.

4.4 Power coupling when pump and Stokes losses are unequal

The equations (4.5) and (4.6) have not been solved analytically, but useful information can be ascertained about the transfer of power from R_ℓ to R_s. Following section 3.3, add the product of Λ and equation (4.5) to equation (4.6):

$$\frac{d}{dZ}(\Lambda R_\ell + R_s) + \beta_\ell \Lambda R_\ell + \beta_s R_s = 0$$

Now define the parameter γ:

$$\gamma(Z) = \frac{\beta_\ell \Lambda R_\ell + \beta_s R_s}{\Lambda R_\ell + R_s} \tag{4.8}$$

Thus

$$\frac{d}{dZ}(\Lambda R_\ell + R_s) + \gamma(Z)(\Lambda R_\ell + R_s) = 0 \tag{4.9}$$

From which:

$$\Lambda R_\ell + R_s = \Lambda \exp\left\{-\int^Z \gamma(Z')dZ'\right\} \tag{4.10}$$

It can be seen that (4.10) is very similar in form to (3.20). It is

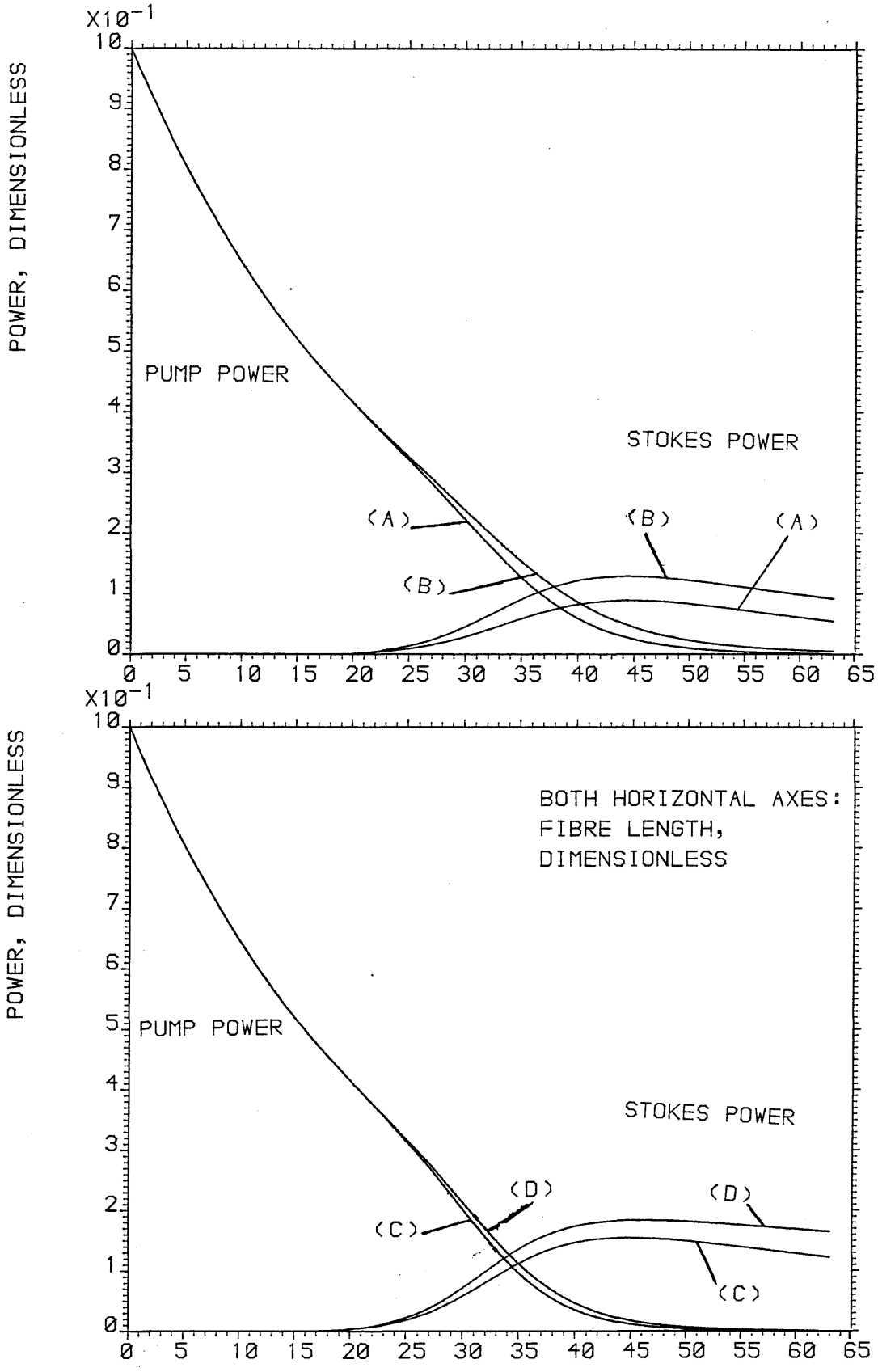

FIG. 4-2 GROWTH OF THE STOKES POWER AND THE CORRESPONDING DEPLETION OF PUMP POWER.
RATIO OF LOSSES; STOKES TO PUMP:
(A) 1.0, (B) .6, (C) .4, (D) .2 .

proportional to the total photon number at length Z in the fibre. The power absorbed by the material scattering centres is $(1 - \Lambda)R_\ell$. It should be noted from (4.8) that γ is Z-dependent. It can be seen from (4.10) that $\gamma(Z)$ is a loss-like term. In (3.20) $\Lambda R_\ell + R_s$ was dependant upon the negative exponential of the Z-integral of the loss. In (4.10) $\Lambda R_\ell + R_s$ depends upon the negative exponential of the integral of the loss-like parameter, γ.

$\gamma(Z)$ is designated here as the power coupling parameter, due to the fact that it plays a central role in describing power conversion from pump to Stokes wavelengths. If the equations (4.5) and (4.6) are restated in terms of physical coordinates and the physical equivalent of γ, say $\gamma(\text{phys})$, is derived in the same way, it can easily be shown that $\gamma(\text{phys})$ has the dimensions of reciprocal length. That is the dimensions of loss.

It is now of interest to draw some simple conclusions about $\gamma(Z)$. Consider equation (4.8). If at any Z-value $R_\ell >> R_s$, then it can be seen that $\gamma \doteq \beta_\ell$. If, on the other hand, for some particular Z-value $R_s >> R_\ell$ then $\gamma \doteq \beta_s$. Thus it can be concluded that for all Z:

If $\beta_s > \beta_\ell$ $\qquad \beta_\ell \leq \gamma(Z) \leq \beta_s$ (4.11)

and if $\beta_s < \beta_\ell$ $\qquad \beta_s \leq \gamma(Z) \leq \beta_\ell$ (4.12)

in the equal loss case:

if $\beta_s = \beta_\ell = \beta$ $\qquad \gamma = \beta$ (4.13)

From equation (4.10) in conjunction with (4.11) and (4.12) it can be seen that the total normalised optical power in the fibre lies in the range:

if $\beta_s > \beta_\ell$; $\exp(-\beta_\ell Z) \leq \Lambda R_\ell + R_s \leq \exp(-\beta_s Z)$

if $\beta_\ell > \beta_s$; $\exp(-\beta_s Z) \leq \Lambda R_\ell + R_s \leq \exp(-\beta_\ell Z)$

At no fibre length does the power $\Lambda R_\ell + R_s$ experience an attenuation outside the range β_ℓ to β_s.

Consider Z = 0. Using initial conditions, equations (3.17) and (3.18), together with (4.8) one can show that:

$$\gamma(0) = \frac{\Lambda\beta_\ell + Q\beta_s}{\Lambda + Q} \doteq \beta_\ell \qquad (4.14)$$

(Since $\Lambda >> Q$.) Suppose the threshold condition, $\Lambda R_\ell = yR_s$ is satisfied. (See equation (3.46)). From equation (4.8), where γ is γ_{th} at threshold,

$$\gamma_{th} = \frac{yR_s\beta_\ell + R_s\beta_s}{yR_s + R_s} = \frac{y\beta_\ell + \beta_s}{y + 1} \qquad (4.15)$$

when y = 1

$$\gamma_{th} = \frac{\beta_\ell + \beta_s}{2}$$

Thus when the threshold condition is that pump and Stokes photon numbers are equal, γ_{th} is the arithmetic mean of the pump and Stokes losses.

$\gamma(Z)$ can be normalised so that it lies between zero and unity if β_s is greater than β_ℓ, and zero and negative unity if β_ℓ is greater than β_s. The normalisation can be performed in two ways:

Define:

$$\varepsilon = \frac{\beta_s - \gamma}{\beta_s - \beta_\ell} \qquad (4.16)$$

So it can be seen that

$$1 - \varepsilon = \frac{\gamma - \beta_\ell}{\beta_s - \beta_\ell} \qquad (4.17)$$

Both ε and $(1 - \varepsilon)$ lie in the range 0 to 1 for all possible values of β_ℓ & β_s. There would appear to be a problem in the equal loss case, where $\beta_\ell = \beta_s = \beta$. In that case ε is defined to be zero. It should be remembere that ε is a function of γ and consequently of Z. ε is designated the normalised power coupling parameter. It can easily be seen that at the $\Lambda R_\ell = R_s$ threshold $\varepsilon = \frac{1}{2}$ and at Z = 0 $\varepsilon \doteq 1$.

By the use of (4.16) (or (4.17)) values of the power coupling parameter can be normalised and hence plotted on the same graph for widely differing values of the ratio β_s/β_ℓ. On Fig. 4.3 $1-\varepsilon$ has been plotted as a function of Z for the cases corresponding to (A), (B), (C) and (D) of Fig. 4.1. $\varepsilon(Z)$ will be discussed in greater detail in appendix 3.

The power, $\Lambda R_\ell + R_s$ (which is directly proportional to the total photon number) can be calculated as a function of Z either by adding directly or by the use of equation (4.10). Fig. 4.4 is a graph of $(\Lambda R_\ell + R_s)/\Lambda$ computed from equation (4.10). When $Z = 0$, $(\Lambda R_\ell + R_s)/\Lambda = 1$. In (A), the equal loss case, $(\Lambda R_\ell + R_s)/\Lambda$ is an exponential, as required by equation (3.20). As the Stokes loss is increased $\Lambda R_\ell + R_s$ deviates increasingly from exponential form until β_s is so high that the Stokes wave, R_s can grow only to a minimal extent. The pump wave, R_ℓ then becomes the dominant contribution to $\Lambda R_\ell + R_s$. As β_s is increased to yet higher levels $\Lambda R_\ell + R_s$ starts to return to an exponential-like form.

The three curves of Fig. 4.5 are $(\Lambda R_\ell + R_s)/\Lambda$ calculated from (4.10), $(\Lambda R_\ell + R_s)/\Lambda$ calculated by direct addition and R_ℓ by itself. The Stokes loss corresponds to curve (D) of Figs. 4.1 and 4.4; $\beta_s/\beta_\ell = 40$. The overlapping dotted and solid lines confirm equation (4.10). The plot of R_ℓ indicates that the major contribution to the total number of photons in the fibre comes from the pump wave when β_s is high. However, the pump wave is the dominant contributor to the total photon number only near the input end when β_s is low.

4.5 Power input-output relationships

An experimental method of testing the predictions of the theories of stimulated Raman scattering in an optical fibre is illustrated in Fig. 3.1. A laser of variable power is launched into a fibre of fixed length. Attempts to vary the fibre length by making successive cuts in a

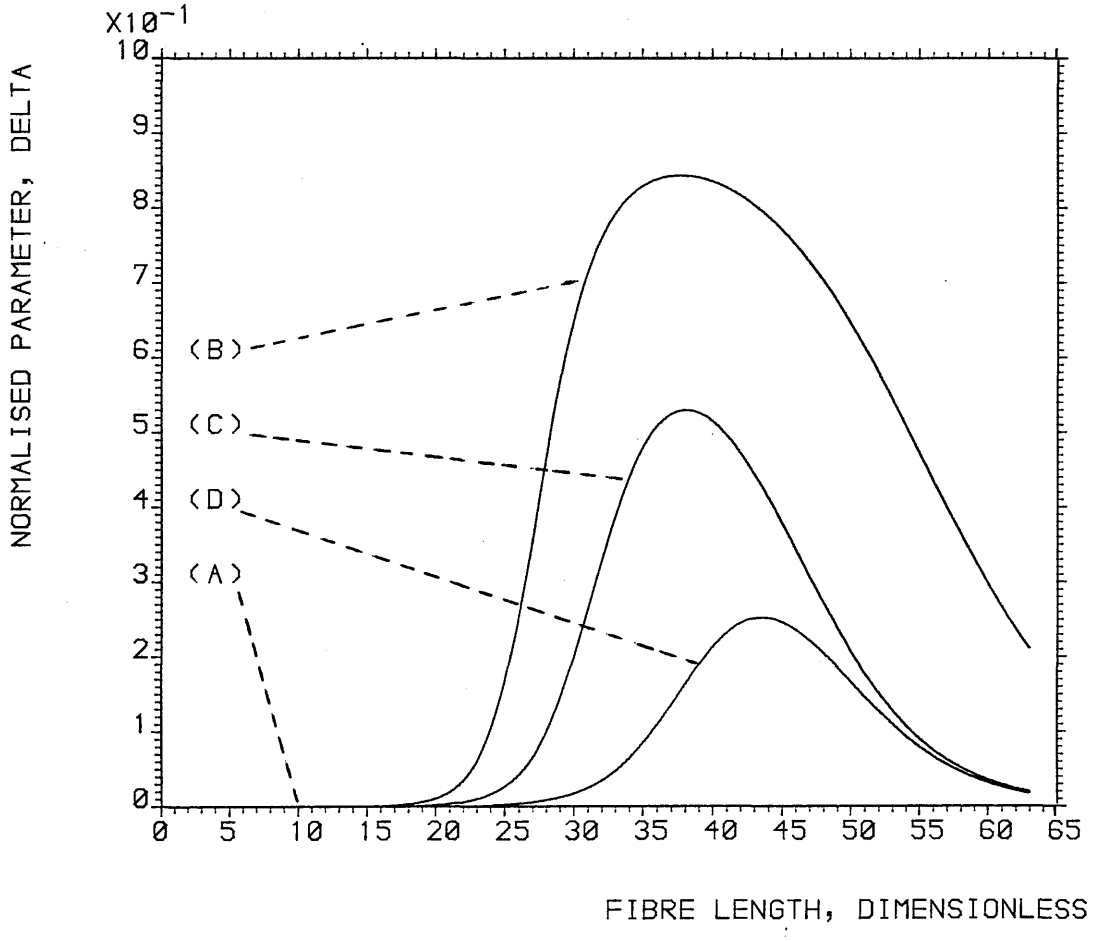

FIG. 4-3 VARIATION OF THE NORMALISED POWER COUPLING PARAMETER (1-EPSILON) WITH RESPECT TO LENGTH.
RATIO OF LOSSES; STOKES TO PUMP:
(A) 1.0, (B) 20.0, (C) 30.0, (D) 40.0
OTHER DATA USED IN COMPUTATIONS ARE IN TABLE 3-1.

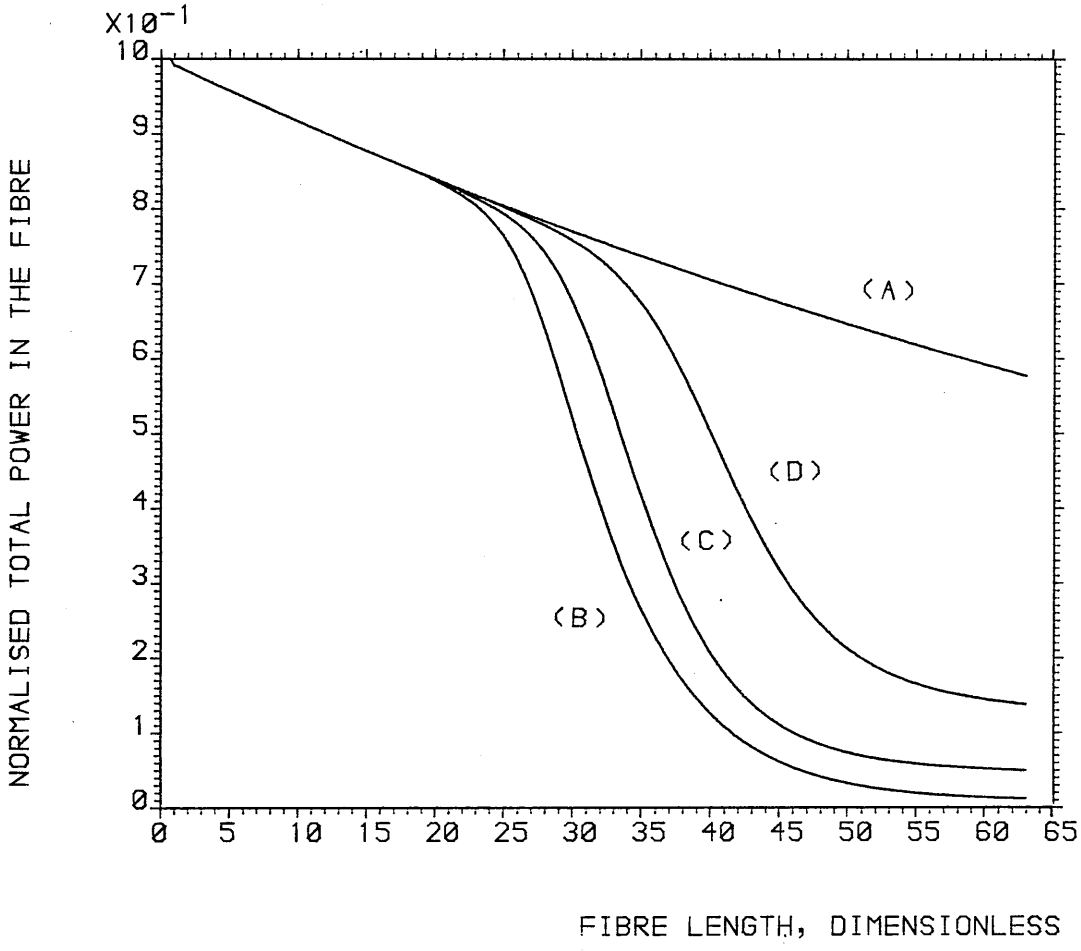

FIG. 4-4 VARIATION OF THE TOTAL POWER IN AN OPTICAL FIBRE WITH RESPECT TO LENGTH, WHEN STIMULATED RAMAN SCATTERING IS OCCURING.
RATIO OF LOSSES; STOKES TO PUMP:
(A) 1.0, (B) 20.0, (C) 30.0, (D) 40.0.
OTHER DATA USED IN COMPUTATIONS ARE IN TABLE 3-1.

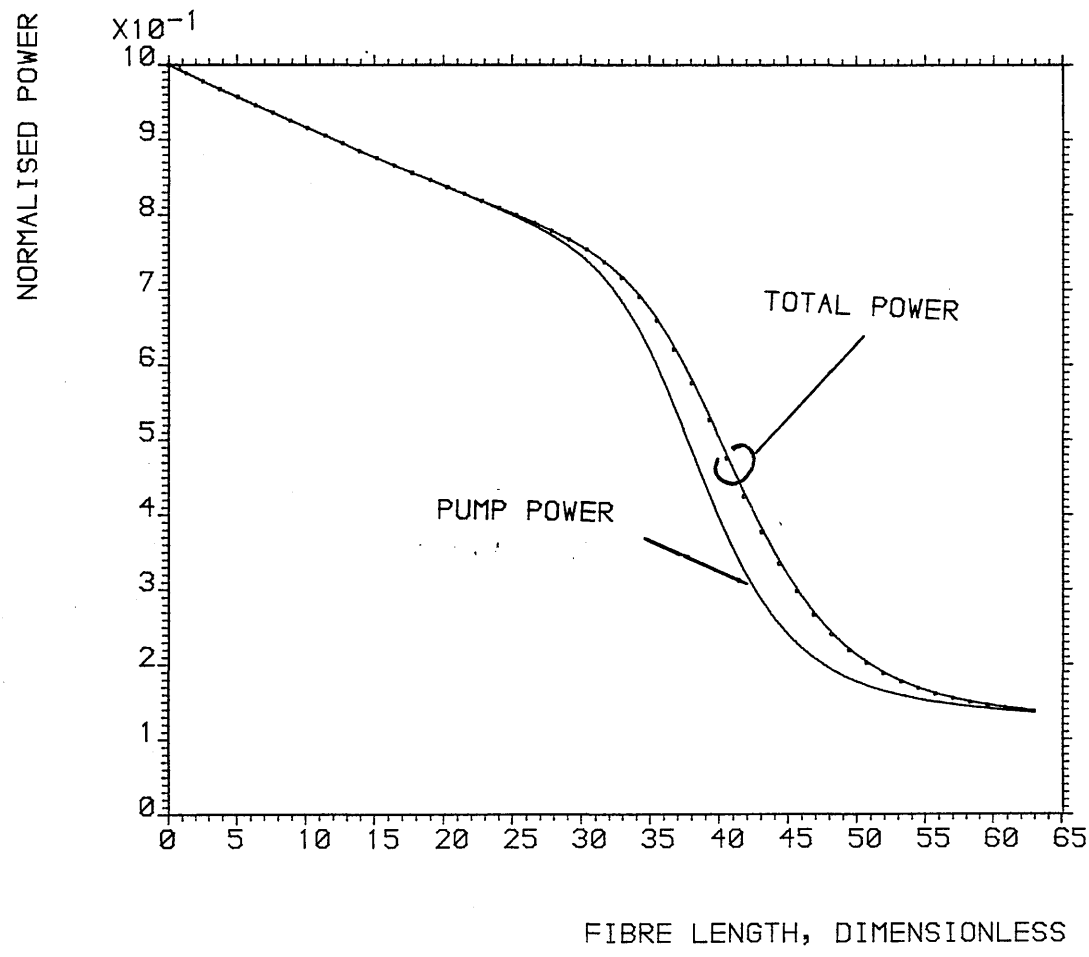

FIG. 4-5 COMPARISON OF THE TOTAL POWER IN THE FIBRE TO THE PUMP POWER IN THE FIBRE FOR THE CASE WHERE THE RATIO OF STOKES TO PUMP LOSS IS 40.0 THE BROKEN LINE IS THE TOTAL POWER CALCULATED BY DIRECT ADDITION OF THE PUMP AND STOKES POWER. OTHER DATA USED IN COMPUTATIONS ARE IN TABLE 1.

long fibre are impractical for three reasons: (a) it is costly, (b) the ends must all be cleaved to an equally high standard, (c) it is possible to disturb the input optics whilst making the cuts, giving rise to inconsistent coupling efficiencies. It is therefore necessary to reconsider the two-wavelength model of S.R.S. in terms of a variable input power rather than a variable length.

The practical implications of the power input-output relationships are most easily understood in terms of physical rather than normalised coordinates. Consider first the equal loss case as expressed by equations (3.23), (3.24) and (3.26). The variable η can be expressed as:

$$\eta(P_o) = [Q(P_o)/\Lambda]\exp(bP_o) \tag{4.18}$$

$Q(P_o)$ is the spontaneous power variation with input power, given by equations (3.42) and (3.35) or (3.36), as appropriate. The analysis that follows is independent of the nature of the gain profile. b is a constant in P_o, given by equation (4.19):

$$b = \frac{\lambda_\ell}{\lambda_s}\frac{g_o}{\alpha A}(1-\exp(-\alpha z)) \tag{4.19}$$

See equations (3.9) to (3.14), inclusive. Thus from (3.23), (3.24) and (3.26):

$$P_\ell(P_o) = \frac{P_o \exp(-\alpha z)}{1+(Q/\Lambda)\exp(bP_o)} \tag{4.20}$$

$$P_s(P_o) = \frac{P_o Q \exp(bP_o).\exp(-\alpha z)}{1+(Q/\Lambda)\exp(bP_o)} \tag{4.21}$$

In most cases $b < 1$.

When P_o is small:

$$P_\ell(P_o) \doteqdot P_o\exp(-\alpha z) \tag{4.22}$$

$$P_s(P_o) \doteqdot 0 \tag{4.23}$$

The physical interpretation of (4.22) and (4.23) is that when the input power is small the fibre behaves as a passive device. When the length is a constant the power, just before being coupled out, is directly proportional to the power just after being coupled in.

When P_o is large:

$$P_\ell(P_o) = 0 \tag{4.24}$$

$$P_s(P_o) = \Lambda P_o \exp(-\alpha z) \tag{4.25}$$

The meaning of (4.25) and (4.26) is that when the input power is high the fibre acts as a linear quantum amplifier. Little power at the pump wavelength emerges from the fibre. All the propagating energy at the output end is in the form of Stokes photons. The factor $\Lambda(=\lambda_\ell/\lambda_s)$ is due to the fact that the packet of energy $h\Delta\nu_R$ is absorbed by the material scattering centres upon each scattering event. See Fig. 2.1 (a) and (c).

Fig. 4.6 is a graph of the physical values of the pump and Stokes output powers, P_ℓ and P_s plotted as functions of the laser input power, P_o from equations (4.1) and (4.2). There are four sets of curves corresponding to α_s/α_ℓ equal to (A) 1.0 (equal loss case); (B) 2.0; (C) 3.0; (D) 4.0. The values of all other constants, including α_ℓ are given in table 3.1.

The curves labelled (A) show the equal loss case. As predicted by equations (4.23) and (4.24), when P_o is small there is little Stokes output and the pump output is proportional to the input. When P_o is large the behaviour follows equations (4.24) and (4.25). There is little remaining pump power and the Stokes output power, P_ℓ is directly proportional to the laser pump input power.

Consider now that the Stokes loss, α_s is unequal to the pump loss α_ℓ. At low input powers one observes the same behaviour as with the equal loss case. However, the more the Stokes loss is increased the more the growth

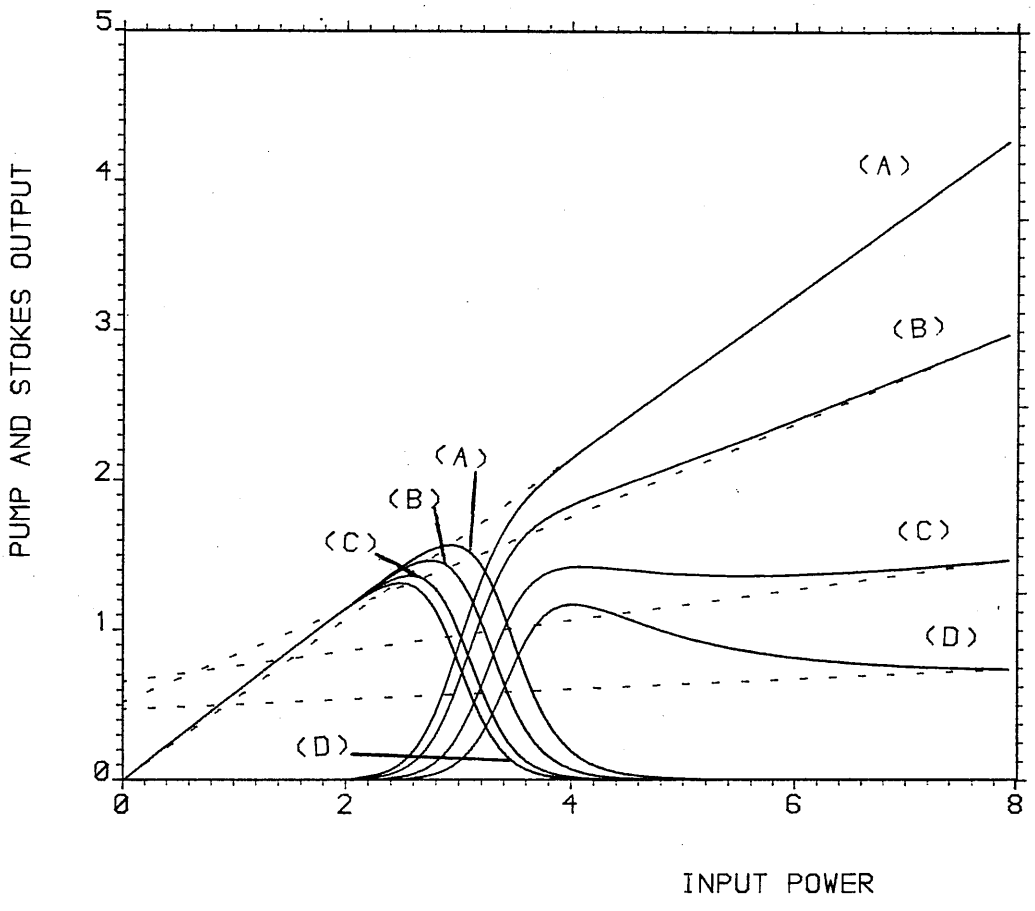

FIG. 4-6 OUTPUT PUMP AND STOKES POWER AS A FUNCTION OF THE INPUT PUMP POWER. THE FIBRE LENGTH IS A CONSTANT.
FIBRE LENGTH = 12000. METRES
RATIO OF LOSSES; STOKES TO PUMP:
(A) 1.0, (B) 2.0, (C) 4.0, (D) 6.0.
OTHER DATA USED IN COMPUTATIONS ARE IN TABLE 3-1.

of the Stokes signal is delayed. The input power necessary to achieve equality of pump and Stokes output is increased as α_s is increased. In all four cases when P_o is large:

$$P_s(P_o) = \Lambda P_o \exp(-\alpha_s z). \tag{4.26}$$

The broken lines in Fig. 4.6 have gradient $\Lambda\exp(-\alpha_s z)$. Due to the fact that no acceptable analytic solution has been found for circumstances where $\alpha_\ell \neq \alpha_s$, it is not possible to give a mathematical expression for the variation of $P_\ell(P_o)$ and $P_s(P_o)$ in the region of maximum Raman conversion. The important implication of Fig. 4.6 is that the performance of single pass Raman lasers are seriously degraded by quite modest increases in the loss at the Stokes wavelength.

Fig. 4.7 is the direct equivalent to Fig. 4.6. It is plotted in dimensionless coordinates, R_ℓ and R_s on the vertical axis as a function of P_o/P_{omax} on the horizontal axis. P_{omax} is 8 watts. At small values of P_o, R_ℓ is a constant, having the value $\exp(-\beta_\ell Z)$, whilst $R_s \doteq 0$. At large values of P_o, $R_\ell \doteq 0$ and R_s is a constant, having the value $\Lambda\exp(-\beta_s Z)$ as P_o becomes infinite. It is interesting to note the similarity between Fig. 4.7 and Fig. 4.1. Terms βZ, which appear in any algebraic step are independent of P_o. See equations (3.23), (3.24) and (3.26). There are no such terms in the analysis for the zero loss limit. See equations (A1.12) and (A1.13). Consequently, in the zero loss limit input power and fibre length can be treated on an identical basis. Thus, the Z-coordinate on the horizontal axis of Fig. A1.1 can be taken to be an input power coordinate where the length is fixed or a length coordinate when the input power is fixed. This symmetry breaks down as soon as one introduces loss into the equations.

Graphs such as Figs. 4-6 and 4-7 illustrate the action of single-pass Raman lasers and aid the comparison of experimental results with theory. See section 8.3.

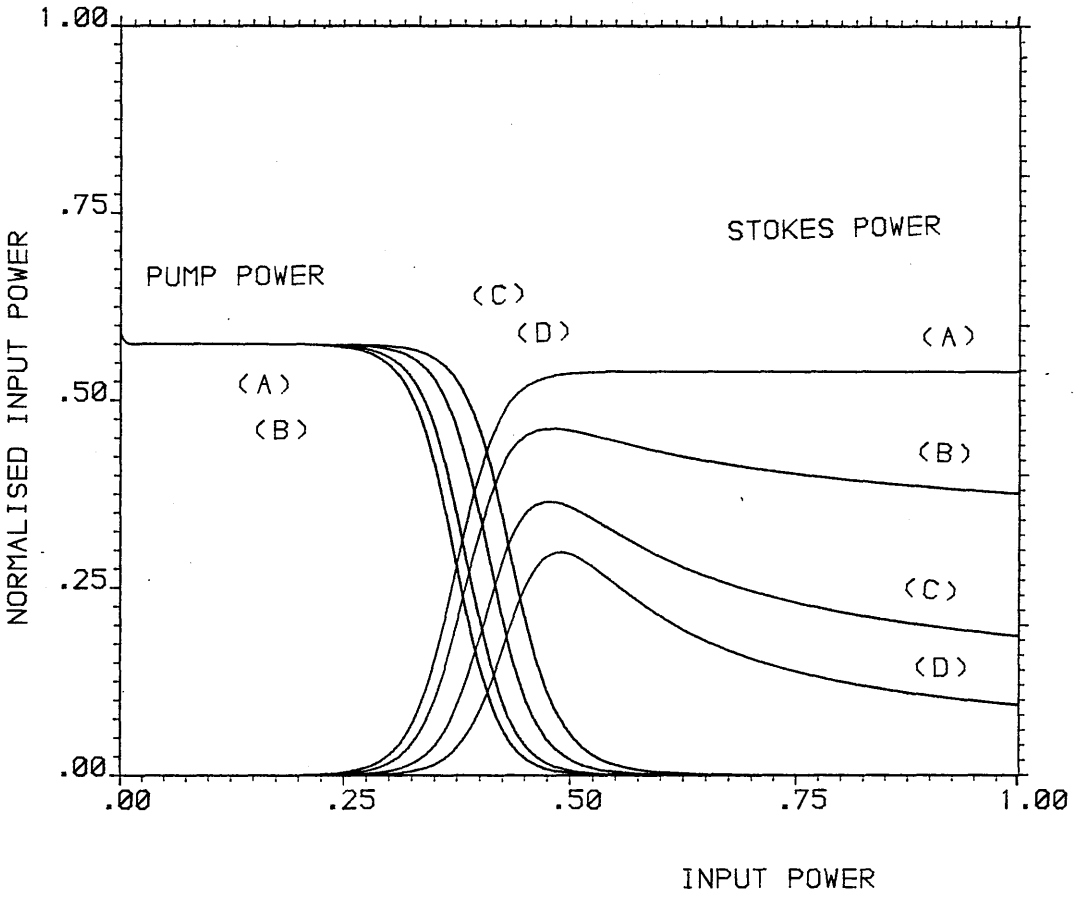

FIG. 4-7 NORMALISED OUTPUT PUMP AND STOKES POWER AS A FUNCTION OF THE INPUT PUMP POWER. THE FIBRE PARAMETERS ARE THE SAME AS THOSE IN FIG. 4-6.

Reference

1. Smith, R.G. "Critical power handling capacity of low loss optical fibres as determined by stimulated Raman and Brillouin scattering. Appl. Optics 11, 2489, (1972).

CHAPTER FIVE

THE MULTI-WAVELENGTH MODEL OF STIMULATED RAMAN SCATTERING IN OPTICAL FIBRES WITH NON-CONSTANT LOSSES

5.1 Introduction

In the previous chapter the evolution of the pump and total Stokes power were described by the two-wavelength model in the form of equations (4.5) and (4.6). However, it is known from experiment[1] that there is a spread of Stokes power over some finite frequency range. It is also known that the optical fibre loss is frequency dependent and hence the loss encountered by one amplified Stokes mode will be different from that encountered by the next. The frequency dependence of Stokes power cannot be computed by equations (4.5) and (4.6) alone. One must use a multi-wavelength model. The problem which then arises is whether one can continue to represent the total Stokes power by a two-wavelength model and if so which value of β_s, the Stokes loss, should be used.

In this chapter a multi-wavelength model is used to examine the evolution of the Stokes spectrum and how it is influenced by the loss distribution. The total Stokes power is given particular attention. It is shown that if one adopts the concept of the effective Stokes loss defined in section 5.4, the results of the computations of the total Stokes power from the multi-wavelength model are equivalent to those of the two-wavelength model of the previous chapter. One can thus assume that provided that $R_s(Z)$ is understood to be the total dimensionless Stokes power, then all of the conclusions of chapter 4 still hold true.

In order to illustrate the effective Stokes loss by analytical and numerical calculations it is necessary to adopt a mathematical model for the optical fibre loss variation over the frequency range covered by the Raman gain profile. For simplicity a linear form was chosen. With more complicated forms there is the danger that analytic solutions cannot be found and hence numerical solutions cannot be cross-checked. The problem with such a simplistic model is that it could only serve as a representation

of a limited class of experimentally determined loss profiles. The extension to cover more complicated loss profiles can therefore be seen as a suggestion for further research as a result of this thesis.

5.2 The equations of the multi-wavelength model

The equations (3.2) and (3.3) account for the power evolution for all q of the Stokes modes and how they combine to deplete the laser pump power. The loss experienced by each of the modes is assumed to be equal to the loss experienced by the laser pump. In a more realistic model the optical fibre loss will vary over the range of wavelengths covered by the gain profile. There is a corresponding "loss profile". Each mode encounters the loss α_{si} (physical coordinates) or β_{si} (dimensionless coordinates). Equations (3.2) and (3.3) are more conveniently expressed in the dimensionless coordinate scheme introduced in section 3.2.

For the i^{th} Stokes mode use:

$$\beta_{si} = \left(\frac{\alpha_{si} A}{g_o P_o}\right) \tag{5.1}$$

$$\Lambda_i = \frac{\lambda_\ell}{\lambda_{si}} \tag{5.2}$$

The i^{th} component of normalised Stokes power is:

$$R_{si} = P_{si}/P_o \tag{5.3}$$

it is also necessary to introduce the segmented lineshape function:

$$\frac{g_i}{g_o} = \mathcal{L}_i \,, \tag{5.4}$$

where $\mathcal{L}_i$ is the weighting of the i^{th} mode according to the part of the Raman lineshape function that it lies within. $0 \leq \mathcal{L}_i \leq 1$. g_o is the

peak Raman gain in the range of frequencies covered by the Raman gain profile (see equation (3.30)).

The multi-wavelength model in dimensionless coordinates is stated as:

$$\frac{dR_\ell}{dZ} + \beta_\ell R_\ell = - R_\ell \sum_{i=1}^{q} \ell_i (R_{si} + Q/q) \qquad (5.5)$$

For each i = 1, 2, ...q:

$$\frac{dR_{si}}{dZ} + \beta_{si} R_{si} = \Lambda_i \ell_i R_\ell (R_{si} + Q/q) \qquad (5.6)$$

The total dimensionless Stokes power is given by:

$$R_s = \sum_{i=1}^{q} R_{si} \qquad (5.7)$$

In practice it is not possible to carry out the computations required to solve (5.5) and (5.6). q is a very large number, typically of the order of 10^8. For the sake of practical computation one segments the frequency range into m, a convenient number, of intervals. There are thus q/m modes per interval. The larger the value of m the more realistic the model, up to the limiting case of m = q. Use equations (5.5) to (5.7), inclusive, with q replaced by m to give m + 1 simultaneous differential equations solved subject to m + 1 initial conditions.

m, the number of segments chosen, is dictated by three factors: computational time, limitations imposed by the software package used and the necessity for accuracy. For the calculations referred to in section 5.3, m = 91. The effect on computational accuracy of varying m is discussed in the succeeding sections. As will be seen, a useful insight into the nature of the multi-wavelength model can be obtained when m is much smaller than q. Further details about computation appear in appendix 4.

In order to perform calculations from equations (5.5) and (5.6) it is necessary to consider the segmented lineshape, the spontaneous Stokes power and the initial pump and Stokes excitation. As a result of the arguments of section (2.5) the lineshape function is taken to be a Lorentzian given by equation (2.10). For computational purposes it was convenient that m should be an odd number. Thus one uses equation (5.8) to compute with a segmented gain profile:

$$\mathcal{L}_i = \frac{(\delta\nu/2)^2}{(\delta\nu/2)^2 + \left[\left(\frac{i - \frac{m+1}{2}}{m}\right)(\nu_{sm}-\nu_\ell)\right]^2} \tag{5.8}$$

Then use equation (5.4) to give Raman gain.

The total initial excitation of the Stokes modes is the dimensionless spontaneously scattered power, Q calculated from (3.40) and (3.42). Assume that the probability of a given Stokes mode being excited is proportional to its position on the gain profile. Thus the initial Stokes excitation follows a Lorentzian distribution, scaled so that the total dimensionless Stokes power at input is Q. Here the thermal population factor, which weights the spontaneous spectrum, is ignored. See section 2.4. The initial conditions for computation are thus:

$$R_\ell = 1 \tag{5.9}$$

$$R_{si} = Q.\frac{(\delta\nu/2\pi).\left(\frac{\nu_{sm}-\nu_\ell}{m}\right)}{\left(\frac{\delta\nu}{2}\right)^2 + \left[\left(\frac{i - \left(\frac{m+1}{2}\right)}{m}\right)(\nu_{sm}-\nu_\ell)\right]^2} \tag{5.10}$$

For i = 1, 2, ...m.

In the work of Au Yeung and Yariv[2] the input distribution of spontaneously scattered Stokes photons was assumed to be a Gaussian with full width at 1/e of the maximum $(\nu_s - \nu_\ell)$ and with a peak magnitude of 10^{10} photons at $\nu = \nu_s$. In practice it is found that the behaviour of

the system of equations (5.5) and (5.6) is not particularly sensitive to the nature of the Stokes input distribution provided that $Q << 1$.

In this section there has been a statement of the equations and initial conditions which constitute the multi-wavelength model, together with a brief description of how they are solved by computer. In the next section there is an examination of the properties of the solutions of the equations.

5.3 A computed example with a linear loss profile

The numerical solution of equations (5.5) and (5.6) given here is an extension of the example used in section 4.3. The data are from table 3.1. The loss increases linearly from $\beta_\ell = 8.73 \times 10^{-3}$ over an 880 cm^{-1} span to the values depicted on lines (B) to (E) in the lower graph of Fig. 5.1. Line (A) of Fig. 5.1 applies to the constant loss case. The upper graph is a digitised representation of the Stokes output spectrum at a fibre length of 6000 metres ($Z = 31.7$). The vertical axis is normalised according to equation (5.3) with $P_o = 8$ watts.

The equal loss case, (A) gives rise to a symmetrical Stokes spectrum, which is centred on ν_s, the frequency of the peak of the Stokes gain profile. As predicted in section 2.3, the exponential nature of the Raman amplification process gives rise to strong discrimination in favour of those modes which lie within the spectral region of highest gain. There is thus considerable line narrowing. The FWHM of the gain profile, $\delta\nu$ is 240 cm^{-1}, whilst that of the resulting Stokes spectrum, $\Delta\nu$ is about 55 cm^{-1}.

The following effects can be observed when the gradient of the loss profile increases as in curves (B) to (E).

1. The most marked effect is a decrease in the overall magnitude of the Stokes spectrum.

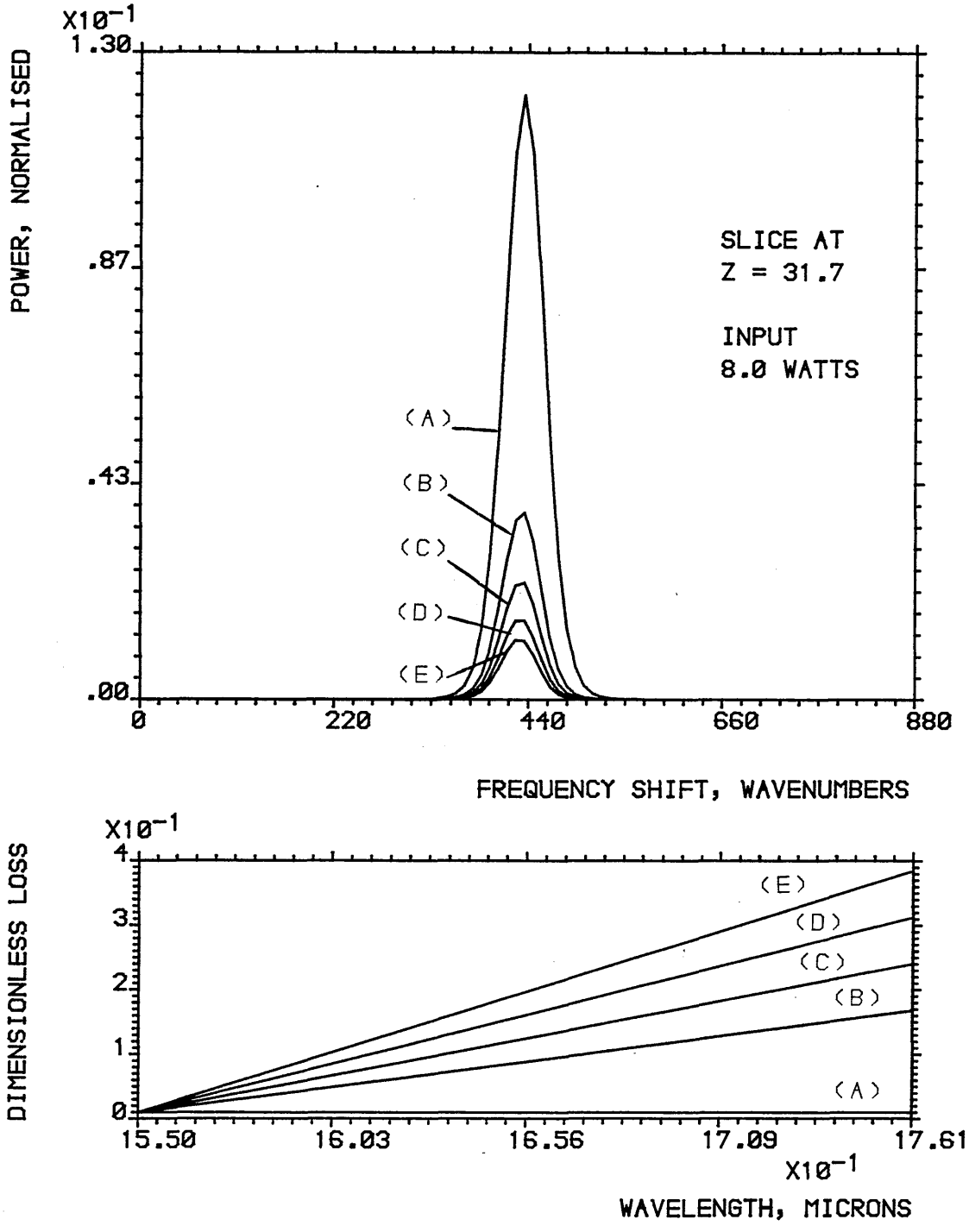

FIG. 5-1: TOP; SIX STOKES SPECTRA COMPUTED USING EQUATIONS (5-5) & (5-6). BOTTOM; THE CORRESPONDING LOSS PROFILES. THE TWO HORIZONTAL SCALES ARE DIRECTLY EQUIVALENT. SEE TABLE 3-1 FOR DATA USED IN COMPUTATION.

2. The spectrum becomes slightly asymmetrical.

3. The full width at half maximum, $\Delta\nu$ remains approximately constant at about 55 cm^{-1}.

It would appear from Fig. 5.1 that the Stokes spectrum is of approximately Gaussian form, which becomes slightly distorted as the gradient of the loss profile is increased. To check that this is the case, the method of the sum of squares of differences, as in section 2.5, was used. Define:

$$\text{diff} = \sum_{i=1}^{91} [R_s(\nu_i) - R_s(\nu_{46}) \exp\{-(\frac{\nu_i - \nu_{46}}{\Delta\nu/2})^2\}]^2 \qquad (5.11)$$

ν_i is the frequency of the i^{th} segment and ν_{46} is the frequency of the central segment at which the maximum of a Gaussian or slightly distorted Gaussian would be expected to occur. $\Delta\nu$ is the adjustable full width at half maximum of the trial Gaussian function. The best fit is that value of $\Delta\nu$ such that diff is minimised.

The first column of entries on table 5.1 are the lowest values of diff for the five Stokes spectra. These are found when $\Delta\nu$ = 55.2 cm^{-1}. In contrast diff was also calculated for the case where the trial function in (5.11) is a Lorentzian. These are the data on the second column of table 5.1.

It can be concluded from table 5.1 that the Stokes spectrum, after experiencing a Lorentzian gain profile, is a close approximation to a Gaussian distribution. The same conclusion was drawn for the purposes of calculating the effective bandwidth in section 3.4. The method for evaluating $\Delta\nu$ was repeated for a length of 2000 metres (Z = 10.6). The best fitting Gaussian required $\Delta\nu$ to be 70.7 cm^{-1}. As concluded in section 3.4, as the Stokes wave grows the Raman spectrum narrows and

Graph number	diff: comparison of data on Fig. 5.1 with a Gaussian	diff: comparison of data on Fig. 5.1 with a Lorentzian
1	0.40×10^{-4}	1.85×10^{-3}
2	1.64×10^{-4}	2.52×10^{-3}
3	3.13×10^{-4}	3.01×10^{-3}
4	4.80×10^{-4}	3.41×10^{-3}
5	6.64×10^{-4}	3.78×10^{-3}

Table 5.1 Calculation of diff, (from equation (5.11)) where the data of Fig. 5.1 are compared with Gaussian and Lorentzian functions of FWHM = 55.2 cm^{-1}.

changes from a Lorentzian to a Gaussian. At lengths greater than that considered there is no continuation of the line narrowing. $\Delta\nu = 55.2\ cm^{-1}$ is the limiting case.

It is interesting to compare $\Delta\nu$ obtained above with the effective bandwidth, B_{eff} calculated from equation (3.36): $B_{eff} = 23.5\ cm^{-1}$. One would expect B_{eff} to be smaller due to the fact that it is computed from a small signal analysis. The amplification experienced by the Stokes modes is overestimated in a small signal result due to the fact that pump depletion is not accounted for. Thus the extent to which line-narrowing occurs is exagerated and B_{eff}, as calculated in section 3.4 is a slight under estimate. Fortunately, it is found both here and elsewhere[3] that the behaviour of the pump and Stokes waves are not particularly sensitive to small variations in the value of the spontaneous power, Q, which is calculated from B_{eff}. Therefore, although there is an inaccuracy in the value for Q in (5.5), (5.6) and (5.10), the effect on the final results is negligible.

Fig. 5.2 is an isometric representation of how the entire Stokes spectrum evolves during travel along the optical fibre in the equal loss case. The pump power does not appear. It can be seen that Fig. 5.1(A) is a cross section of Fig. 5.2 at Z = 31.7. The information which can be extracted from such projections is qualitative rather than quantitative.

The variation of pump and total Stokes power with respect to length are plotted on Fig. 5.3 by the use of (5.5), (5.6) and (5.7). Loss profiles (A), (C) and (E) were used. The striking feature about Fig. 5.3 is the similarity in form with Fig. 4.1, in which only two coupled equations were solved. In the rest of the chapter is is shown that if one uses a single loss value, referred to here as the effective Stokes loss, then the m + 1 equations used to calculate the pump and total Stokes

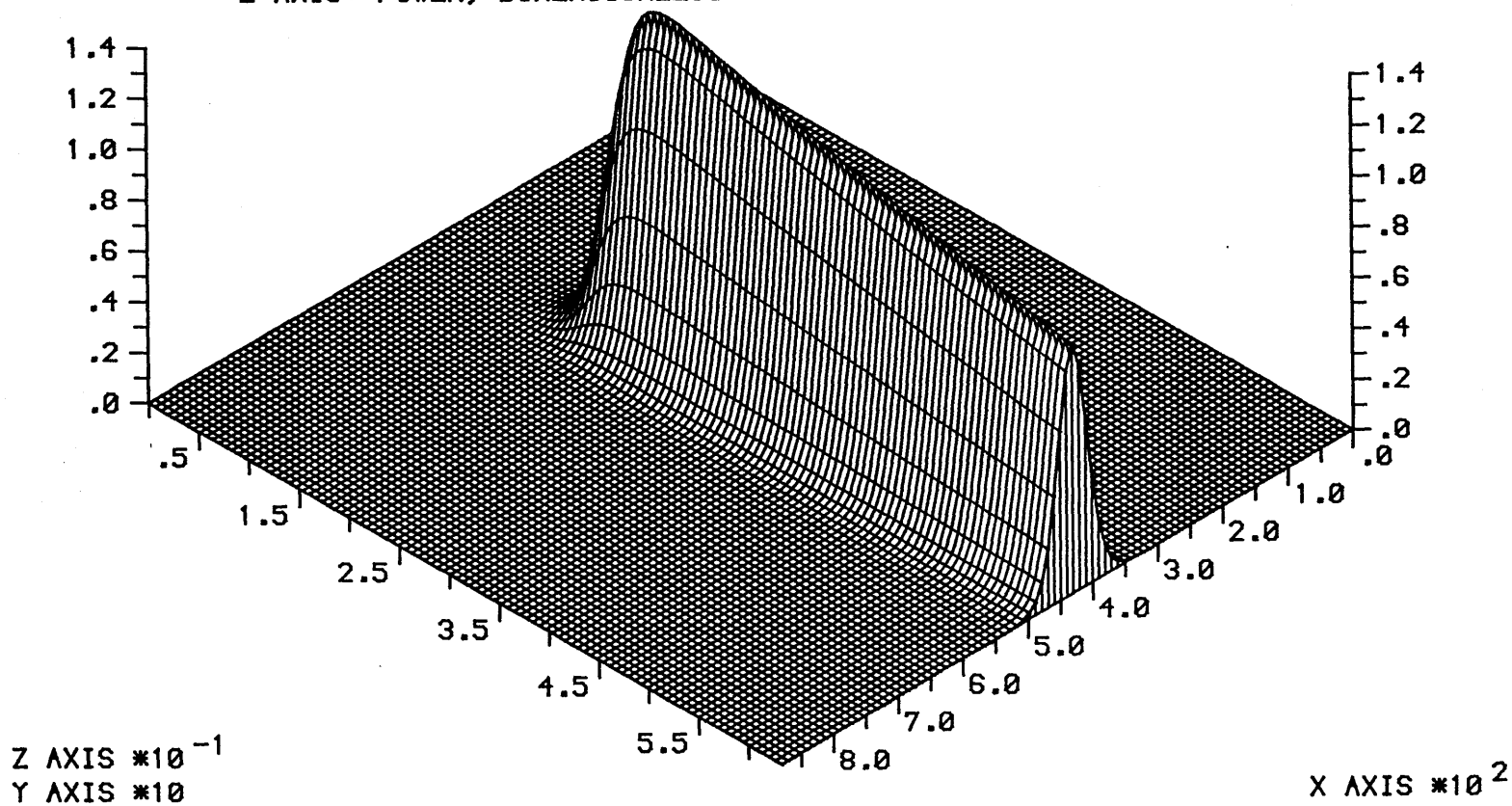

FIG. 5-2 ISOMETRIC PROJECTION REPRESENTING THE EVOLUTION OF THE POWER SPECTRUM ALONG THE LENGTH OF A MONOMODE STEP-INDEX OPTICAL FIBRE. INPUT POWER =8.0 WATTS. THE LOSS SPECTRUM IS (A) OF FIG 5-1, BOTTOM. OTHER DATA USED IN COMPUTATIONS ARE IN TABLE 3-1.

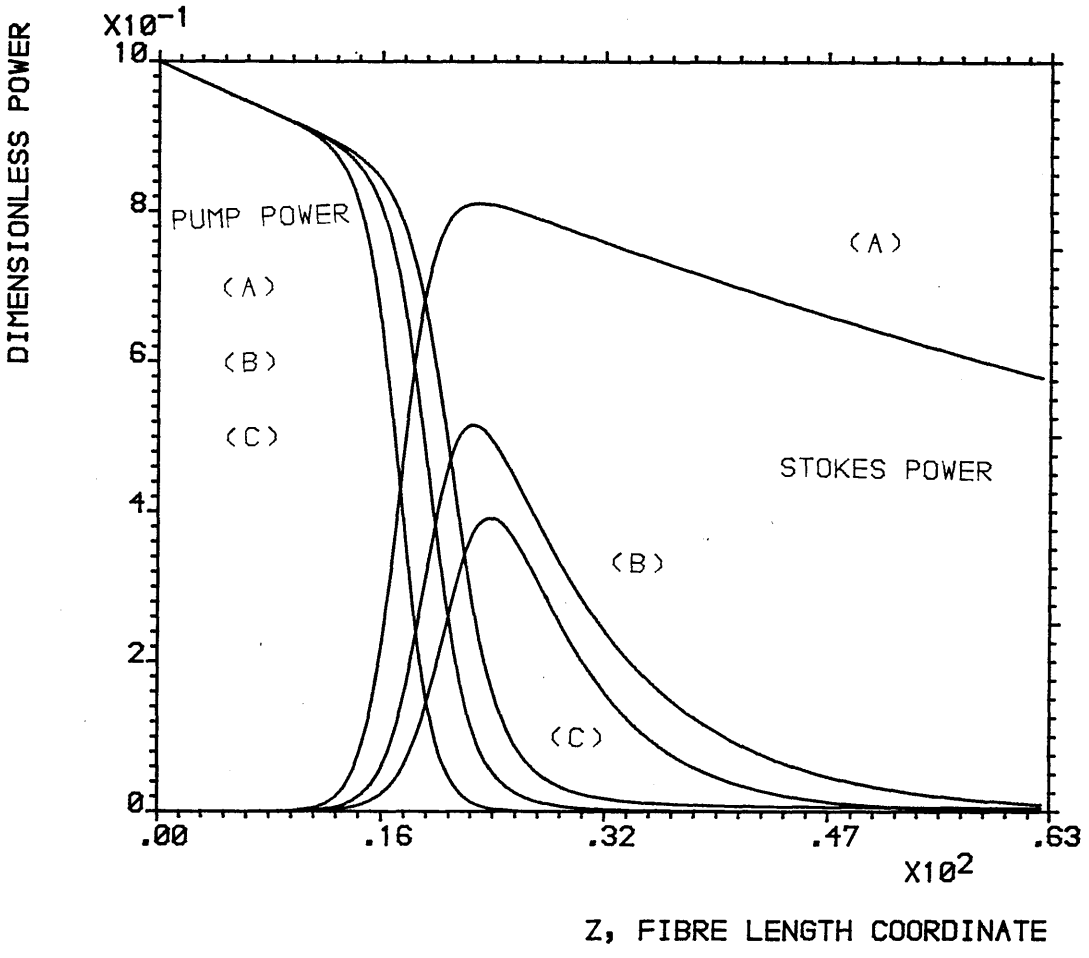

FIG. 5-3 DEPLETION OF THE PUMP POWER WITH THE CORRESPONDING GROWTH OF THE STOKES POWER. THE LATTER IS COMPUTED BY SPLITTING THE STOKES SPECTRUM INTO 91 ELEMENTS AND SUMMING THE POWER CONTRIBUTIONS FROM EACH.
INPUT POWER = 8.0 WATTS.
LOSS AT PUMP WAVELENGTH, BETA-L = .0087
THE LOSS SPECTRA FOR THE STOKES WAVELENGTHS ARE LINES (A), (C) AND (E) OF THE LOWER GRAPH OF FIG.5-1.
OTHER DATA USED IN COMPUTATIONS ARE IN TABLE 3-1.

power evolution can be replaced with only two equations. One would therefore expect the similarity of form with Fig. 4.1.

5.4 The effective Stokes loss

The problem arising from section 5.3 is: how does one replace all of the individual losses, β_{si} by a single loss β_s so that the two wavelength model is equivalent to the multi-wavelength model? Introduce the effective Stokes loss:

$$\beta_s = \frac{\sum_{i=1}^{q} \beta_{si} R_{si}}{\sum_{i=1}^{q} R_{si}} \qquad (5.12)$$

Then combine (5.12) with (5.6) and (5.7) to give equation (5.13) to represent the total Stokes power:

$$\frac{d}{dZ} \sum_{i=1}^{q} R_{si} + \beta_s \sum_{i=1}^{q} R_{si} = R_\ell \sum_{i=1}^{q} \Lambda_i \ell_i (R_{si} + Q/q) \qquad (5.13)$$

Equations (5.12) and (5.13) are directly equivalent to equations (4.5) and (4.6). Therefore by using β_s in conjunction with the effective bandwidth, B_{eff}, as introduced in section 3.4, the multi-wavelength model can be reduced to the two-wavelength model. It is important to note that R_s from the two-wavelength model is the total Stokes power. The two-wavelength model gives no information about the distribution of power between the Stokes modes.

An important property about the effective Stokes loss, β_s can be deduced. If $\beta_s(\min)$ and $\beta_s(\max)$ are the minimum and maximum losses covered by the Stokes profile, respectively then:

$$\beta_s(\min) \leq \beta_s \leq \beta_s(\max) \qquad (5.14)$$

(5.14) can easily be proved as follows:

From (5.12) it can be seen that:

$$[\beta_s(\max) \sum_{i=1}^{q} \frac{\beta_{si} R_{si}}{\beta_s(\max)}] / \sum_{i=1}^{q} R_{si} \leq \beta_s(\max) \qquad (5.15)$$

Because

$$\sum_{i=1}^{q} \frac{\beta_{si} R_{si}}{\beta_s(\max)} \leq \sum_{i=1}^{q} R_{si},$$

due to the fact that each β_{si} is individually less than or equal to $\beta_s(\max)$. In a similar way it can be seen that:

$$[\beta_s(\min) \sum_{i=1}^{q} \frac{\beta_{si} R_{si}}{\beta_s(\max)}] / \sum_{i=1}^{q} R_{si} \geq \beta_s(\min) \qquad (5.16)$$

Each β_{si} is individually $\geq \beta_s(\min)$. Thus from equations (5.15) and (5.16) it can be seen that (5.14) holds.

The consequence of equation (5.14) is that the effective Stokes loss is some loss value which is intermediate between the minimum and maximum values of the Stokes loss profile. The value of β_s relative to $\beta_s(\min)$ and $\beta_s(\max)$ is dependent upon the mathematical form of the Stokes loss profile. As with the Raman gain profile, it is necessary to postulate some simple mathematical function to represent the loss profile.

In order to calculate β_s analytically it is necessary to replace the summations over the q Stokes modes in (5.8) by integrations over the range of frequencies in the Raman gain profile. The argument in favour of doing so is the same as that appealed to in using integration in equation (3.34). The Stokes modes are so closely spaced that the loss profile is a slowly varying function in comparison. So use:

$$\beta_s = \frac{\int_{\nu_\ell}^{\nu_{smax}} R_s(\nu) . \beta(\nu) d\nu}{\int_{\nu_\ell}^{\nu_{smax}} R_s(\nu) d\nu} \qquad (5.17)$$

$\beta(\nu)$ is the frequency dependent loss profile.

In order to evaluate (5.17) it is necessary to assume that the frequency variation of the normalised Stokes power is constant with length. In practice β_s is slowly varying with length. See section 5.5.

It is convenient to introduce a normalised effective loss:

$$\beta_{sN} = \frac{\beta_s - \beta_s(\min)}{\beta_s(\max) - \beta_s(\min)} \tag{5.18}$$

β_{sN} is useful for the purposes of section 5.5. β_{sN} lies between zero and unity.

5.5 Analytical computation of the effective Stokes loss arising from a linear loss profile

The effective Stokes loss, β_s, is calculated by the use of equation (5.17). Due to the appearance of $R_s(\nu)$ in the integrals in both the numerator and the denominator one need only consider the Frequency variation of R_s. Multiplicative constants do not play any roll in the integrations and so will cancel out. Following Fig. 5.1, the frequency dependence is given by a Gaussian:

$$R_s(\nu) \propto \exp\{-(\frac{\nu - \nu_s}{\Delta\nu/2})^2\}. \tag{5.19}$$

The full width at half maximum of the Gaussian, $\Delta\nu$, is undetermined. It is assumed that in (5.19) only the constant of proportionality is Z-dependent.

It is appropriate at this stage to give a word of caution about the use of (5.19). One cannot assume that (5.19) is applicable in the calculation of β_s for all effective Stokes loss profiles. In general one will have to derive or approximate a function for $R_s(\nu)$

for each type of loss profile. Consequently one would expect a marked decrease in the ease with which one could calculate β_s when the functional form of the loss profile is chosen to be more complicated.

For the purposes of this section $\beta_N(\nu)$ is a straight line. At $\nu = \nu_\ell, \beta_N(\nu) = \beta_\ell$. ν_{sm} is the maximum Stokes frequency considered at which $\beta_N(\nu_{sm}) = \beta_{sm}$. The gradient of the profile is $1/(\nu_{sm} - \nu_\ell)$. Thus the equation of the straight line which represents the normalised loss profile in dimensionless units is:

$$\beta_N(\nu) = \left(\frac{\nu - \nu_\ell}{\nu_{sm} - \nu_\ell}\right) - \left(\frac{\beta_\ell}{\beta_{sm} - \beta_\ell}\right) \tag{5.20}$$

The normalised effective Stokes loss is calculated by the use of equations (5.17) to (5.20):

$$\beta_{sN} = \frac{\int_{\nu_\ell}^{\nu_{sm}} \left(\frac{\nu - \nu_\ell}{\nu_{sm} - \nu_\ell}\right) . \exp\left\{ -\left(\frac{\nu - \nu_s}{\Delta\nu/2}\right)^2 \right\} d\nu}{\int_{\nu_\ell}^{\nu_{sm}} \exp\left\{ -\left(\frac{\nu - \nu_s}{\Delta\nu/2}\right)^2 \right\} d\nu} - \frac{\beta_\ell}{\beta_{sm} - \beta_\ell} \tag{5.21}$$

Substitute: $\nu' = \dfrac{\nu - \nu_s}{\Delta\nu/2}$

The denominator of the term involving integrations becomes:

$$\frac{\Delta\nu\sqrt{\pi}}{4}\left[\operatorname{erf}\left(\frac{\nu_{sm} - \nu_s}{\Delta\nu/2}\right) + \operatorname{erf}\left(\frac{\nu_s - \nu_\ell}{\Delta\nu/2}\right)\right]$$

erf is the error function. If the argument of erf is greater than or approximately equal to 3 erf = 1 to better than 2 decimal places. In the above expression this is generally so, giving:

$$\frac{\Delta\nu\sqrt{\pi}}{2}$$

The term in the numerator where the Gaussian is multiplied by $-\nu_\ell/(\nu_{sm} - \nu_\ell)$ becomes:

$$\left(\frac{-\nu_\ell}{\nu_{sm} - \nu_\ell}\right) \frac{\Delta\nu\sqrt{\pi}}{2}$$

by the same reasoning.

The remaining term in the numerator also requires the substitution:

$$\nu' = \left(\frac{\nu - \nu_s}{\nu/2}\right)$$

to give:

$$\frac{\Delta\nu}{2}\sqrt{\pi}\left(\frac{\nu_s}{\nu_{sm} - \nu_\ell}\right) - \frac{\Delta\nu}{2}\int_{(\nu_\ell - \nu_s)/(\Delta\nu/2)}^{(\nu_{sm} - \nu_s)/(\Delta\nu/2)} \nu' \exp(-\nu'^2)\, d\nu'$$

The integral can be evaluated by making the further substitution $\nu'' = \nu'^2$ to give the expression for the normalised effective Stokes loss:

$$\beta_{sN} = \left(\frac{\nu_s - \nu_\ell}{\nu_{sm} - \nu_\ell}\right) - \left(\frac{\beta_\ell}{\beta_{sm} - \beta_\ell}\right) - \frac{1}{\sqrt{\pi}}\left\{\exp\left[-\left(\frac{\nu_{sm} - \nu_s}{\Delta\nu/2}\right)^2\right] + \exp\left[-\left(\frac{\nu_\ell - \nu_s}{\Delta\nu/2}\right)^2\right]\right\} \qquad (5.22)$$

Note that all of the terms in equation (5.22) are individually less than unity, but greater than zero. The exponential terms are generally small and can be ignored. In silica with a Lorentzian model for the gain profile $\nu_s - \nu_\ell = 440\ \text{cm}^{-1}$ and $\nu_{sm} - \nu_\ell = 900\ \text{cm}^{-1}$. However, in section 2.5 it was found to be convenient to terminate the Lorentzian at $880\ \text{cm}^{-1}$, giving $(\nu_{sm} - \nu_\ell) = 2(\nu_s - \nu_\ell)$. In that case:

$$\beta_{sN} = \frac{1}{2} - \left(\frac{\beta_\ell}{\beta_{sm} - \beta_\ell}\right) \qquad (5.23)$$

β_{sN} is thus always less than $\frac{1}{2}$. When the maximum Stokes loss, β_{sm} is very much larger than the pump loss, β_ℓ $\beta_{sN} \doteq \frac{1}{2}$. In the general case where $(\nu_{sm} - \nu_\ell) \neq 2(\nu_s - \nu_\ell)$:

$$\beta_{sN} \doteqdot \left(\frac{\nu_s - \nu_\ell}{\nu_{sm} - \nu_\ell}\right), \text{ when } \beta_{sm} \text{ is large.}$$

In deriving (5.22) the FWHM of the Gaussian spectrum, $\Delta\nu/2$ was not specified. Provided that the exponential terms in (5.22) can be ignored, β_{sN} is independent of $\Delta\nu/2$. However, it should not be assumed that β_{sN} can be taken to be independent of the Stokes spectral bandwidth for all loss profiles. The above result is derived only in the linear case.

5.6 Numerical computation of the effective Stokes Loss arising from a linear loss profile

The effective Stokes loss, β_s is calculated numerically by application of the defining equation, (5.12), where the summation is over the m computational segments, rather than the q Stokes modes. In Fig. 5.4(A) and (B) the normalised effective Stokes loss, β_{sN} is plotted as a function of fibre length for each of the three loss profiles of Fig. 5.4(C). In Fig. 5.4(A) and (B) m = (A) 21 and (B) 91. The first point to be made is that the improvement in accuracy by increasing m is noticeable, but slight, which suggests that accurate predictions can be made when $m << q$.

Consider, now Fig. 5.4(B): in all three curves β_{sN} is slowly varying in Z, with the exception of curve (2) in the region of $Z \doteqdot 3$. Curves (2) and (3) agree well with the theoretical prediction of section 5.5 that β_{sN} has a value slightly less than $\frac{1}{2}$ when the maximum Stokes loss is considerably larger than the pump loss. Curve (1) corresponds to the case where the Stokes loss at all wavelengths is only slightly greater than the pump loss and in accordance with equation (5.19) has a value of β_{sN} significantly less than $\frac{1}{2}$.

In the top graph of Fig. 5.5 β_{sN} is calculated at Z = (1) 6.3

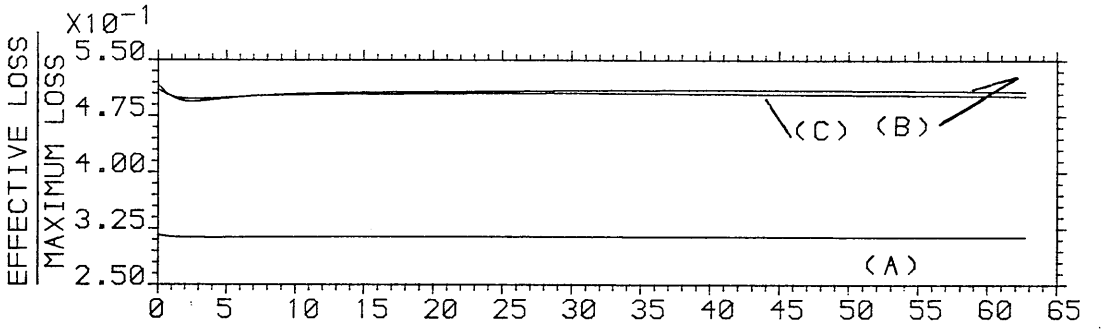

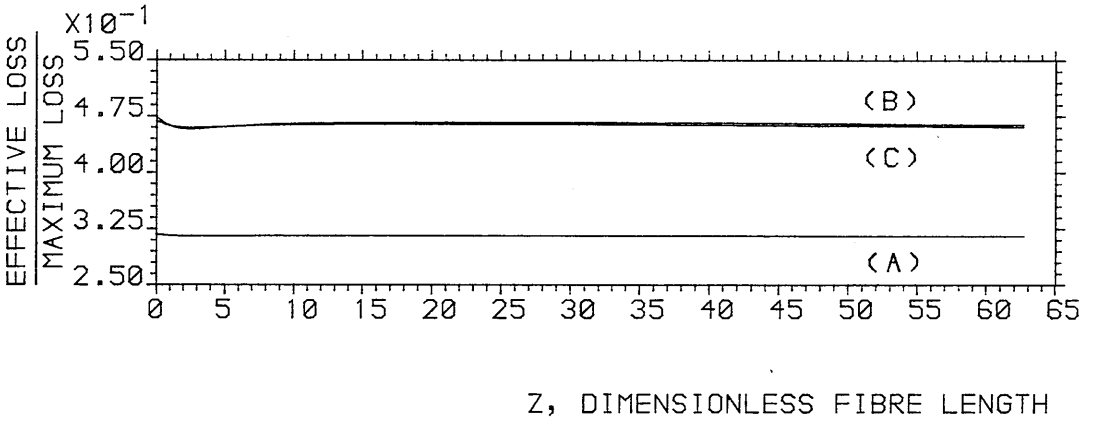

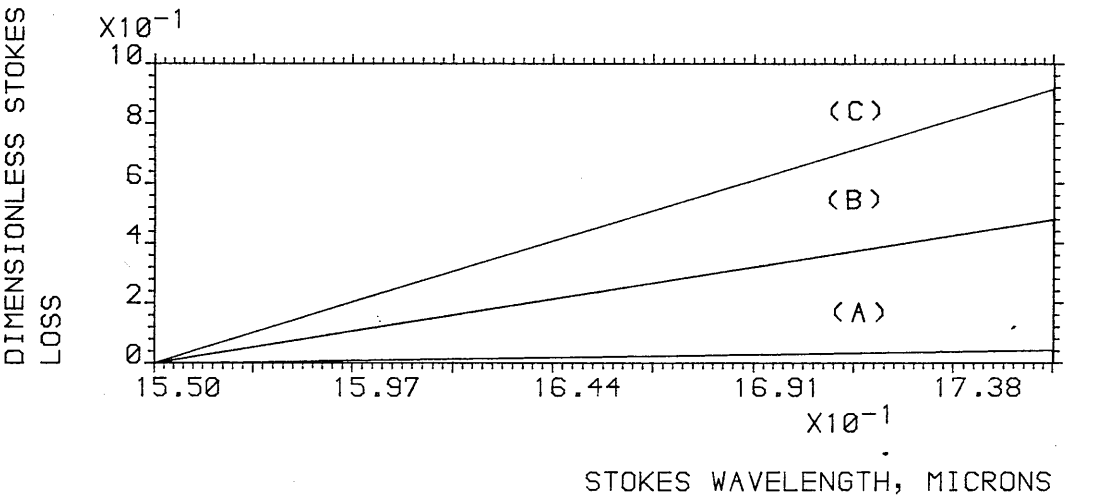

FIG.5-4 (A)-(C): (A) & (B) ARE THE VARIATION OF THE NORMALISED EFFECTIVE LOSS WITH RESPECT TO WAVELENGTH, WHERE (A) 21 AND (B) 91 SIMULTANEOUS EQUATIONS ARE USED TO REPRESENT THE STOKES POWER EVOLUTION.
(C) IS THE LOSS PROFILE.
SEE FIGS. 3-2 & 3-3 AND TABLE 3-1.

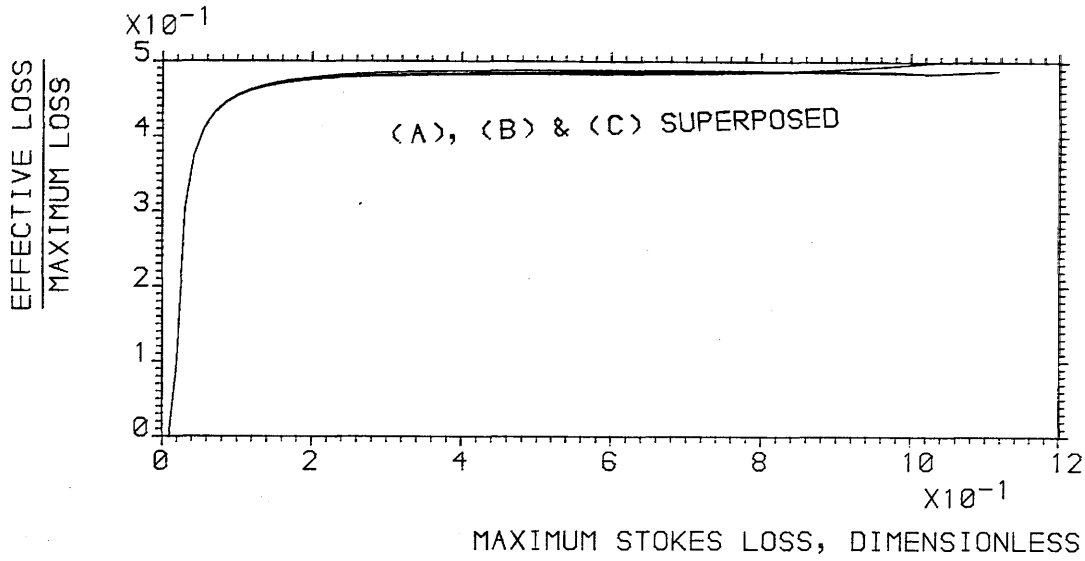

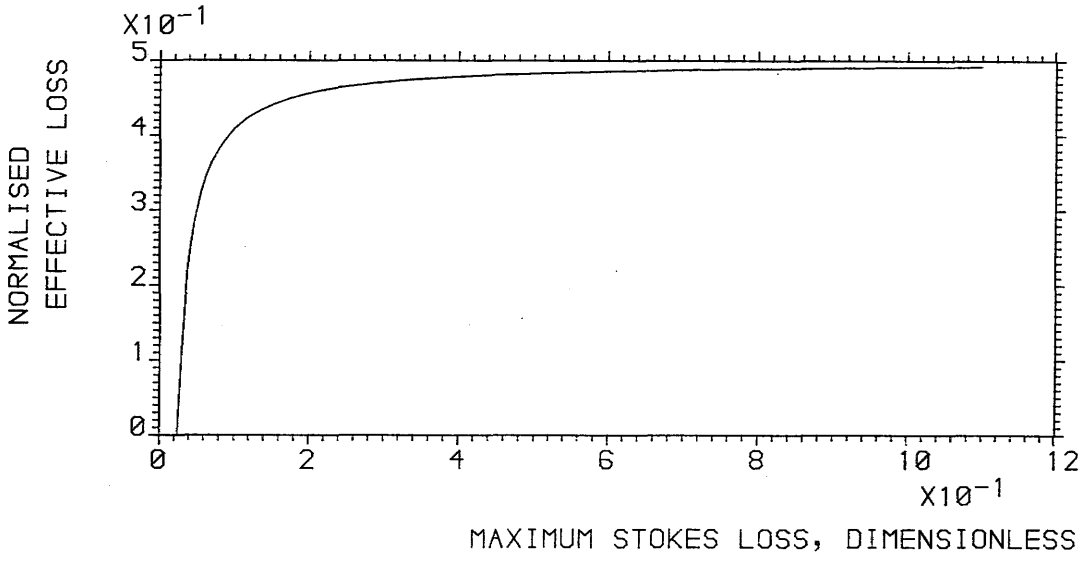

FIG. 5-5 (A) , (B) & (C) VARIATION OF THE NORMALISED EFFECTIVE STOKES LOSS WITH THE MAXIMUM STOKES LOSS. THE PUMP LOSS IS HELD CONSTANT AT 0.2 dB/km. AND THE LOSS PROFILE IS LINEAR. FIBRE LENGTHS: Z= (A) 6.3, (B) 31.6, (C) 63.3.

(2) 31.6 and (3) 63.3. The value of β_{sm}, the maxmimum Stokes loss, and hence the gradient of the loss profile is varied. It can be seen that the shape of all three curves are so similar that the lines virtually overlap. When $\beta_{sm} \gtrsim 0.3$, β_{sN} assumes an almost constant value of about 0.48. However below $\beta_{sm} = 0.3$, β_{sN} is strongly dependent upon β_{sm}. β_{sN} is zero when the loss profile is a constant. β_{sN} is plotted as a function of β_{sm} on the lower graph from equation (5.23). β_{ℓ} is held constant. It can be seen that there is good agreement between the top and bottom graphs of Fig. 5.5.

The influence of m, the number of differential equations employed to model the Stokes spectrum, is illustrated in Fig. 5.6. The two graphs apply where Z = 6 and Z = 30, respectively. The three curves on each graph are for loss profiles (1), (2) and (3) of Fig. 5.4(C). As m is increased β_{sN} asymptotically approaches the appropriate values on the corresponding curves of Fig. 5.5. Consequently, even with a small number of equations one would expect to find a value of β_{sN} not far from the limiting value as m = q.

Fig. 5.7 is an illustration of the equivalence of the two methods of calculating the power evolution using: (a) the multi-wavelength method with m = 91 in conjunction with the loss profiles of Fig. 5.4(C); (b) the two wavelength method in conjunction with the effective Stokes loss. The values of β_{sN} used are the same as those in Fig. 5.4(B) at Z = 30. It can be seen that there is good agreement between the two methods of computation.

In deriving an expression for β_{sN} in section 5.5, three assumptions were made: 1. the loss and gain profiles are slowly varying on the scale of quantisation of the individual Stokes modes; 2. the functional form of $R_s(\nu)$ is independent of length for a given loss profile; 3. $R_s(\nu)$

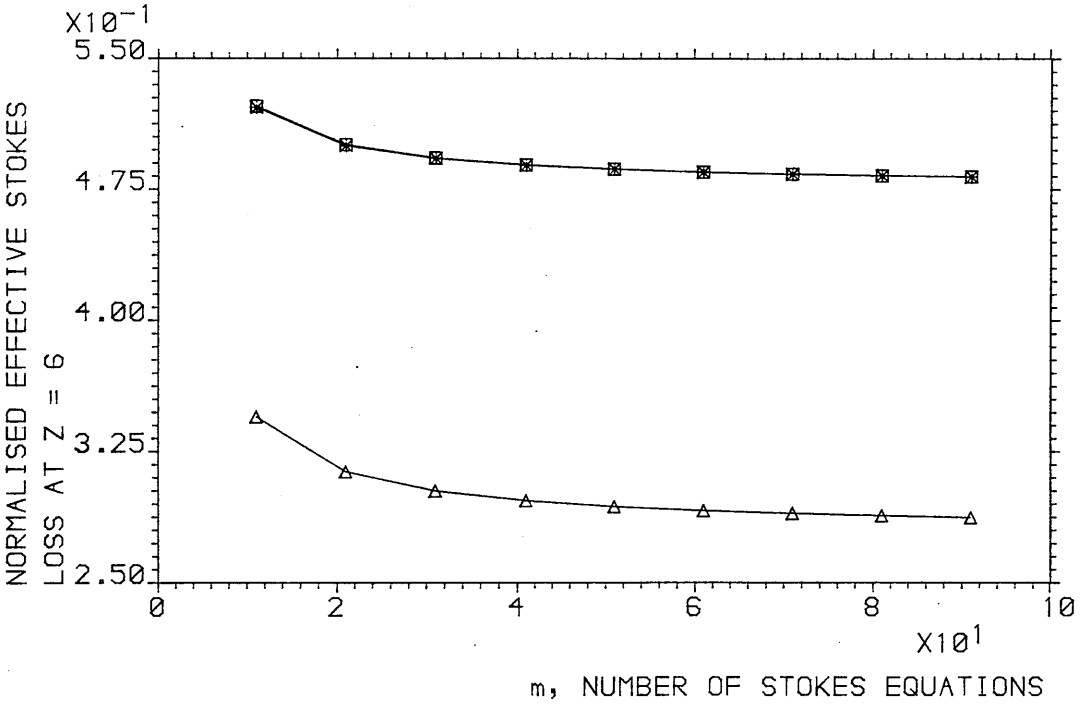

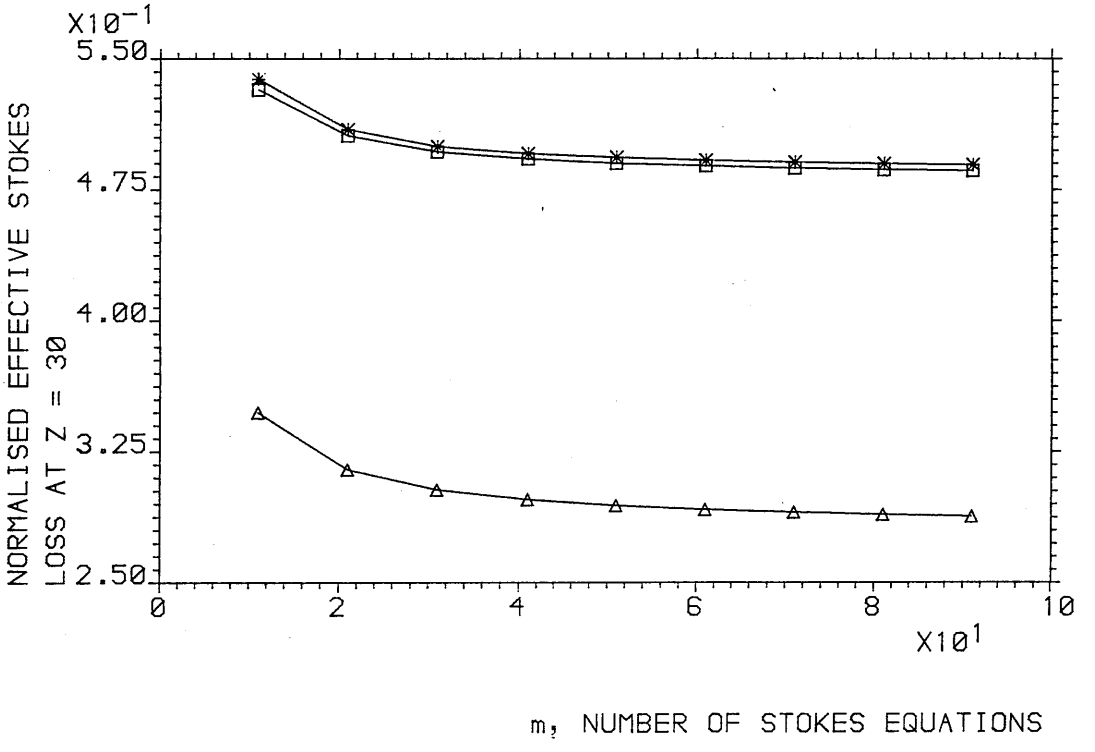

FIG. 5-6 VARIATION OF THE NORMALISED EFFECTIVE STOKES LOSS WITH THE NUMBER OF SIMULTANEOUS EQUATIONS REPRESENTING THE STOKES POWER.
VALUES OF THE EFFECTIVE STOKES LOSS WITH m=91:
Z=6 : (A) .2969, (B) .4890, (C) .4888
Z=30: (A) .2976, (B) .4925, (C) .4957
Δ =(A), $\square$ =(B), $*$ =(C).

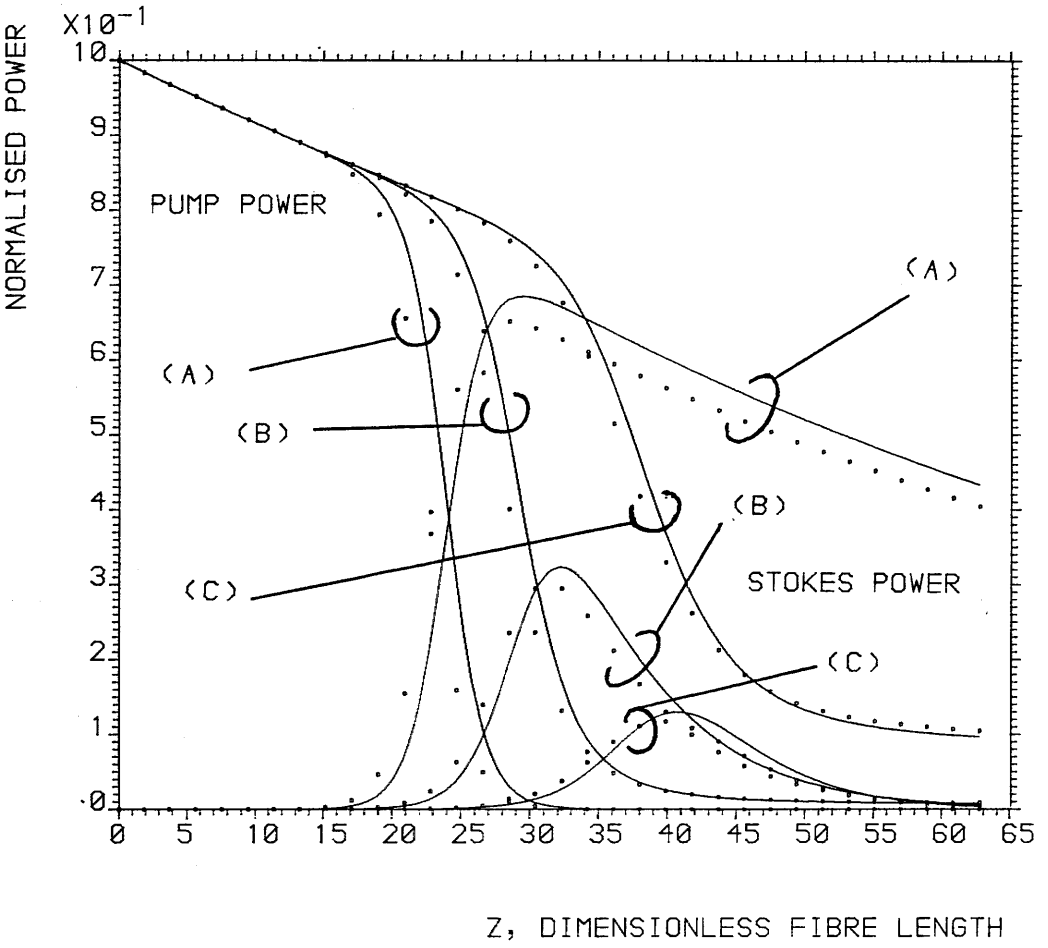

FIG. 5-7 COMPARISON OF TWO METHODS OF SOLUTIONS. SOLID LINES: SOLUTION BY SPLITTING THE STOKES SPECTRUM INTO 91 ELEMENTS AND SUMMING THE POWER CONTRIBUTIONS FROM EACH. BROKEN LINES: BY THE USE OF THE EFFECTIVE STOKES LOSS AND ONLY ONE EQUATION TO REPRESENT THE STOKES POWER EVOLUTION. THE LOSS SPECTRA FOR THE STOKES WAVELENGTHS ARE LINES (A), (B) & (C) OF FIG 5-4 (C). NORMALISED EFFECTIVE STOKES LOSSES: (A) .2873 , (B) .4823, (C) .4823 OTHER DATA USED IN COMPUTATIONS ARE IN TABLE 3-1.

can be modelled by a Gaussian regardless of the gradient of the loss profile. The limitations of the first assumption are implicit in Fig. 5.7. The second and third assumptions are validated by numerical computations with two minor exceptions. The failure of assumption two would appear to account for the slight deviation from flatness at about Z = 3 in Fig. 5.4(A) and (B) as the functional form of $R_s(\nu)$ evolves towards a Gaussian. The small scale differences between the top and bottom graphs of Fig. 5.5 are due to the fact that as β_{sm} increases the Gaussian Stokes spectrum becomes progressively distorted. By careful inspection this distortion can be seen in Fig. 5.5.

References

1. Lin, C., Cohen, L.G., Stolen, R.H., Tasker, G.W., French, W.G. "Near infrared sources in the 1-1.3μm region by efficient stimulated Raman emission in glass fibres," Optics Commun. 20, 427 (1977).

2. Au Yeung, J. and Yariv, A. "Spontaneous and stimulated Raman Scattering in long low loss fibres." I.E.E.E. J. Quantum Electron. QE14, 347 (1978).

3. von der Linde, D., Maier, M., Kaiser, W. "Quantitative investigations of the stimulated Raman effect using subnanosecond light pulses." Phys. Rev. 178, 11, (1969).

CHAPTER SIX

THE EFFECTIVE CORE AREA

6.1 Introduction

In the calculations of the evolution of pump and Stokes power (chapters 3 to 5) the area of interaction between the pump and Stokes beams was taken to be some value called the effective core area, which is approximately equal to the actual core area. The effective core area and its dependence on the fibre waveguiding properties is determined in this chapter.

A summary of monomode fibre waveguiding properties appears in section 6.2. For further details, there are numerous reviews in the literature[1,2,3,4,5]. The multi-wavelength model is used in section 6.3 to determine a general expression for the effective core area. It is then shown that an analytic evaluation can be made if the fibre transverse energy distributions are approximated by Gaussians.

In section 6.4 there is a discussion of how the effective core area varies over the range of wavelengths covered by the gain profile. It can thus be shown, as in section 6.5, how a frequency dependent effective core area can be incorporated into the two-wavelength model. To do so one must use the effective core area computed from the interaction of the transverse modes at the laser and peak Stokes wavelengths, together with a weighted gain profile. Thus one can incorporate a frequency-shift dependent effective core area into the two-wavelength model.

The justification for the V-values and effective core area in table 3.1 is presented in section 6.6. The final section, 6.7 considers the possibility of a length-dependent effective core area and gives a qualitative discussion of why such a phenomenon may not be too important.

In this chapter it is assumed that the gain of the core and cladding are equal. The core-cladding interface of a circularly-symmetric fibre

is taken to be a step-function. Only the lowest order mode is considered. Further research is required to determine the effects of departures from these conditions. See section 1.3.

6.2 Monomode fibre waveguiding properties

Consider a cylindrical optical fibre which is specified relative to the coordinates r, θ, z, as illustrated in Fig. 6.1. The core, of radius a, has refractive index n_1 and the cladding of radius very much greater than a, has the lower refractive index, n_2.

Define the relative refractive index difference:

$$\Delta = \frac{n_1 - n_2}{n_2} \qquad (6.1)$$

Gloge[6] shows that if $\Delta << 1$ one can obtain approximate analytic solutions. The mathematical formalism is known as the weakly guiding analysis and gives a good description of the mode structure. It has widespread application in studies of optical fibres. In weakly guiding fibres the solutions are constructed in terms of Bessel and Hankel functions for the core and cladding, respectively. The solution of interest here is that referring to the fundamental mode, which Gloge[6] refers to as the LP_{01} mode ("linearly polarised").

A particularly important parameter in weakly guiding analysis is the normalised frequency or "V-value":

$$V = \frac{2\pi a}{\lambda} (n_1^2 - n_2^2)^{\frac{1}{2}} \doteq \frac{2\pi a}{\lambda} n_1 \sqrt{(2\Delta)} \qquad (6.2)$$

The V-value of a fibre is a measure of the extent to which light is confined to the core. A fibre can only support one mode if $V \leq 2.405$. When $V > 2.405$ a higher mode can propagate as well. V is always positive.

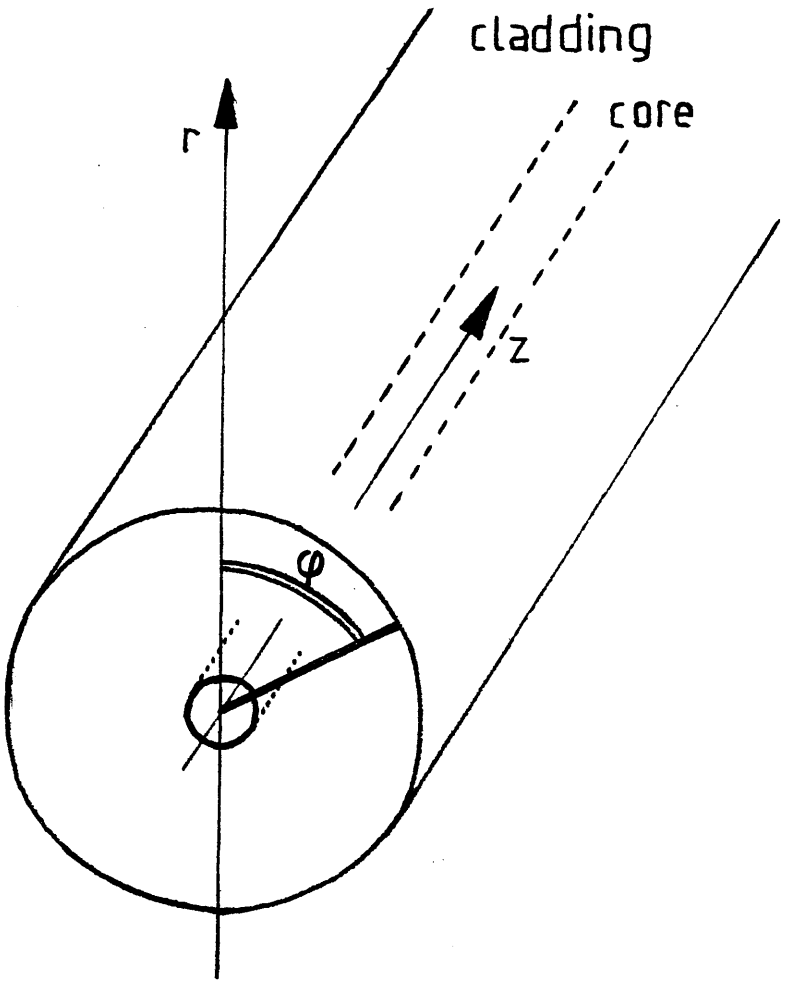

FIG. 6-1: Monomode optical Fibre; system of coordinates

The ratio of power in the cladding to the total power in the fibre at some particular length is

$$\frac{P(CLAD)}{P} = \frac{u^2}{V^2}(1 - \kappa) \tag{6.3}$$

where for the LP_{01} mode:

$$u(V) = \frac{(1 + \sqrt{2})V}{1 + (4 + V^4)^{\frac{1}{4}}} \tag{6.4}$$

and

$$\kappa = 1 - (1 + V^2 - u^2)^{\frac{1}{2}} \tag{6.5}$$

The approximations (6.4) and (6.5) lead to small inaccurancies at low V-values. The total power, P is the sum of the power in the cladding plus the power in the core, thus:

$$\frac{P(CORE)}{P} = 1 - \frac{P(CLAD)}{P} \tag{6.6}$$

Equation (6.3) is plotted in Fig. 6.2 where the fibre V-value is the ordinate. It can be seen that for fibres with low V-values a large percentage of the propagating power is in the cladding. An increase in V-value gives rise to an increase in the extent to which light is confined to the core.

The radial variation of intensity is given by:

$$I(r,\theta,z) \propto I^{rad}(r,\theta) = \begin{cases} J_0^2(\frac{ur}{a}) & 0 \leq r \leq a \\ K_0^2((V^2 - u^2)^{\frac{1}{2}}\frac{r}{a}) & a \leq r < \infty \end{cases} \tag{6.7}$$

$I^{rad}(r,\theta)$ is the normalised radial component of intensity. J_0 and K_0 are zero order Bessel and Hankel functions, respectively. Equation (6.7) is plotted for eight V-values in Fig. 6.3, where a is defined to be unity. The peak value of $I^{rad}(r,\theta)$, which occurs on the fibre axis, is also defined to be unity. Note that $J_0(0) = 1$. It can be seen that as the V-value decreases more power is spread out into the cladding, which is consistent with Fig. 6.2.

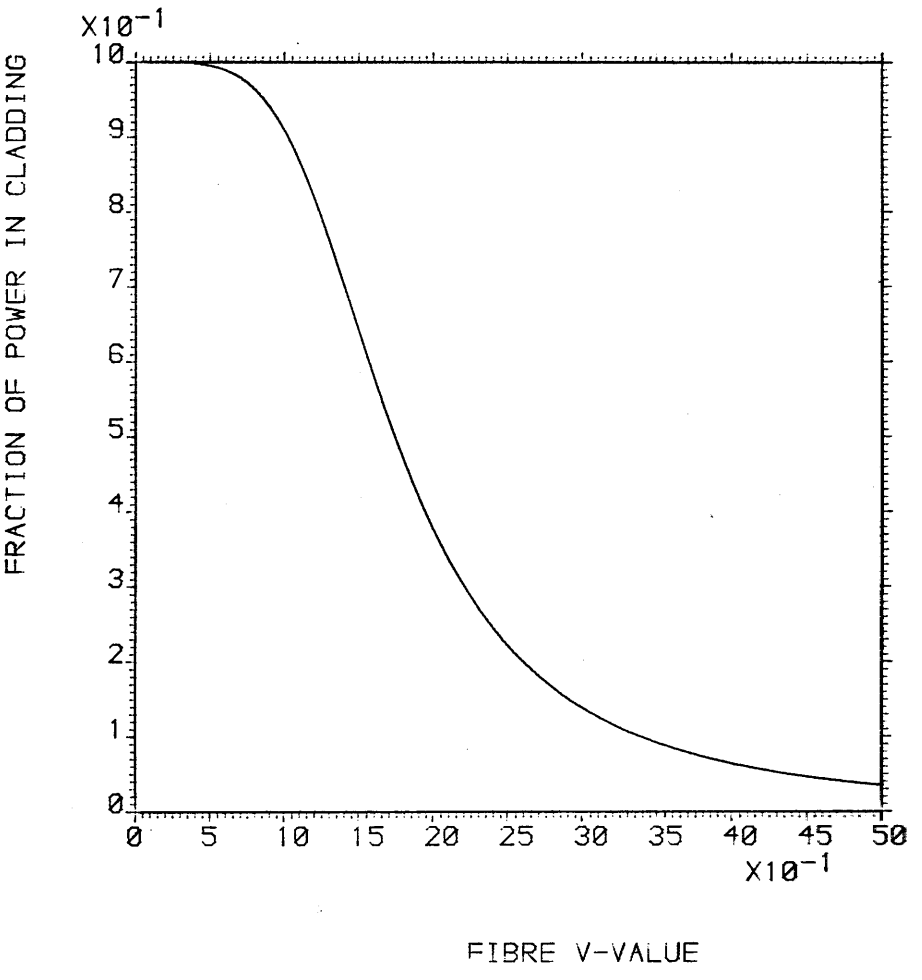

FIG. 6-2 FRACTION OF TRANSMITTED POWER IN FIBRE CLADDING AS A FUNCTION OF V-VALUE, FOR MONOMODE, STEP-INDEX OPTICAL FIBRES.

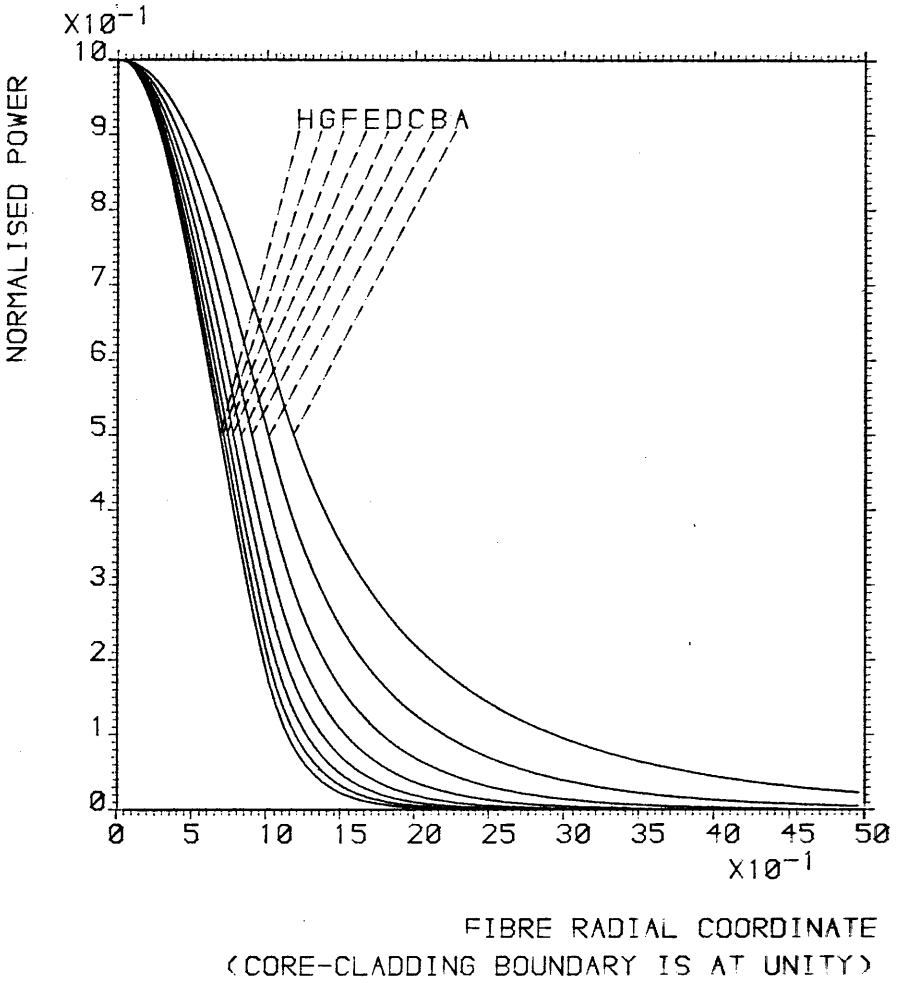

FIG. 6-3 EIGHT MODE PROFILES FOR MONOMODE STEP-INDEX FIBRES WITH THE V-VALUES: (A) 1.0, (B) 1.2, (C) 1.4, (D) 1.6, (E) 1.8, (F) 2.0, (G) 2.2, (H) 2.4.

A radial intensity distribution which is expressed in terms of special functions, as in equation (6.7) requires time consuming numerical computations or difficult analytical computations. It is thus desirable to find some simple function which will give a good approximation. Marcuse[7,8] has shown that the transverse intensity distribution in a monomode fibre can be approximated by a Gaussian:

$$I(r,\theta,z) \propto \overset{rad}{I}(r,\theta) = \exp(-\frac{r^2}{W^2}) \qquad (6.8)$$

In order for (6.8) to be useful, the full width at 1/e maximum of the Gaussian, W must be expressed in terms of the V-value of the fibre. It has been found empirically that there is good agreement between Bessel/ Hankel solutions and Gaussian solutions if:

$$W = \frac{a}{\sqrt{2}} (0.65 + \frac{1.619}{V^{3/2}} + \frac{2.879}{V^6}) \qquad (6.9)$$

The factor $1/\sqrt{2}$ is required for computations of radial intensity, but not the radial variation of electric and magnetic fields.

Once the concept of effective core area is defined it will be possible to compare solutions from (6.8) with those of (6.7). See section 6.4.

6.3 The effective core area in the multi-wavelength model

In the analysis of pump and Stokes power evalution the interaction area was taken to be A, some value of similar magnitude to the core area, πa^2. In section 6.2 it was shown that a significant percentage of the total power in the fibre was carried by the cladding. The confinement of light in the core is dependent upon the V-value and hence the wavelength of the light. Consequently, there is a different transverse intensity distribution for the pump and each of the q longitudinal Stokes modes. It will be shown that the effective core area associated

with the interaction between the pump and i^{th} Stokes longitudinal mode is the overlap integral of their transverse intensity distributions.

The effective core area for the pump -i^{th} Stokes longitudinal mode interaction is A_i and is derived from the multi-wavelength model stated in terms of intensity. I_ℓ, I_{si} and I_{spi} are the intensities of the laser pump, the i^{th} stimulated Stokes longitudinal mode and one spontaneously scattered Stokes photon, respectively. All are in physical units. Assume that there is no mutual mode coupling.

$$\frac{dI_\ell}{dz} + \alpha_\ell I_\ell = - g_o I_\ell \sum_{i=1}^{q} \mathcal{L}_i (I_{si} + I_{spi}) \qquad (6.10)$$

and:

$$\frac{dI_{si}}{dz} + \alpha_{si} I_{si} = g_o \Lambda_i \mathcal{L}_i I_\ell (I_{si} + I_{spi}) \qquad (6.11)$$

In equations (6.10) and (6.11) the terms I, with the appropriate subscripts, will in general be variable with respect to the r,θ,z coordinate system of Fig. 6.1. However, the LP_{01} transverse mode is axially symmetric and so there is no θ-dependence. It is an assumption of the theory used here that the radial dependence of all the intensity terms remains constant as the waves propagate along the fibre. Depletion and growth in intensity take place only in the z-direction. One can thus separate each intensity term:

$$I = I^{rad}(r,\theta) \cdot I^{ax}(z) \qquad (6.12)$$

All three terms in (6.12) are subscripted ℓ, si or spi as appropriate. The superscripts rad and ax refer to the radial and axial variations in intensity, respectively.

The power in the fibre, subscripted ℓ, si or spi as appropriate is given by the integral of the intensity:

$$P(z) = \int_0^{2\pi} \int_0^{\infty} I(r,\theta,z) r \, dr d\theta$$

$$= 2\pi \int_0^{\infty} I(r,z).rdr$$

$$= \langle I(r,z) \rangle \qquad (6.13)$$

Now, by equations (6.12) and (6.13):

$$\langle I(r,z) \rangle = \overset{ax}{\langle I(z) \rangle} \overset{rad}{\langle I(r) \rangle}$$

$$= \overset{ax}{I(z)} \overset{rad}{\langle I(r) \rangle} \qquad (6.14)$$

Thus:
$$\overset{ax}{I(z)} = \frac{P(z)}{\overset{rad}{\langle I(r) \rangle}} \qquad (6.15)$$

Now integrate equations (6.10) and (6.11) with respect to r and θ to give equations in terms of power:

$$\frac{d\langle I_\ell \rangle}{dz} + \alpha_\ell \langle I_\ell \rangle = -g_o \sum_{i=1}^{q} \mathcal{L}_i \langle I_\ell (I_{si} + I_{spi}) \rangle \qquad (6.16)$$

and for each i=1,2 ....q:

$$\frac{d\langle I_{si} \rangle}{dz} + \alpha_{si} \langle I_{si} \rangle = g_o \mathcal{L}_i \Lambda_i \langle I_\ell (I_{si} + I_{spi}) \rangle \qquad (6.17)$$

Now use (6.14) and (6.15) to give:

$$\frac{dP_\ell}{dz} + \alpha_\ell P_\ell = -g_o \sum_{i=1}^{q} \mathcal{L}_i \frac{\overset{rad}{\langle I_\ell(r) \rangle} \overset{rad}{\langle I_{si}(r) \rangle}}{\overset{rad}{\langle I_\ell(r) \rangle} \overset{rad}{\langle I_{si}(r) \rangle}} P_\ell (P_{si} + P_i) \qquad (6.18)$$

and for each i=1,2, ...q:

$$\frac{dP_{si}}{dz} + \alpha_{si} P_{si} = g_o \Lambda_i \mathcal{L}_i \frac{\overset{rad}{\langle I_\ell(r) \rangle} \overset{rad}{\langle I_{si}(r) \rangle}}{\overset{rad}{\langle I_\ell(r) \rangle} \overset{rad}{\langle I_{si}(r) \rangle}} P_\ell (P_{si} + P_i) \qquad (6.19)$$

In obtaining equations (6.18) and (6.19) the fact that the radial components of the spontaneous and stimulated Stokes intensities are equal was used:

$$I_{si}^{rad}(r) = I_{spi}^{rad}(r)$$

In (6.18) and (6.19) p_i is the power associated with the i^{th} spontaneous Stokes photon.

Compare equations (6.18) and (6.19) with (4.1) and (4.2). The effective core area for the interaction between the pump wave and the i^{th} Stokes longitudinal mode can be identified as:

$$A_i = \frac{<I_{\ell}^{rad}(r)><I_{si}^{rad}(r)>}{<I_{\ell}^{rad}(r).I_{si}^{rad}(r)>} \qquad (6.20)$$

There is a separate effective core area for the interaction between the pump and each of the q Stokes longitudinal modes. The effective core area is an overlap integral. It depends upon the parameters which dictate the extent to which the pump and Stokes guided waves are confined to the core. A_i is thus dependent upon the fibre V-value. A_i is independent of z, the propagation distance.

If the radial variation of intensity used to evaluate (6.20) is that of the weakly guiding analysis one must resort to numerical integration. However, if the Gaussian approximation can be employed, A_i can be evaluated analytically. V_{ℓ} and V_{si} are the V-values at the pump and i^{th} Stokes wavelength, respectively. Thus $W_{\ell} = W(V_{\ell})$ and $W_{si} = W(V_{si})$. See equation (6.9). The i^{th} component of the effective core area is expressed as:

$$A_i = \frac{4\pi^2 \int_o^\infty \exp(\frac{-r^2}{W_\ell^2}) r dr \int_o^\infty \exp(\frac{-r^2}{W_{si}^2}) r dr}{2\pi \int_o^\infty \exp[-r^2 (\frac{W_\ell^2 + W_{si}^2}{W_\ell^2 W_{si}^2})] r dr} \qquad (6.21)$$

Which can be shown to be:

$$A_i = \pi(W_\ell^2 + W_{si}^2) \qquad (6.22)$$

In the work done by Stolen[9], the transverse modal profile of the Stokes wave was assumed to be approximately equal to that of the laser pump. Thus $W_\ell^2 \doteqdot W_{si}^2 = W^2$, for all i.

Therefore: $$A_i = 2\pi W^2 \qquad (6.23)$$

This approximation is referred to here for convenience as the self interaction approximation.

6.4 Variation of the effective core area with V-value

Assume firstly that the difference in radial intensity distribution between the pump guided wave and any of the Stokes guided waves is negligible One therefore uses the self interaction approximation. The ratio of the effective core area to the actual core area is plotted as a function of V-value in Fig. 6.4. The calculation is performed in two ways: (A) by the use of equations (6.9) and (6.23) and (B) by numerical integration of the solutions from weakly guiding analysis, equation (6.7).

Two important features are evident from Fig. 6.4. Firstly, in both curves the effective core area increases with a decrease in the V-value. Secondly, the Gaussian and weakly guiding solutions agree well at high V-values. At lower V-values the best fitting Gaussians assign too much

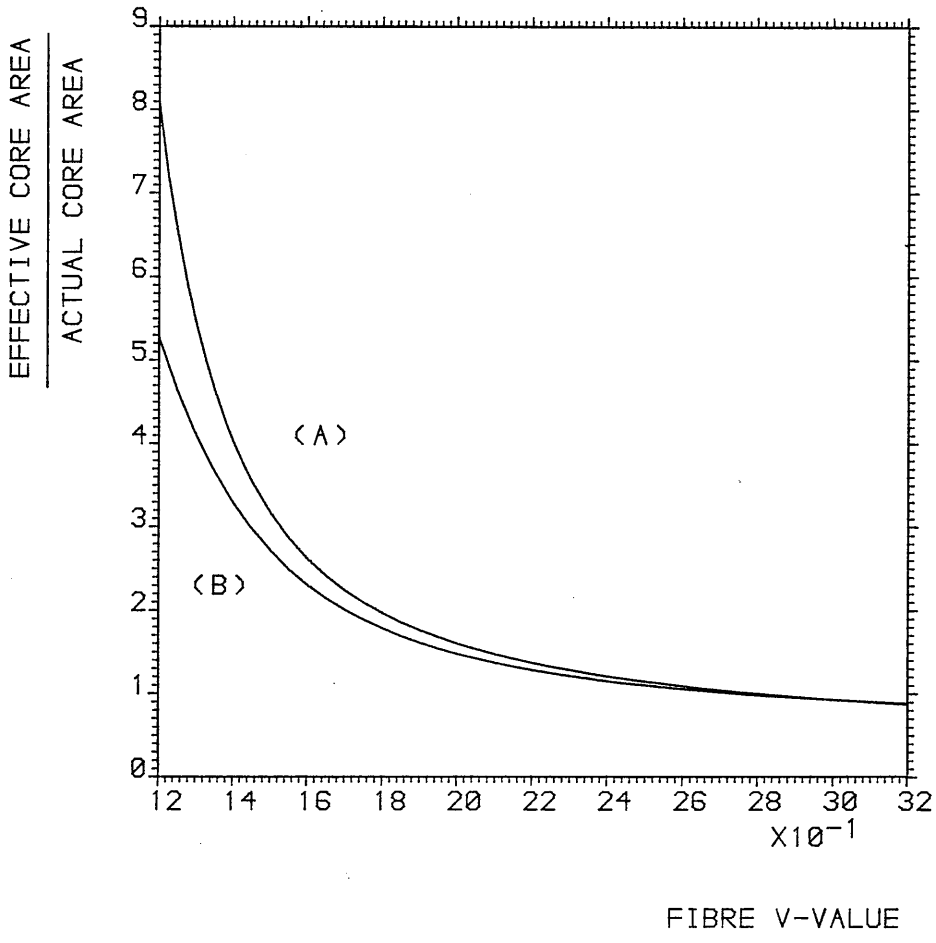

FIG. 6-4 GRAPH OF EFFECTIVE CORE AREA AS A FUNCTION OF V-VALUE FOR A SINGLE MODE STEP-INDEX OPTICAL FIBRE. THE CALCULATION IS PERFORMED USING (A) GAUSSIAN AND (B) WEAKLY GUIDING APPROXIMATIONS TO THE TRANSVERSE FIELD.

power to the fibre cladding, giving values of the effective core area which are too high.

From now on only weakly guiding solutions are considered due to their greater accuracy. However, it is a simple matter to rework what is said in terms of the Gaussian approximation.

In a fibre which is pumped at 1.55μm and has a Stokes spectrum covering $880cm^{-1}$ (such as that described in table 3.1) there will be a range of effective core areas experienced by the q longitudinal Stokes modes. Fig. 6.5 shows the V-value variation of $A_i/\pi a^2$ for longitudinal modes corresponding to six equally spaced frequency shifts between 0 and $880cm^{-1}$. The horizontal axis is the V-value at the pump wavelength. It can be seen that $A_i/\pi a^2$ increases as the frequency shift of the Stokes mode increases. The line labelled (A) on Fig. 6.5 is the same as (B) on Fig. 6.4.

The importance of Fig. 6.5 is that over the range of wavelengths covered by the gain profile the V-value decreases with frequency shift and hence the effective core area increases. The variation of $A_i/\pi a^2$ with respect to V-value is illustrated on Fig. 6.6 for a fibre with a V-value of 1.50 at the laser wavelength and 1.32 at a maximum Stokes frequency shift of $880cm^{-1}$.

6.5 Reduction to a dimensionless two wavelength model with a weighted lineshape function

The multi-wavelength model is stated in physical units in equations (6.18), (6.19) and (6.20). Both the Lorentzian lineshape function, $\mathcal{L}$ and the effective core area, A are frequency dependent. The term $\mathcal{L}_i/A_i$ appears on the right hand side of all equations. There are two functions in Fig. 6.7: (A) is the lineshape function having a peak

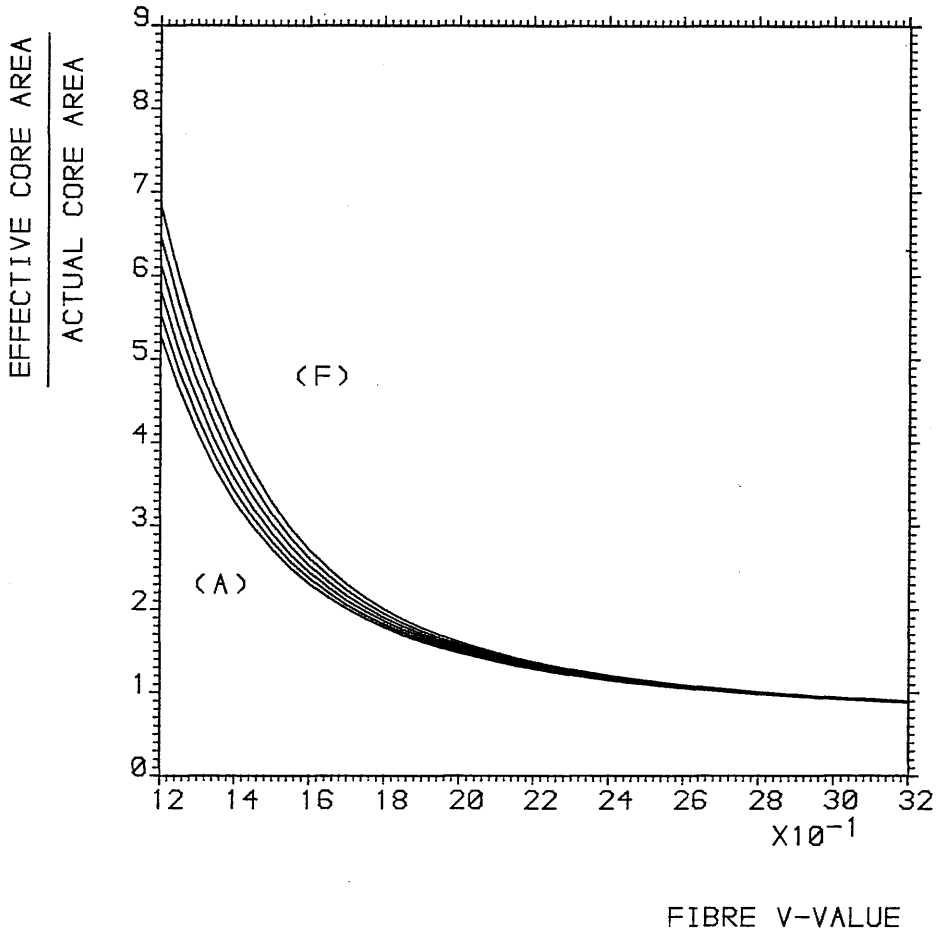

FIG. 6-5 GRAPH OF EFFECTIVE CORE AREA AS A FUNCTION OF V-VALUE FOR A SINGLE MODE STEP-INDEX OPTICAL FIBRE. V-VALUE DIFFERENCE BETWEEN PUMP AND STOKES WAVES:
(A) 0, (B) 0.36E-1, (C) 0.72E-1,
(D) 1.08E-1, (E) 1.44E-1, (F) 1.80E-1.

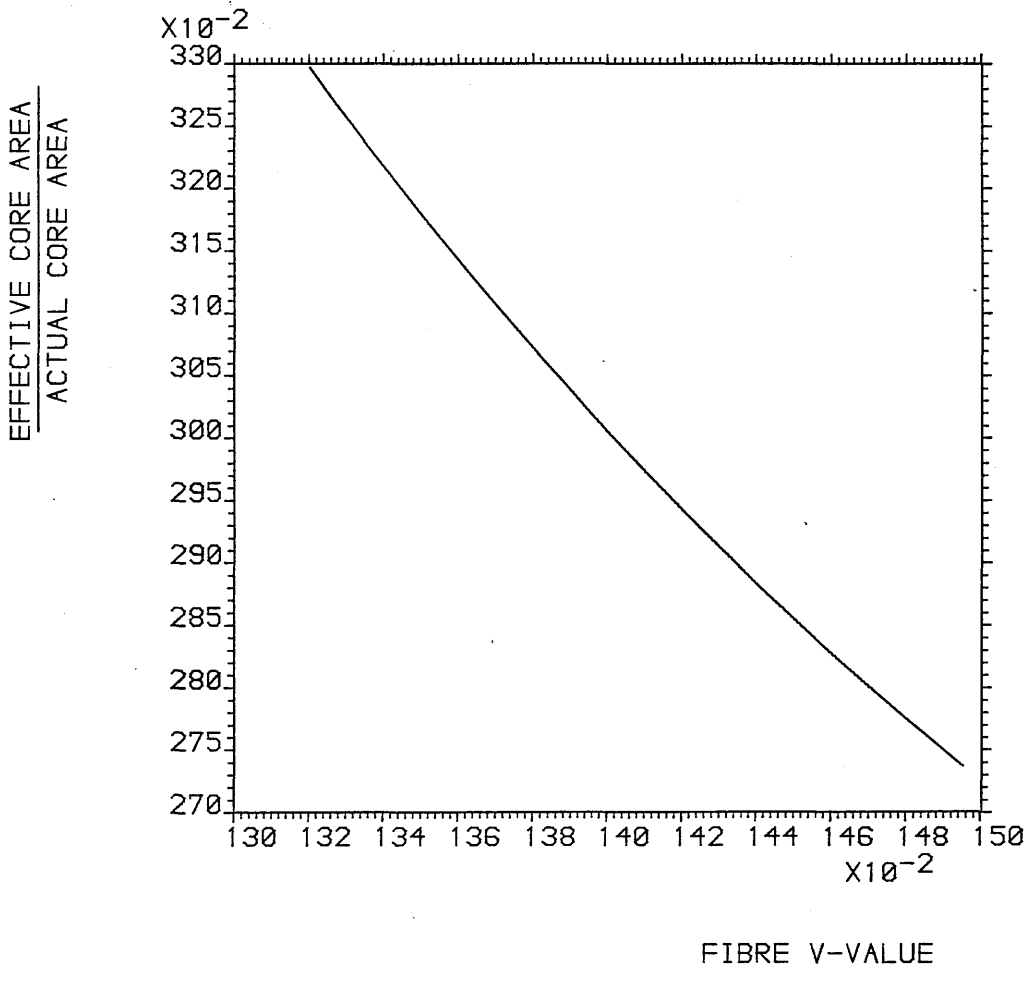

FIG. 6-6 GRAPH ILLUSTRATING THE INCREASE IN THE NORMALISED EFFECTIVE CORE AREA AS A RESULT OF THE OVERLAP INTERACTION BETWEEN A PUMP WAVE OF WAVELENGTH 1.55 MICRONS AND ALL OF THE POSSIBLE STOKES WAVES SPANNING 880 WAVENUMBERS SHIFT. THE V-VALUE AT THE PUMP WAVELENGTH IS 1.5, THE FURTHEST RIGHT POINT ON THE GRAPH.

frequency shift of 440cm^{-1} and a full width at half maximum of 240cm^{-1}, in accordance with table 3.1. (B) is the lineshape function weighted so that A_i at the laser wavelength is unity and A_i at the Stokes wavelengths increase in proportion to the variation in effective core area in Fig. 6.6.

Fig. 6.7 shows that the effective core area can be regarded as a constant provided that the lineshape function is weighted so as to account for the variation of the overlap integral with Stokes wavelength. One can choose which of the A_i is to be taken as the constant. Two values would appear to be useful: (a) A_i calculated from the self interaction approximation and (b) A_i calculated from the overlap of the transverse mode at the laser wavelength with the transverse mode at the peak Stokes wavelength, λ_s. The choice of (b) is found to be more convenient due to the fact that the weighted Lorentzian lineshape function has the value of unity at λ_s.

The multi-wavelength model in physical units thus becomes:

$$\frac{dP_\ell}{dz} + \alpha_\ell P_\ell = -\left(\frac{g_o}{A_{s\ell}}\right) \sum_{i=1}^{q} \mathcal{L}_{Wi} P_\ell (P_{si} + p_i) \qquad (6.24)$$

For each i = 1,2, ...q:

$$\frac{dP_{si}}{dz} + \alpha_{si} P_{si} = \left(\frac{g_o}{A_{s\ell}}\right) \Lambda_i \mathcal{L}_{Wi} P_\ell (P_{si} + p_i) \qquad (6.25)$$

Where $\mathcal{L}_{Wi}$ is the weighted Lorentzian lineshape function and $A_{s\ell}$ is the effective core area for the interaction between the laser guided wave and the guided wave of the peak longitudinal Stokes mode. Equations (6.24) and (6.25) can be rendered dimensionless by the same scheme used in section 5.2 provided that $A_{s\ell}$ is substituted for A and $\mathcal{L}_{Wi}$ for $\mathcal{L}_i$.

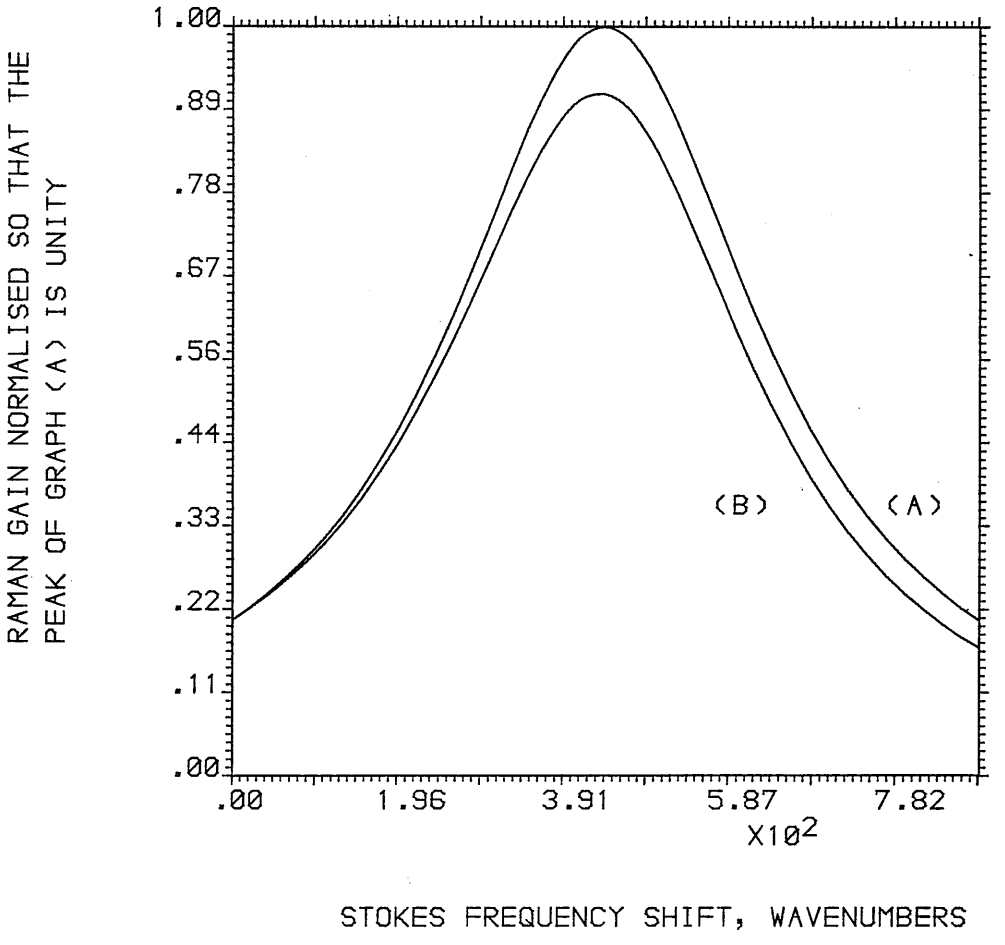

FIG. 6-7 GRAPH OF NORMALISED RAMAN GAIN:
(A) THE EFFECTIVE CORE AREA IS ASSUMED CONSTANT
(B) THE PROFILE IS WEIGHTED SO AS TO ACCOUNT
FOR A VARIABLE EFFECTIVE CORE AREA
PUMP WAVELENGTH = 1.55 MICRONS
V-VALUE AT PUMP WAVELENGTH = 1.5
F.W.H.M. OF RAMAN GAIN PROFILE = 240 WAVENUMBERS

In order to reduce (6.24) and (6.25) to a two-wavelength model it is necessary to calculate the effective Stokes bandwidth, B_{eff} from equation (3.36). B_{eff} calculated with the use of $\mathcal{L}_{Wi}$ will, in principal, be different from B_{eff} calculated with the use of $\mathcal{L}_{i}$. However, it was shown in section 3.4 that B_{eff} calculated using parabolic and Lorentzian lineshape functions gave results which were approximately equal. It can therefore be seen that after an exponential amplification process the slight asymmetries in $\mathcal{L}_{Wi}$ will have a negligible effect upon the resulting Stokes spectrum. Thus B_{eff} arising from a weighted Lorentzian function also can be well approximated by equation (3.36). In order to complete the reduction to a two wavelength model one must use the effective Stokes loss as discussed in chapter 5.

6.6 Justification of the entries for the V-value and effective core area in table 3.1

Dispersion[1] is the variation of group delay per unit length and determines the distance one can propagate two signals of slightly different wavelength before they become unacceptably separated in time. In a weakly guiding monomode fibre there are two dispersive effects: material dispersion and waveguide dispersion. The former is determined by the wavelength dependence of refractive index and the latter by the modal confinement within the fibre. An important aim of optical fibre design is to achieve a waveguide dispersion which is equal and opposite to the material dispersion, giving zero total dispersion at the operating wavelength. In table 3.1 the V-value at 1.55μm is 1.50 for two reasons: (a) it has been shown [10] that zero total dispersion can be achieved in such a fibre and (b) V = 1.50 illustrates well the spread of effective core areas over an $880cm^{-1}$ gain profile.

The effective core area is justified as follows: the core

diameter required for zero total dispersion at λ_ℓ = 1.55μm and V = 1.5 is 4.5μm[10]. The actual core area is thus 1.59 x 10^{-11} m^2. It can be seen from Fig. 6.6 that the fibre V-value at 440cm^{-1} peak frequency shift is 1.41. The ratio of effective core area to actual core area at V = 1.41 is 2.99. Thus the entry in table 3.1 for effective core area, $A_{s\ell}$ is computed to be 4.75 x 10^{-11} m^2. See section 6.5.

6.7 The effect of non-planar wavefronts on amplification properties

In deriving the expression (6.20) for the effective core area, it was assumed that the transverse intensity distribution was independent of length. Thus the intensity at any point in the fibre could be expressed as the product of a radial and an axial component. See equation (6.12). In reality this separation can only be made for a plane wave interaction when Raman conversion is occurring.

The product of the intensity terms on the right hand side of (6.10) and (6.11) indicate that the Raman amplification is proportional to the local intensity of the pump and Stokes waves. Thus there is greater Stokes growth and pump depletion on the axis of the fibre, showing a decrease with radius. Von der Linde, et al[11] have treated this situation for a Gaussian radial profile from a TEM_{oo} laser beam propagating in free space. The transverse profiles of the pump and Stokes waves are being changed as they propagate, giving rise to an overlap integral which is length dependent.

It is assumed for the purpose of this thesis that the effect just described is not important in optical fibres and therefore A is very slowly varying with z. A possible reason is that the wave-guiding action of the fibre re-forms the pump and Stokes waves so that they always have intensity distributions which are close approximations to

those which would exist in the absence of the Raman interaction. The effect is thus similar to that of a plane wave interaction.

References

6.1 Contributions to: Miller, S.E. and Chynoweth, A.G. (Eds.) "Nonlinear properties of optical fibres". Academic Press, New York (1979).

6.2 Garrett, I., Todd, C.J., "Components and systems for long wavelength monomode fibre transmission", Optical and Quant. Electron., 14, 95, (1982).

6.3 Snyder, A.W. and Love, J.D., "Optical waveguide theory", Chapman and Hall, London, (1983).

6.4 Sodha, M.S. and Ghatak, A.K., "Inhomogeneous optical waveguides", Plenum, New York (1977).

6.5 Unger, H.G., "Planar optical waveguides and fibres", Oxford University Press (1977).

6.6 Gloge, D. "Weakly guiding fibres", Appl. Optics 10, 2252, (1971).

6.7 Marcuse, D. "Loss analysis of single mode fibre splices", Bell Syst. Tech. J., 56, 703, (1977).

6.8 Marcuse, D. "Gaussian approximation of the fundamental modes of graded-index fibres", J. Opt. Soc. Am., 68, 103, (1978).

6.9 Stolen, R.H. "Fibre Raman lasers", in "Fibre and integrated optics", Vol. 3, Ostrowsky, D.B. (Ed.) Plenum (1980).

6.10 Sugimura, A., Daikoku, D., Imoto, N., Miya, T. "Wavelength dispersion characteristics of single mode fibres in low-loss region", I.E.E.E. J. Quantum Electron., QE-16, 215 (1980).

6.11 Von der Linde, D., Maier, M., and Kaiser, W. "Quantitative investigations of the stimulated Raman effect using subnanosecond light pulses", Phys. Rev., 178, 11 (1969).

CHAPTER SEVEN

THE DESIGN OF SYSTEMS FREE FROM STIMULATED RAMAN SCATTERING

7.1 Introduction

The subject matter of the previous chapters will now be collected together to develop a simple method of design of a source, optical fibre and detector system, which can operate free of cross-talk due to stimulated Raman scattering. In this chapter the two-wavelength model, which was discussed in chapters 3 and 4 is used. The loss, β_s is the effective Stokes loss from chapter 5 and the area, A is the effective core area from chapter 6. It will be shown how the two-wavelength model with non-zero β_ℓ and β_s relate to the zero-loss model from appendix 1.

Section 7.2 gives a discussion of the basic design concept, using an example of an equal-loss fibre with respect to the criterion of equal photon number threshold. It should be emphasised that the design method here does not consider all of the possible restrictions upon optical fibre parameters, one obvious omission being dispersion. Further research is required to generalise the method. Section 7.3 illustrates what happens when $\beta_\ell \neq \beta_s$ and section 7.4 is a brief discussion of alternative threshold criteria, one of which is a proposal for further research. Section 7.5 concerns the design of fibres to promote Raman conversion.

The numerical computations in this chapter were time-consuming, involving many iterations. Repetition of the calculations with the multi-wavelength model substituted for the two wavelength model could not be contemplated with the computing facilities available. It is thus important, as in chapters 5 and 6, to reduce the problem of pump and Stokes power evolution to one which can be stated as a two-wavelength model.

7.2 The design of Raman-free systems with equal pump and Stokes losses

The evolution of pump and Stokes waves with respect to length, where β_ℓ, β_s, Q and Λ are known constants was examined in chapters 3, 4 and 5. This only gives information about one particular fibre. A Raman-free source-fibre-detector system can be designed by examining how the length of fibre that allows the threshold criterion to be satisfied varies with β_ℓ, when β_s/β_ℓ, Q and Λ are held constant. The criterion for threshold considered here is equality of pump and Stokes photon number. See equation (3.45).

Fig. 7.1 is the locus of (β_ℓ, Z) coordinates which exactly satisfy (3.45), plotted on logarithmic axes. Here $\beta_\ell = \beta_s = \beta$. Calculations were made by the method described in appendix 4: the differential equations (4.1) and (4.2) are solved for all values of Z above threshold until (3.45) is satisfied. Unstable solutions were obtained for values of β greater than 0.066, however, as will be seen, such solutions are of little interest and can be ignored. $\Lambda = 0.939$, see table 3.1.

It has been shown in section 3.4 that with a Lorentzian gain profile Q depends upon $\beta^{\frac{1}{2}}$, provided that fibre lengths are large and β is not too low. It has been decided here to calculate Q from a constant high value. Q is calculated from an effective bandwidth which is equal to $2\Delta\nu$, the complete range of frequencies covered by the gain profile. There are two advantages of doing so: doubts about β and Z variations of B_{eff} are removed and such a large value gives rise to the most pessimistic forecast of lengths at which threshold will be reached, as will be seen, the system is relatively insensitive to variations in Q and so inaccuracies caused are only slight.

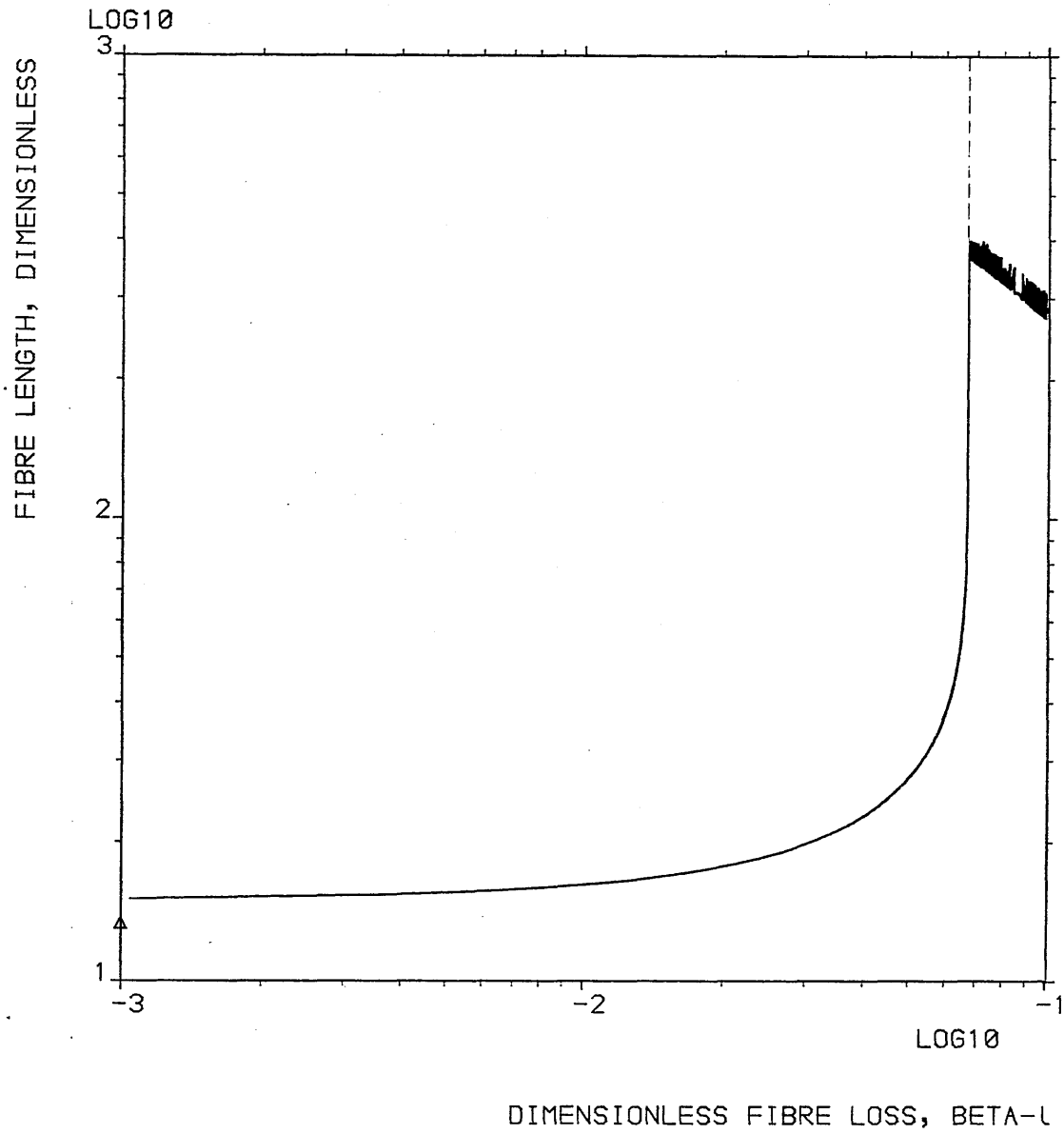

FIG. 7-1 THRESHOLD FREE TRANSMISSION DISTANCE AS A FUNCTION OF FIBRE LOSS ACCORDING TO THE CRITERION OF EQUALITY OF PUMP AND STOKES POWER. IN COMPUTATIONS.

At low β-values the curve is approximately horizontal. The triangle marker on the vertical axis is the Z-value, Z_{min}, calculated from zero-loss theory, below which threshold cannot be achieved. See equation (A1-17) and section 3.7. Another feature of the theory of chapter 3 was that there is a maximum loss, β_{max}, above which threshold is never reached and that $\beta_{max} = 1/Z_{min}$. It is easy to check that the value of β where the broken line cuts the horizontal axis is the reciprocal of Z_{min}. The jagged line to the right of β_{max} indicates numerically unstable solutions. Here both the pump and the Stokes waves are behaving like exponentials. See fig. 3.3. Fortunately, such high-loss fibres are seldom of interest and can be ignored.

Fig. 7.2 illustrates how the locus of β, Z Raman-threshold coordinates can be incorporated into a design concept. Zone 1 is the set of points representing fibres which cannot be manufactured in practice. Solutions to equations with β less than 8.73×10^{-3} ($\alpha < 0.2$ dB/km) are mathematically, but not physically realisable in silica-based fibres.

In a telecommunications fibre operating at a known loss and input power, in the absence of nonlinear phenomena, the receiver sensitivity will impose a limit to the length of fibre over which useful operation is possible. If P_{min} is the minimum power at the pump wavelength, to which the detector is sensitive, then in physical coordinates:

$$P_{min} = P_o \exp(-\alpha z) \qquad (7.1)$$

The maximum length for a detectable signal in dimensionless coordinates is thus:

$$Z_{max} = -\frac{1}{\beta_{min}} \mathrm{Ln}(R_{min}) \,. \qquad (7.2)$$

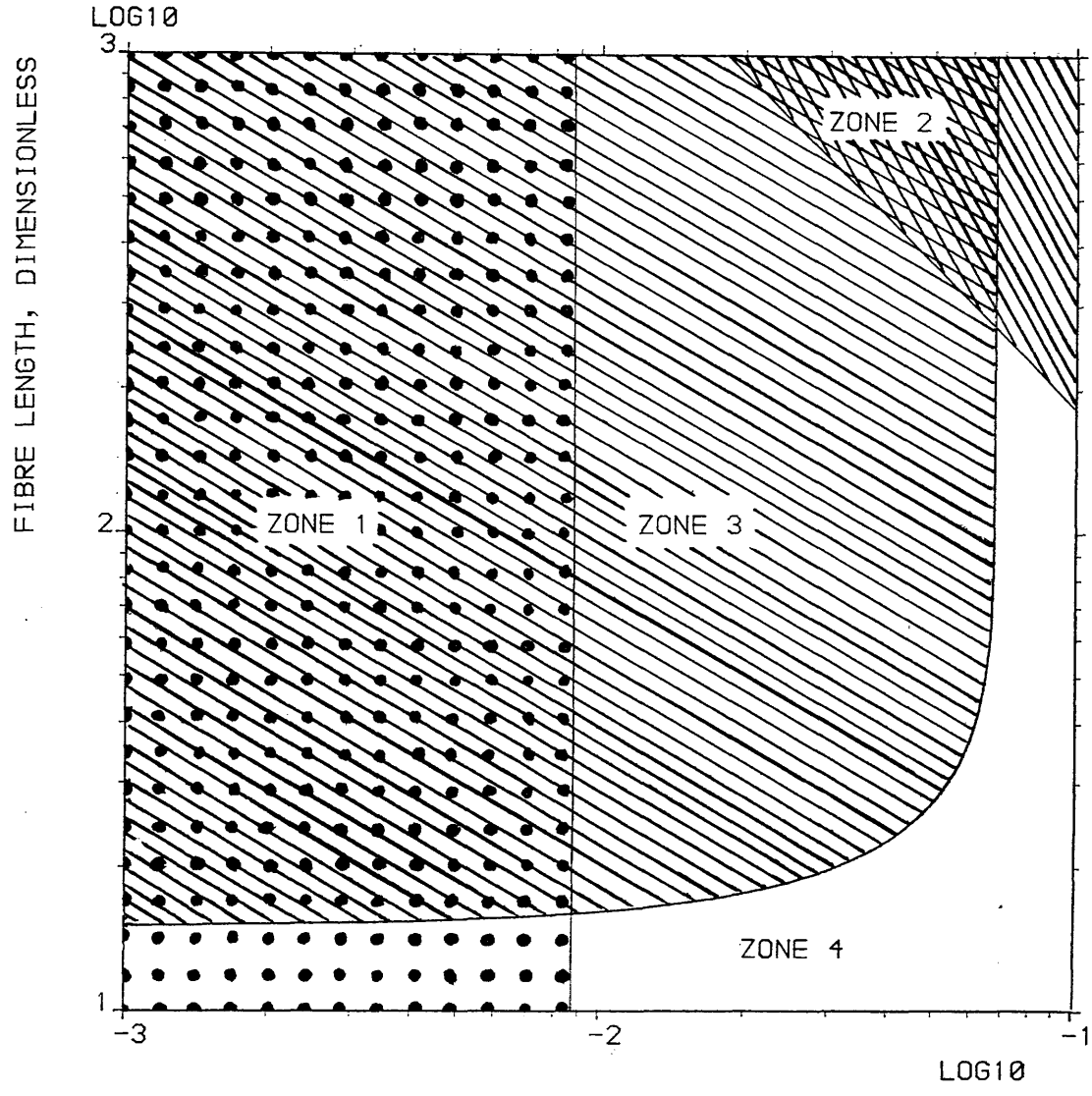

FIG. 7-2 THRESHOLD FREE TRANSMISSION DISTANCE AS A FUNCTION OF FIBRE LOSS ACCORDING TO THE CRITERION OF EQUALITY OF PUMP AND STOKES POWER.
ZONE 1: LOW LOSS FIBRES WHICH CANNOT BE MANUFACTURED IN PRACTICE. ZONE 2: BEYOND LIMIT OF DETECTOR SENSITIVITY. ZONE 3: RAMAN PRONE FIBRES. ZONE 4: RAMAN-FREE FIBRES.
SEE TABLE 3-1 FOR DATA USED IN COMPUTATIONS.

where $R_{min} = P_{min}/P_o$. Zone 2 in Fig. 7.2 is the range of Z, which is greater than Z_{max}. P_{min} is taken to be 10^{-7} watts (-40dBm)[1] and P_o = 8 watts, as in table 3.1. An increase or decrease by one order of magnitude in P_{min} causes little alteration in the position of the boundary of zone 2.

Points which lie in zone 3 are Raman prone and points which lie in zone 4 are Raman-free. The vertical boundary of zone 3 is drawn by extrapolating Z at $\beta = \beta_{max}$ to infinity. It can be seen that the numerically unstable solutions in Fig. 7.1 lie well within zone 2 and are thus of little interest.

There is a set of points, defined by the unshaded region on Fig. 7.2, for which detectable transmission, in currently available silica fibres ($\alpha \geq$ 0.2dB/km), which do not satisfy the Raman threshold criterion, (3.45 is possible. The important feature of this region is that the greatest transmission length does not occur at the lowest possible loss. It occurs where $\beta = \beta_{max} = 1/Z_{min}$ in equation (7.2). Thus

$$Z_{max}^{opt} = Z_{min}\, Ln[\frac{1}{R_{min}}] \qquad (7.3)$$

Z_{max}^{opt} is the optimal transmission length. Z_{min} is given by equation (A1.17).

Finally, consider how the threshold locus depends upon the physical parameters q, P_o, λ_ℓ/λ_s, g_o and A. It was seen from the dimensionless analysis of the zero loss limit that the threshold length depends only on Q and Λ (equation (A1.17) with y = 1). Both Q and Λ are independent of g_o and A. Thus Z_{min} and β_{max} are independent of g_o and A. The curve of Fig. 7.2 is universal for all values of g_o and A. The effect of varying g_o and A is completely

explained by Fig. 7.2 when equations (3.13) and (3.12) are used to convert the axes back to physical units.

The position of Z_{min} and hence β_{max} depend upon Q and Λ and hence q, P_o and λ_ℓ/λ_s. It can be seen from (A1.17) that for small changes in λ_ℓ/λ_s, Z_{min} is approximately proportional to λ_ℓ/λ_s. Z_{min} is also proportional to $Ln(P_o)$ and Ln (1/q), due to the fact that $Q \propto q/P_o$ (see section 3.4). Thus Z_{min} and β_{max} are altered slightly relative to the axes of Fig. 7.2. The change in the curve with values of P_o varied over the range 1/8 watts to 8 watts is illustrated on Fig. 7.3. The same change in the β,Z threshold curve is produced when 1/q is varied over the same range.

7.3 The loss-length variation in the presence of unequal pump and Stokes loss

In this section the threshold criterion of equation (3.45) is used to evaluate the range of Raman free coordinates when $\beta_\ell \neq \beta_s$. Due to the lack of an analytic treatment in such circumstances, one must rely entirely upon numerical solutions to obtain physical insight into the problem. Fig. 7.4 is a series of equivalent curves to those of Figs 7.1 and 7.2. The indications of constraints due to minimum fibre loss and maximum propagation length, imposed by receiver sensitivity are omitted. Curves (A) and (B) are for $\beta_\ell > \beta_s$, (C) for $\beta_\ell = \beta_s$ and (D) to (J) for $\beta_\ell < \beta_s$.

All curves where $\beta_s > \beta_\ell$, gave unstable solutions similar to those of Fig. 7.1. The lengths at which such instabilities occurred were considerable and inside zone 3 in all cases. (C) to (J) of Fig. 7.4 were extended vertically upwards whenever the instability occurred. All curves were computed to a high degree of segmentation in the horizontal coordinate. Special care had to be taken with the tight bends in (H),

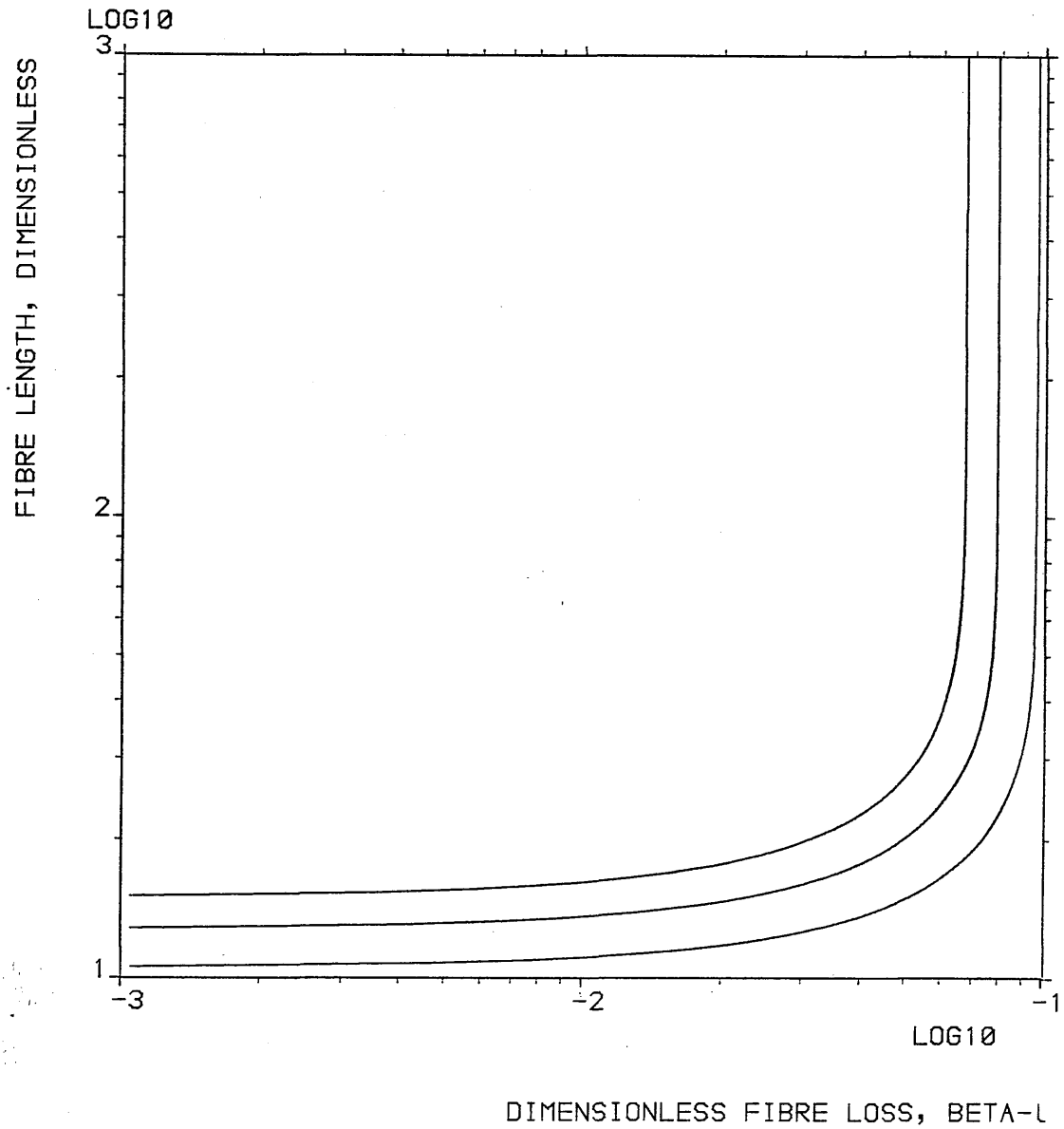

FIG. 7-3 THRESHOLD FREE TRANSMISSION DISTANCE AS
A FUNCTION OF FIBRE LOSS ACCORDING TO THE CRITERION
OF EQUALITY OF PUMP AND STOKES POWER.
THE PUMP AND STOKES LOSSES ARE EQUAL.
PUMP POWER: (A) 1/8, (B) 1, (C) 8 WATTS.
DATA USED IN COMPUTATIONS ARE IN TABLE 3-1.

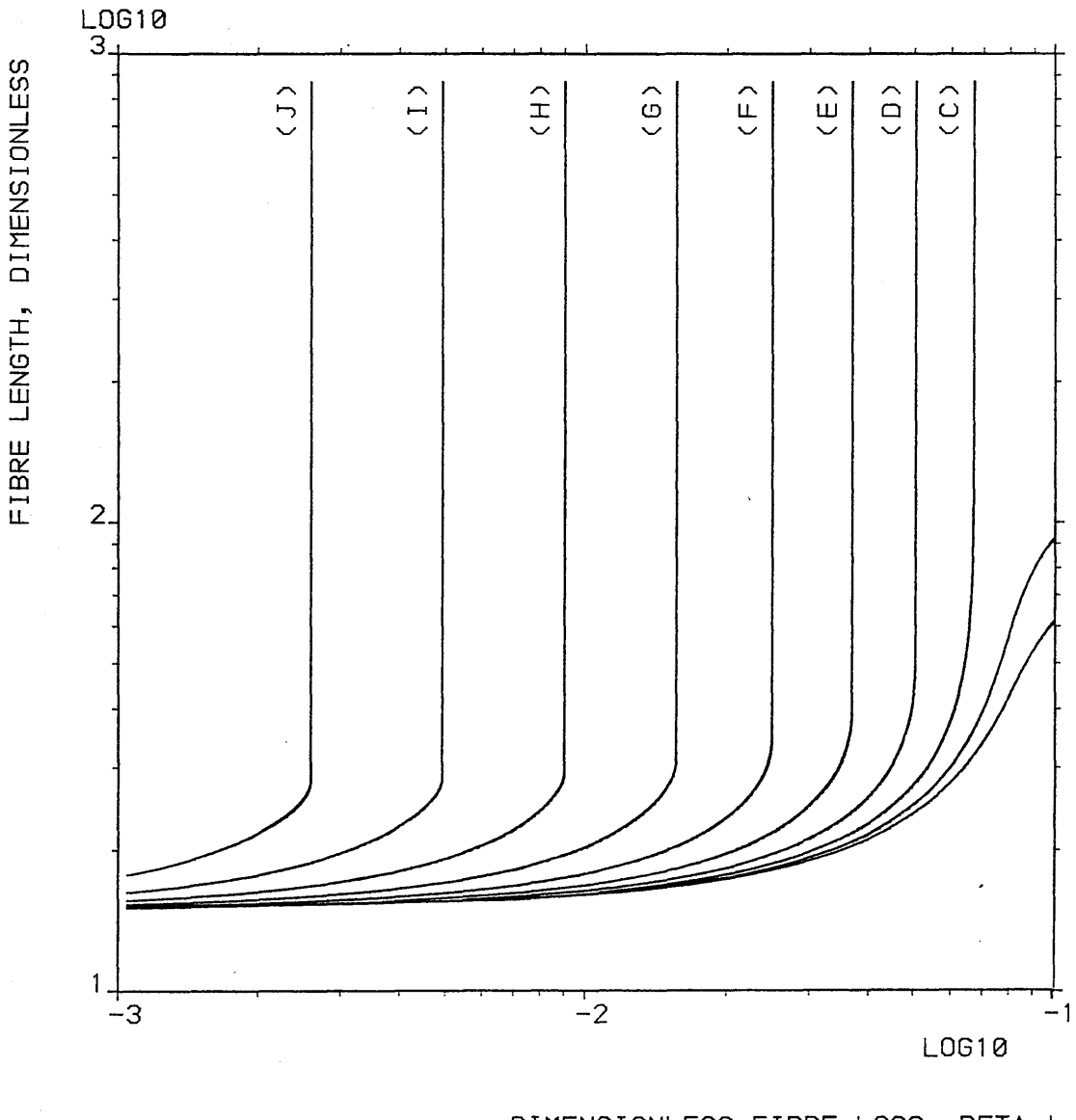

FIG. 7-4 THRESHOLD FREE TRANSMISSION DISTANCE AS A FUNCTION OF FIBRE LOSS ACCORDING TO THE CRITERION OF EQUALITY OF PUMP AND STOKES POWER.
RATIO OF STOKES LOSS TO PUMP LOSS:
(A) 0.25, (B) 0.5, (C) 1, (D) 2, (E) 4,
(F) 8, (G) 16, (H) 32, (I) 64, (J) 128.
DATA USED IN COMPUTATIONS ARE IN TABLE 3-1.

(I) and (J). See appendix 4. In all curves as β_ℓ decreases Z asymptotically approaches Z_{min}. In (C) to (J), where $\beta_s > \beta_\ell$ there is some value of loss, $\beta_{\ell max}$ above which threshold cannot occur according to the criterion of (3.45). It is obvious that only in (C) does the relationship $\beta_{\ell max} = 1/Z_{min}$ hold. Due to the lack of an analytic solution the relationship between $\beta_{\ell max}$, Z_{min} and β_ℓ/β_s is not clear. It has been found that $\beta_{\ell max}$ is dependent upon the physical parameters P_o, qp and λ_ℓ/λ_s.

Finally, consider how Fig. 7.4 compares with the characteristics of Fig. 4.1. Although different Q-values have been used, it is still instructive to carry out a qualitative comparison. When β_ℓ has a given value, say 8.73×10^{-3}, the value in Fig. 4.1, threshold is possible only where β_s/β_ℓ is less than some well defined value. For example, a line extended perpendicular to the horizontal axis at $\beta_\ell = 8.73 \times 10^{-3}$ will cut curves (A) to (H) but not (I) and (J). Clearly, there is some ratio of β_s/β_ℓ between 32 and 64 above which the threshold criterion is never satisfied. By interpolating the values of $\beta_{\ell max}$ by eye it would appear that threshold can occur only when β_s/β_ℓ is less than about 40.

The discussion of section 4.3 has made clear the limitations upon equality of pump and Stokes photon number as a criterion of threshold. These limitations are also manifest in Fig. 7.4. Firstly, even at ratios of β_ℓ/β_s greater than that which gives rise to $\beta_{\ell max} = 8.73 \times 10^{-3}$ there is considerable depletion of the pump signal which cannot be accounted for by linear loss alone. Secondly, Fig. 7.4 gives no indication of the ambiguity in threshold length which is shown in Fig. 4.1(c). This is because Fig. 7.4 is the locii of the lowest Z-values which satisfy threshold condition (3.45).

In the next section there is a short discussion of possible alternative criteria for threshold to overcome the problems discussed above.

7.4 Alternative threshold criteria

It was argued in chapter 3 that there is no natural criterion for threshold. Equation (3.45) can easily be modified to give (3.46): threshold occurs when the Stokes photon number grows to 1/y of the pump photon number. The method of sections 7.2 and 7.3 can easily be adapted to accommodate such a modification. The parameter y plays exactly the same roll as Q in determining Z_{min}. See equation (A1.17). The equal loss curve, (C) of Fig. 7.4 is merely translated up and to the left in the same way as would be expected for an increase in Q. The other curves (A), (B) and (D) to (J) would have to be recomputed each time the parameter y is adjusted.

From the point of view of the pump and Stokes evolution in the fibre, there is no natural value of y to choose. See Fig. 4.1. However, the decision could possibly be made by considering how strong a signal at a frequency shift $\Delta\nu$ from ν_ℓ that the detector can tolerate within acceptable error rate requirements.

So far attention has concentrated upon the relationship between the pump and Stokes wave. A possibly more useful criterion could arise from considering the pump wave by itself. A proposition for further research is thus to consider the derivative of the pump power. It can be seen from equation (4.5) and Fig. 4.1 that dR_ℓ/dZ is negative at all Z-values. However, there is some value of Z for which $|dR_\ell/dZ|$ is a maximum and hence the second derivative d^2R_ℓ/dZ^2 is zero. It can be shown from equations (4.5) and (4.6) that the criterion $d^2R_\ell/dZ^2 = 0$ is the equivalent to equation (7.4):

$$[\beta_\ell + (R_s + Q)]^2 + [\beta_s R_s - \Lambda R_\ell (R_s + Q)] = 0 \qquad (7.4)$$

One would thus use the condition (7.4) in conjunction with the method described in appendix 4. It is shown in section A1.2 that in the zero loss limit the threshold length is identical to that required for the criterion of equation (3.45) nevertheless, one would expect a different shape of curve to those of Fig. 7.4 for higher losses.

A final idea which was considered was to take as threshold that length such that the derivative of the pump wave is m times its original value at Z = 0. The problems are firstly, that there is no obvious choice for m and secondly, if m = 2 the zero loss theory of section A1.2.3 gives an infinite Z_{min}. The more promising approach would be to choose the zero second derivative criterion outlined above.

7.5 The design of optimised Raman prone fibres

The method considered in this chapter could in principle be extended to designing fibres so that they promote the most efficient possible Raman conversion. The differential equations (4.5) and (4.6) are solved for all length values until the derivative of the Stokes power is zero. This situation has been considered in section 3.8 for the equal loss case and in section A1.2.4 for the zero loss limit.

Reference

1. See for example: section 7 of Garrett, I. and Todd, C.J. "Components and systems for long-wavelength monomode fibre transmission", Optical and Quantum Electron. 14, 95 (1982).

8.1 Introduction

Some of the theoretical predictions of the previous chapters will now be compared with reported experimental observations of stimulated Raman scattering in optical fibres. No original experimental data due to the author is reported here. The experimental details are kept to a minimum. For further information the actual publications should be consulted.

Three topics are considered in sections 8.2 to 8.4: (a) the bandwidth of the amplified Stokes wave and thus the spontaneous Stokes power; (b) the relationship between the pump and Stokes power at output with the pump power at input; (c) the validity of the assumption used throughout that reflections from fibre ends, giving rise to resonances do not play a significant roll in the prediction of threshold power levels.

It will be shown in this chapter that the theoretical framework of the previous chapters agrees well with published experiments. It has not been possible to find any published data which contradicts any of the predictions in this thesis. The Stokes loss referred to is the effective Stokes loss. Where the effective core area is computed the Bessel/Hankel-function solutions of the weakly-guiding analysis are used.

8.2 The effective bandwidth and spontaneous Raman scattering

The Stokes spectral output due to amplified spontaneous scattering from a monomode fibre with a germania-silica core was observed by Ikeda[1]. The required data for computations are given as experiment 1 of table 8.1. The pump power is the average output power of an optical parametric oscillator (O.P.O.) radiating at 1.017μm. The pulse characteristics of the O.P.O. were not reported, but are assumed to be sufficiently long to be taken as approximately CW[2]. The fibre loss is not given and

CHAPTER EIGHT

COMPARISON OF THEORY WITH EXPERIMENT

Experiment number	Fibre length (km)	Maximum input power (W)	Core radius (μm)	Cut-off wavelength (μm)	λ_ℓ (μm)	λ_s (μm)	Effective core area (m^2)	Loss at λ_ℓ	Loss at λ_s	Semi-gain $(mW)^{-1}$	Calculated reflectivity by (8.1),%
1	1.3	>1.2	2.4	1.0	1.017	1.064	2.35×10^{-11}	Not stated	Not stated	4.8×10^{-14}	Not applicable
2	35	6.0	3.7	1.54	1.064	1.12	3.49×10^{-11}	1.13	Not stated	4.6×10^{-14}	$\mathcal{R}(\alpha_\ell)=8.3$
3	35	2.1	3.7	1.27	1.064	1.12 & 1.114	cannot be calculated	1.30	1.09	4.6×10^{-14}	$\mathcal{R}(\alpha_\ell)=97.5$ $\mathcal{R}(\alpha_s)=31.7$

TABLE 8.1 Data for the three experiments described in this chapter. The calculation of the effective core area in experiment 3 is beyond the scope of the thoery of chapter 6. The reflectivities in experiment 3 are calculated using the actual core area.

so guessed to be 1.0dB/km at all wavelengths of interest. The characteristics of the gain profile were assumed to be the same as those of pure silica.

By the use of equation (3.40) $B_{eff} = 66.7\ cm^{-1}$, which compares well with the experimentally observed value of 88 cm^{-1} (Fig. 3(d) in paper). The reported spectrum was highly spiked. Various explanations are possible, for example: competing nonlinear effects such as four-wave mixing, mutual coupling of some of the Stokes modes but not others, the fact that the fibre core was not pure silica, pulse-to-pulse irregularities in the output from the O.P.O. and resolution of the detecting instrumentation.

In a recent experiment[3] the power levels of a slightly amplified second-order Stokes wave grown from a spontaneous background were reported. A true comparison with theory is not possible because: (a) the second order Stokes wave is being stimulated by a first-order Stokes wave, which is a broad-band source and (b) it is not clear whether or not the laser pump would be fully saturated when the second spontaneous Stokes power is at the levels reported. When the input at the laser wavelength was 1 watt in the fibre, the observed slightly amplified 2nd Stokes power was 5×10^{-7} watts. The only conclusion to be drawn here is that such a value is of the order of magnitude that one would expect from the theory of section 3.4.

8.3 Power input-output relationships

As discussed in section 4.5, it is not convenient to test theoretical predictions by measuring pump and Stokes power output from a fibre which is successively shortened. In the experiments described here the fibre length was kept constant whilst the laser input power was varied. The computer program employed in section 4.5 was re-run with the data

for experiments 2 and 3 of table 8.1. These experiments were performed by Sasaki, et al[4] and Ohmori, et al[5], respectively.

In "experiment 2" a CW Neodymium-YAG laser radiating at 1064nm in the TEM_{00} mode was coupled into a fibre which operated exclusively at the LP_{01} mode at wavelengths greater than 1.54μm. The experimental arrangement was similar to that of Fig. 3.1. A mode stripper, consisting of the fibre coiled round a small radius drum and immersed in a bath of high refractive index liquid, was added after the input lens. Cladding and high order core modes were removed so that only the LP_{01} mode propagated. The fibre core was a silica germania composite glass, so that one might expect the gain characteristics to be different from those of pure silica. The gain in table 8.1 is the polarisation-corrected value for pure silica. The effective core area was calculated by the method of section 6.5.

The lowest Stokes power which could be detected by the power meter at the output end corresponded to a pump wave input of 0.6 Watts. Equality of pump and Stokes power were observed at an input level of 1.25 Watts and the first signs of a 2nd Stokes wave were with a 4.8 Watt input.

It has not been possible to obtain a good agreement between theory and experiment if the gain is taken to be that of pure silica as in table 8.1. However, if the gain is increased to 11.6×10^{-14} mW^{-1}, there is a convincing correlation. Fig. 8.1 is a graphical comparison of theoretical and experimental results. Compare with Figs. 4.6 and 4.7. The theoretical curves on Fig. 8.1 are computed numerical solutions to equations (4.1) and (4.2) where $g_o = 11.6\times10^{-14}$ mW^{-1}. The Stokes loss was not stated. It was found that the value which gave closest agreement between theory and experiment was $\alpha_s = 0.99\alpha_\ell = 1.12$dB. km^{-1}.

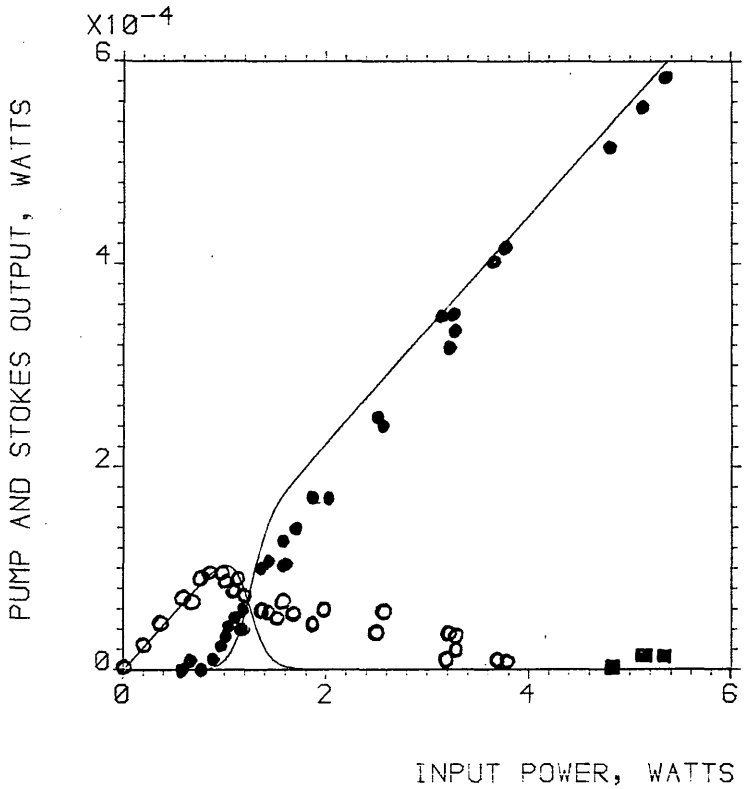

FIG. 8-1: COMPARISON WITH EXPREIMENT:
OUTPUT PUMP AND STOKES POWER AS A FUNCTION
OF THE INPUT PUMP POWER. THE FIBRE LENGTH
IS A CONSTANT.
RATIO OF LOSSES; STOKES TO PUMP = .99.
O PUMP POWER, ● 1st STOKES POWER,
■ 2nd STOKES POWER.
SEE TABLE 8-1 FOR THE OTHER DATA USED
IN COMPUTATIONS.

The most likely explanation for the large gain value required is the GeO_2 doping of the core. It has been reported[6] that the gain of pure germania is 7.4 times that of pure silica. In the fibre used in the experiment the relative core-cladding refractive index difference was 0.86%. One would thus expect a 8.3% GeO_2 concentration[7] in the core. If the scaling of gain with GeO_2 doping level is linear the gain of a 8.3% GeO_2 core is 7.0×10^{-14} mW^{-1}, which is closer to the value required for the best agreement with experiment. It should be noted that there is no reason to believe that the scaling of gain with GeO_2 concentration should be linear. However, the above calculation suggests that the presence of GeO_2 in the core could account for the necessity for an increased value of g_o to give good agreement with experiment.

It can be seen from Fig.8.1 that, although the curves and experimental data overlap well, there is a small difference in behaviour at pump and Stokes powers slightly above the cross-over threshold. The pump power is not depleted as rapidly as predicted and the Stokes power does not grow as rapidly as predicted. The most likely explanation is that discussed in section 6.7: the effective core area is variable with length for a fixed input power and variable with input power for a fixed length. The fact that there is a reasonable agreement between theory and experiment suggests that A is only slowly varying with P_o and the fact that the pump to Stokes conversion observed was less pronounced than the theoretical prediction suggests that A increases slightly with P_o.

The relative values of α_s and α_ℓ can be justified by modelling an 880 cm^{-1} range of Stokes losses as a straight line which decreases with an increase in wavelength. Use the theory of effective Stokes loss; equation (5.23), in which it is assumed that the maximum Stokes shift, 880 cm^{-1} is twice the shift of the peak. For a given input

power $\alpha_\ell \propto \beta_\ell$, $\alpha_s \propto \beta_s$ and $\alpha_{sm} \propto \beta_{sm}$, all with the same proportionality constant. Thus from (5.23), α_{sm} = 0.723 dB/dm and so $\alpha(\nu_s)$ = 0.927 dB/km. The loss at the peak Stokes wavelength was not reported, however the value calculated here is what one would expect at 1.12μm in SiO_2-GeO_2 fibres.[7]

In experiment 3 a mode locked, but not Q-switched Nd:YAG laser operating at 1.064μm was launched into an optical fibre with a 1.27μm cut-off. As above the core was SiO_2-GeO_2. The experimental equipment was that illustrated in Fig. 3.1. No mode-stripper was used.

The train of pulses at 1.064μm would normally differ in group velocity from the corresponding train at 1.120μm which they generate due to dispersion, causing pulse "walk-off". The problem was overcome by arranging that the pump wave propagated in LP_{11} (2nd order) fibre mode and the Stokes wave in the LP_{01} (1st order) fibre mode. By the use of the weakly guiding analysis[8] of modal dispersion in fibres, Ohmori, et al[5] showed that the transit time of a pulse at 1.064μm in the LP_{11}-mode is equal to the transit time of a pulse at 1.114μm in the LP_{01} mode. 1.114μm is equivalent to a frequency shift of 390 cm^{-1} and so does not correspond to the peak of the silica gain profile. See Fig. 2.7. It was found that at low input powers the output Stokes spectrum was centred upon 1.114μm and at higher powers (P_o > 1.65μm) the output was centred upon 1.120μm (440 cm^{-1} shift).

The experiment described here is outside the scope of this thesis because (a) the fibre is not monomode, (b) the Raman interaction is forced to operate at a frequency shift removed from the Stokes spectral centre and (c) the input laser is pulsed. However, it is shown that one can come close to accounting for the observed behaviour in terms of the two-wavelength model.

The smallest Stokes output detectable was with a 0.9 watt input, pump and Stokes equality was at 1.65 watts and the first signs of a 2nd order Stokes spectrum was at 1.95 watts. The sudden jump in peak Stokes wavelength occurred at an input power close to that which was necessary to obtain pump and Stokes equality (1.65 watts). The most likely reason for the sudden wavelength jump would appear to be that thermal absorption in the fibre gives rise to a slight change in refractive index and hence waveguiding properties. If so the fact that the jump occurs close to the input power which gives rise to equal pump and Stokes output is a coincidence.

The effective bandwidth, effective Stokes loss and effective core areas cannot be computed from the results of chapters 3, 5 and 6, respectively. When $P_o < 1.65$ W the gain is not that of the peak of the gain profile and in all cases the transverse modal overlap is between LP_{01} and LP_{11} modes. Thus in comparing theory with experiment the values of α_s and g_o/A in the two wavelength model of equations (4.1) and (4.2) were adjusted by trial and error to give the best agreement with experimental results.

Fig. 8.2 illustrates the comparison of theory with experiment. The pump loss α_ℓ and the wavelengths λ_ℓ and λ_s are those values given in table 8.1. The best fit with the experimental data were found when $\alpha_s = 0.81\ \alpha_\ell = 1.05$dB/km; $g_o/A\ (P_o < 1.65W) = 2.55 \times 10^{-3}$; $g_0/A\ (P_o > 1.65W) = 2.77 \times 10^{-3}$. The conclusion to be drawn from Fig. 8.2 is that, although the validity of the theoretical work in this thesis is not sufficiently wide-ranging to predict the appropriate values of the constants g_o, A and α_s to be used, the two-wavelength model in the form of (4.1) and (4.2) is a good representation of the physical process.

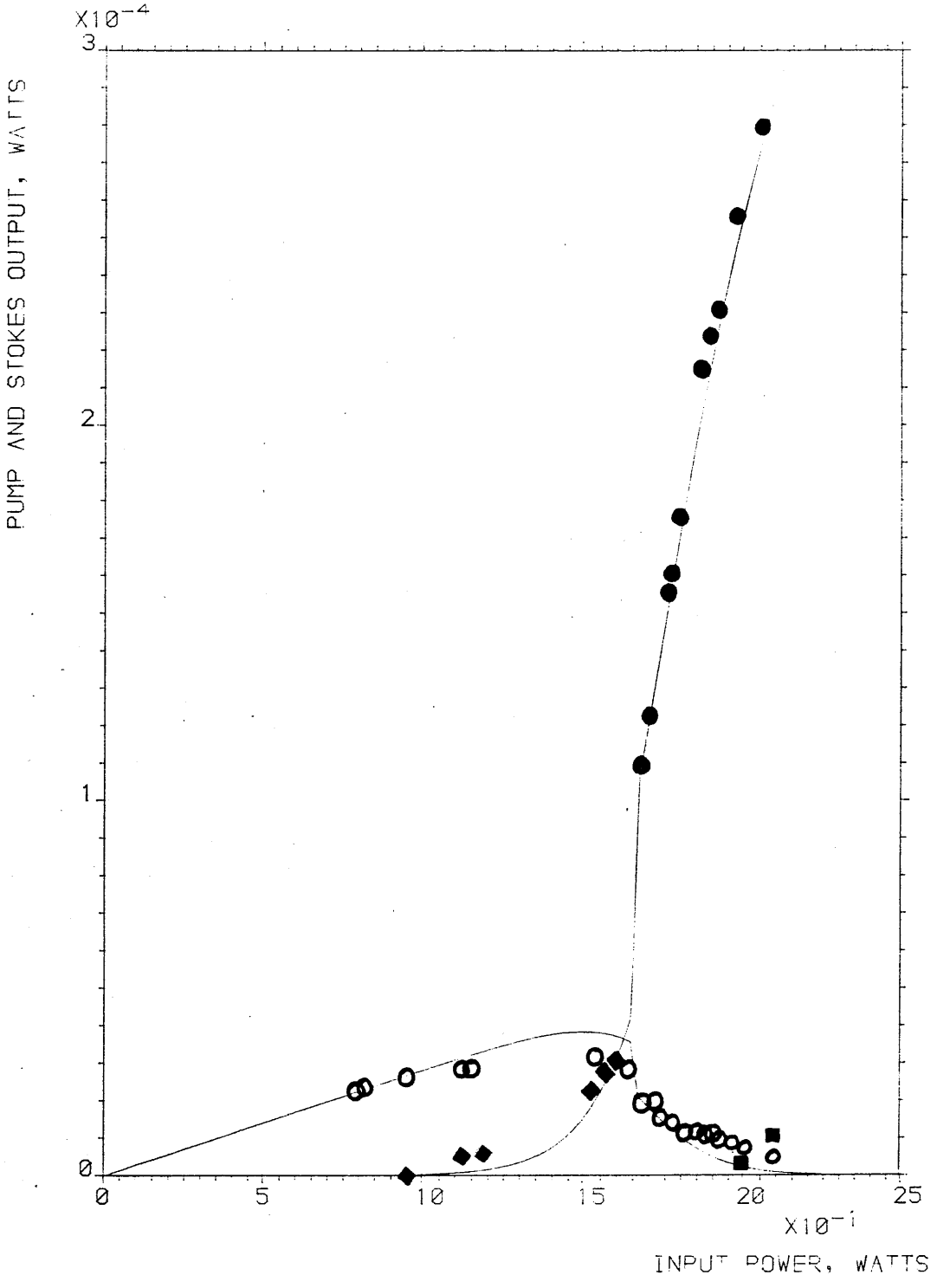

FIG. 8-2: COMPARISON WITH EXPERIMENT: OUTPUT PUMP AND STOKES POWER AS A FUNCTION OF THE INPUT PUMP POWER.
FIBRE LENGTH = 35000.0 METRES
RATIO OF LOSSES; STOKES TO PUMP = .81
○ PUMP POWER; ● 1st STOKES POWER AT 1.114 um;
◆ 1st STOKES POWER AT 1.12; ■ 2nd STOKES POWER.
SEE TABLE 8-1 FOR THE OTHER DATA USED IN COMPUTATIONS.

Finally, two further experiments are mentioned, but not described. Stolen[9] has shown that despite evidence of mutual Stokes longitudinal mode coupling, an equivalent analysis to that of chapter 3 gives a realistic prediction of threshold powers. Aoki, et al[10] have shown that the small signal analysis of Smith[11] gives good agreement with experiment at low input powers.

8.4 The possible effect of fibre end reflections

Assumption (d) of section 1.3 was that the effect of reflections from the fibre ends was negligible. Au Yeung and Yariv[12] developed a theory of fibre Raman oscillators which could be applied in such circumstances. The idea is that the small amount of light at the pump and Stokes wavelengths reflected from the fibre ends would participate in the interaction. The fibre would become a low-reflectivity resonant cavity and the threshold lowered as a result. The threshold[12] according to the criterion of equality of pump and Stokes power (not photon number) in physical units was shown to be:

$$P_{th} = \left(\frac{\alpha A}{g_o}\right)\left[\frac{\alpha L - \mathrm{Ln}(\Re)}{1 - \exp(-\alpha L)}\right] \qquad (8.1)$$

The losses at all wavelengths are equal to α. P_{th} is the threshold input pump power and L is the fibre length. It is assumed that the reflectivities of both ends are equal to $\Re$ at all wavelengths.

The hypothesis to be examined is that the threshold power in the two experimental situations described in section 8.3 were effected significantly by fibre reflections. The hypothesis is tested by solving equation 8.1 for $\Re$. If the hypothesis is correct then $\Re$ should have a value close to the 4% characteristic of an air-glass interface. The last two columns of table 8.1 give $\Re$ calculated from equations 8.1. In the second experiment α is α_ℓ and α_s, respectively. In neither case

are the predicted end reflectivities even within an order of magnitude of 4%. For a physically realisable oscillator $0 < \mathcal{R} < 1$. It is therefore proposed that reflection from the fibre ends is not an important mechanism in single pass stimulated Raman scattering. Approximation (d) in section 1.3 is thus a valid one.

References

1. Ikeda, M., "Stimulated Raman amplification characteristics in long-span single mode fibres", Optics Commun. 39, 148, (1981).
2. Stolen, R.H., "Nonlinear properties of optical fibres" in "Optical Fibre Telecommunications", Miller, S.E. and Chynoweth, A.G. (Eds.), Academic Press, New York, (1979).
3. Nakamura, K., Kimura, M., Yoshida, S., Hidaki, T., Mitsuhashi, Y., "Raman amplification of 1.50μm laser diode light in a low fibre loss region", J. Lightwave Technol. LT-2, 379, (1984).
4. Sasaki, Y., Ohmori, Y., Kawachi, M., Edahiro, T., "C.W. single-pass Raman generation in optical fibres", Electron. Lett., 17, 315, (1981).
5. Ohmori, Y., Sasaki, Y., Edahiro, T., "Single-pass Raman generation pumped by a mode-locked laser", Electron. Lett., 17, 595, (1981).
6. Galeener, F.L., Mikkelsen, J.C., Geils, R.H., Mosby, W.J., "The relative Raman cross-sections of viterous SiO_2: SiO_2; B_2O_3 and P_2O_5", Appl. Phys. Lett., 32, 34, (1978).
7. Garrett, I., Todd, C.J., "Components and systems for long-wavelength monomode fibre transmission", Optical and Quantum Electron., 14, 95 (1982).
8. Gloge, D.,"Dispersion in weakly guiding fibres", Appl. Opt., 10, 2442, (1971).
9. Stolen, R.H., Lee, C., Jain, R.K., "Development of stimulated Raman spectrum in single-mode silica fibres", J. Opt. Soc. Am., B1, 652, (1984).
10. Aoki, Y., Kishida, S., Honmou, H., Washio, K., Sugimoto, M., "Efficient backward and forward pumping C.W. Raman amplification for InGaAsP laser light in silica fibres", Electron. Lett., 19, 620, (1983).

11. Smith, R.G., "Critical power handling capacity of low loss optical fibres as determined by stimulated Raman and Brillouin scattering", Appl. Optics, 11, 2483, (1972).

12. Au Yeung, J., and Yariv, A., "Theory of C.W. Raman oscillation in optical fibres", J. Opt. Soc. Am., 69, 803, (1979).

CHAPTER NINE

CONCLUSIONS AND SUGGESTIONS FOR FURTHER RESEARCH

9.1 Conclusions

A summary of the subject matter of the thesis is given in section 1.2. Here the emphasis is upon the conclusions as they arose in the preceding chapters. Section 9.2 is a compilation of suggestions for further research arising from these conclusions.

The discussion of Raman gain profiles of optical fibre glasses in chapter 2 lead to a consideration of which mathematical function best represented the gain profile of pure silica. Three were considered: a parabola, a Lorentzian and a triangle. It was argued with the aid of a simple curve-fitting procedure that the most appropriate was the Lorentzian. Thus a Lorentzian model for the Raman gain was given preferential treatment in the remaining chapters. The mathematical treatments in the literature, to date have not argued explicitly why a Lorentzian is the best fit.

It was shown in chapter 3 that by the use of a dimensionless coordinate scheme the calculation of pump and Stokes power evolution can be simplified. In the derivation of appendix 2 the opportunity was taken to correct some algebraic mistakes that existed in the literature[1].

The following features appear in chapter 3 that are not in the original work on equal loss power evolution: (a) the most accurate expressions for $R_\ell(Z)$ and $R_s(Z)$ are in terms of the special function Mei, (see appendix 2) but can be approximated by exponentials (b) the effective bandwidth was calculated from a triangular gain profile, (c) threshold lengths were calculated according to the more general criterion of Stokes power growing to 1/y of the pump, (d) the relationship between the minimum length and the maximum loss at which threshold can occur, $Z_{min} = 1/\beta_{max}$ is general for all gain profiles and values of y.

Chapter 4 is the first study of power evolution in fibres solved by the two wavelength model with unequal losses which does not resort to a small signal analysis[2]. The negative conclusion was that there is unlikely to be an exact analytical solution. However, the positive conclusions were (1) that it is possible to describe power transfer and dissipation from the system without an analytic solution, (2) when the Stokes loss is much greater than the pump loss there is considerable depletion of the pump wave, despite negligible Stokes wave growth, and (3) by varying the initial condition for the pump power and keeping the length constant one can describe the power input-output relationships at the pump and Stokes wavelengths. The importance of (2) is that one must reconsider the condition for threshold, whilst the importance of (3) is that one has a method suitable for direct comparison of theory with experiment. The physical interpretation of the analytical expression for the power input-output relationships for the unequal loss case was considered. This was not discussed by Au Yeung and Yariv[1].

The examination of the variation of the Stokes spectrum with respect to Stokes loss in chapter 5 demonstrated that the spectral distribution changed little from a Gaussian when the gradient of a linear loss profile was increased. The only significant effect was a reduction in the peak Stokes magnitude. In chapter 5 it was shown for the first time that the multiwavelength model can be reduced to a two wavelength model for total power when there is a variation of loss over the range of wavelengths covered by the gain profile. In order to do so, it is necessary to adopt the concept of an effective Stokes loss. The effective Stokes loss was derived for the particular case of a linear loss profile, which was found to agree well with numerical computation. The importance of the reduction to a two wavelength model is an increase in computation speed.

The effective core area was derived in chapter 6 from the multi-wavelength model of S.R.S. Prior to this work the effective core area had only been derived from a two-wavelength small signal model. It was therefore possible, using both Gaussian and weakly-guiding approximations to the transverse energy distribution, to describe the variation of the effective core area with respect to frequency shift under the gain profile. The main conclusion of chapter 6 (which has not been considered before) is that one single value of the effective core area can be chosen for use in the two wavelength model. One chooses the effective core area calculated from the overlap integral between the transverse energy distributions of the pump and peak Stokes fields. The Lorentzian lineshape function is weighted but it is argued that the resulting change of the effective bandwidth and hence spontaneous power is negligible.

Chapter 7 was a discussion of a novel design method. The design of source fibre and detector systems were easily understood in terms of the locus of fibre lengths, as a function of pump loss which satisfy the chosen threshold criterion. In chapter 7 attention was concentrated upon the criterion of pump and Stokes photon number equality. It was shown that when the receiver sensitivity and S.R.S. threshold length are considered, the optimum loss for Raman-free transmission is $\beta_{\ell max}$, the maximum loss that will satisfy the threshold criterion. In the case where the pump and Stokes losses are equal there is a simple algebraic expression for the optimum transmission length at $\beta_{\ell max}$.

In chapter 8 the theoretical basis of this thesis was compared with published experimental results. There is generally good agreement with the two wavelength model, although there are indications that a length dependence of effective core area (see section 6.7) may influence the pump and Stokes power levels. The models for effective bandwidth and

hence spontaneous power give numerical values which are consistent with experimental data. Finally, the effect of reflection from fibre ends was shown to be insignificant.

In this thesis the theoretical analysis of stimulated Raman scattering has been significantly extended so that it is now possible to predict with some degree of confidence the Raman threshold in a practical long distance communication system.

9.2 Suggestions for further research

It was found in chapter 2 that the gain profile of silica could reasonably be modelled by a Lorentzian. There is little in the literature about the gain of other materials of actual or porential importance to optical communications. The absolute values of gain are of special significance. The variation of the profile of silica with the percentage of germania doping would be an experiment of particular interest. One could use the technique of section 2.5 to find empirical mathematical representations. Various workers[3] have suggested that future generations of fibres could be made of vitreous or crystalline media not based upon silica, offering exceptionally low losses at mid-infra red wavelengths. A knowledge of the gain characteristics[4] of such media would therefore be required.

The suggestion for further work which arose from chapter 5 was to calculate effective Stokes losses due to more complicated loss profiles. Two important empirical loss profiles would be (a) higher order polynomials, starting with the quadratic function and (b) the Lorentzian form. The constants in these functions are adjustable and could model, for example, the infrared absorption edge at long wavelengths and the 1.38μm OH-overtone in silica, respectively. Obviously, the degree of difficulty of calculating the effective Stokes loss would increase with the degree

of complexity of the empirical model for the loss profile.

The main assumption employed in chapter 6 was that the effective core area remains constant at all fibre lengths. It was ascertained from chapter 8 that whilst this may be a good first approximation, there is experimental evidence to suggest that it may lead to minor inaccuracies in the prediction of threshold length. There is obviously a need for theoretical clarification.

The extension to the work of chapter 7 of immediate importance is to consider the second derivative criterion of S.R.S. threshold (see section 7.5). It would also be useful to find an empirical relationship between the maximum pump loss and the minimum length for threshold in circumstances where the pump and Stokes losses are unequal. An exact relationship is unlikely to be found if the two wavelength unequal-loss model cannot be solved analytically.

Further work required is suggested from the list of assumptions in section 1.3. Recently there have been various treatments of S.R.S. when the Stokes input is not only from noise.[5,7,8,9] There is a second "signal" laser at some wavelength within the Raman gain profile. Such circumstances are of particular importance for wavelength division multiplexing. The concepts developed here for example the effective Stokes loss and the design method, would have to take such circumstances into account. Finally, a multiwavelength model which included second order Stokes growth would allow more accurate assessment of the first Stokes power evolution at long lengths of fibre. The extra difficulty that would arise is that the first order Stokes radiation (which stimulates the second order Stokes growth) cannot be approximated as a narrow linewidth source.

References

1. Au Yeung, J. and Yariv, A., "Spontaneous and stimulated Raman scattering in long low loss fibres", I.E.E.E. J. Quantum Electron. QE-14, 347, (1978).

2. Smith, R.G., "Critical power handling capacity of low loss optical fibres as determined by stimulated Raman and Brillouin scattering", Appl. Optics, 11, 2489, (1972).

3. Miyashita, T., Toyotaka, T., "Infra-red optical fibres", I.E.E.E. J. Quantum Electron., QE-18, 1432, (1982).

4. Heiman, D., Hellwarth, R.W., Hamilton, D.S., "Raman scattering and nonlinear refractive index measurements of optical glasses", J. Non-Crystalline solids, 34, 63, (1979).

5. Nakamura, K., Kimura, M., Yoshida, S., Hidaka, T, and Mitsuhashi, Y., "Raman amplification of 1.50μm laser diode light in a low fibre loss region", I.E.E.E. J. Lightwave Technology, LT-2, 379, (1984).

6. Aoki, Y., Kishida, S., Honmuou, H., Washio, K., Sugimoto, M. "Efficient backward and forward pumping CW Raman amplification for InGaAsP laser light in silica fibres", Electron. Lett., 19. 620, (1983).

7. Hill, A.M., Cotter, D. and Wright, J.V., "Nonlinear crosstalk due to stimulated Raman scattering in a two-channel wavelength-division-multiplexed system", Electron. Lett., 20, 247, (1984).

8. Chraplyvy, A.R., "Optical power limits in multi-channel wavelength-division-multiplexed systems due to stimulated Raman scattering", Electron. Lett., 20, 58, (1984).

9. Tomita, A., "Cross talk caused by stimulated Raman scattering in single-mode wavelength-division multiplexed systems", Optics. Lett., 8, 412, (1983).

APPENDICES

APPENDIX ONE: THE ZERO LOSS LIMIT FOR STIMULATED RAMAN SCATTERING

A1.1 Evolution of the pump and Stokes power

The two wavelength model, in the form of equations (3.15) and (3.16), is restated in the case where β is set to zero. See equations (A1.1) and (A1.2):

$$\frac{dR_\ell}{dZ} = - R_\ell(R_s + Q) \qquad \text{(A1.1)}$$

$$\frac{dR_s}{dZ} = \Lambda R_\ell(R_s + Q) \qquad \text{(A1.2)}$$

The effective bandwidth, B_{eff} and hence the spontaneously scattered power, Q are calculated from a rectangular model of the Raman gain profile. B_{eff} is thus independent of loss. See section 3.4.

Add the product of equation (A1.1) and Λ to equation (A1.2) to give:

$$\frac{d}{dZ}(\Lambda R_\ell + R_s) = 0 \qquad \text{(A1.3)}$$

so that:

$$\Lambda R_\ell + R_s = C$$

In (A1.4) C is a constant which is determined from the initial conditions, equations (3.17) and (3.18). Thus:

$$\Lambda R_\ell + R_s = \Lambda + Q \qquad \text{(A1.5)}$$

Equation (A1.4) and hence (A1.5) is a statement of conservation of photon number in the fibre. The power $(1 - \Lambda)R_\ell$ is absorbed by the molecular scattering centres.

Now substitute (A1.5) into (A1.1) to give:

$$\frac{dR_\ell}{dZ} + R_\ell(\Lambda + 2Q) = \Lambda R_\ell^2 \qquad \text{(A1.6)}$$

Equation (A1.6) has been decoupled. R_ℓ is the only dependent variable. There is an equivalent decoupled equation with R_s as the only dependent variable:

$$\frac{dR_s}{dZ} = \Lambda R_s + Q(\Lambda + Q) - R_s^2 \qquad \text{(A1.7)}$$

Both equations (A1.6) and (A1.7) are nonlinear, first order differential equations with constant coefficients. Equation (A1.6) is a Bernoulli equation and equation (A1.7) is a Ricatti equation. They should be compared with equations (3.21) and (3.22) respectively. Both equations (A1.6) and (A1.7) are capable of being reduced to linear differential equations[A1]. The Bernouilli equation yields a more straight-forward solution.

Make the substitution $R_\ell = 1/x$:

$$\frac{dx}{dZ} - x(\Lambda + 2Q) = -\Lambda \qquad \text{(A1.8)}$$

Equation (A1.8) is a standard linear first order differential equation with constant coefficients. One uses the integrating factor method of solution to give:

$$x = \exp[(\Lambda + 2Q)Z]\left(C' - \Lambda \int \exp[-(\Lambda + 2Q)Z]dZ\right)$$

so
$$x = C'\exp[(\Lambda + 2Q)Z] + \frac{\Lambda}{(\Lambda + 2Q)} \qquad \text{(A1.9)}$$

C' is a constant to be determined from the initial conditions, (3.17) and (3.18). When Z = 0:

$$C' = \frac{2Q}{\Lambda + 2Q}$$

Now Q is several orders of magnitude smaller than Λ, so

$$C' \doteq \frac{2Q}{\Lambda} \qquad \text{(A1.10)}$$

Substitute (A1.10) into (A1.9) and again use the fact that $Q << \Lambda$ to give (A1.11):

$$x \doteq 1 + (\frac{2Q}{\Lambda})\exp(\Lambda Z) \qquad \text{(A1.11)}$$

Use the fact that $R_\ell = 1/x$ to obtain the variation of normalised power with respect to the dimensionless Z-coordinate:

$$R_\ell(Z) = \frac{1}{1 + (\frac{2Q}{\Lambda})\exp(\Lambda Z)} \qquad \text{(A1.12)}$$

Now, in order to obtain the equivalent equation for $R_s(Z)$ one does not have to go back to (A1.7) and solve. A much simpler method is to use the conservation condition, (A1.5) to give:

$$R_s(Z) = Q + \Lambda[1 - (1 + (\frac{2Q}{\Lambda})\exp(\Lambda Z))^{-1}]$$

$$\doteq Q + \frac{\Lambda(\frac{2Q}{\Lambda})\exp(\Lambda Z)}{1 + (\frac{2Q}{\Lambda})\exp(\Lambda Z)} \qquad \text{(A1.13)}$$

Equations (A1.12) and (A1.13) describe the evolution of pump and Stokes power, respectively. They should be compared to (3.24) and (3.25), respectively, in conjunction with (3.26).

Equations (A1.12) and (A1.13) can be converted to physical coordinates, by the use of equations (3.9) to (3.14), inclusive to give:

$$P_\ell = P_o[1 + \frac{2qp}{P_o}(\frac{\lambda_s}{\lambda_\ell})\exp(\frac{\lambda_\ell}{\lambda_s}\ \frac{P_o g_o z}{A})] \qquad \text{(A1.14)}$$

and also:

$$P_s = P_o(\frac{\lambda_\ell}{\lambda_s})[1 - (1 + \frac{2qp}{P_o}(\frac{\lambda_s}{\lambda_\ell})\exp(\frac{\lambda_\ell}{\lambda_s}\ \frac{P_o g_o z}{A}))^{-1}] \qquad \text{(A1.15)}$$

As usual the dimensionless equations have a more elegant appearance.

Now, going back to (A1.12) and (A1.13) it is worth considering when Z = 0:

$$R_\ell(Z = 0) = \frac{1}{1 + (2Q/\Lambda)} \doteq 1 \quad (\text{As } Q << \Lambda)$$

and

$$R_s(Z = 0) = Q + \Lambda[1 - \frac{1}{1 + \frac{2Q}{\Lambda}}] \doteq Q$$

The reason why R_ℓ and R_s are not exactly equal to 1 and Q, respectively, as the initial conditions require, is because of the fact that $Q << \Lambda$ was used in approximations to obtain (A1.12) and (A1.13).

Equations (A1.12) and (A1.13) are the most important results of appendix 1. They are used to produce the solid line curves of Fig. A1.1. The superposed dotted line curves are as a result of numerical computations by the method discussed in chapter 4.

A1.2 Conditions for threshold and optimal conversion in the zero loss limit:

Three threshold conditions and one condition for optimal conversion are considered.

A1.2.1 Ratio of Stokes to pump power:

The threshold length is that fibre length such that the Z-coordinate reaches a value such that:

$$\text{(Stokes power)} = \Lambda/y \text{ (pump power)}$$

Then $Z = Z_{th}^{(1)}$. R_{th} is the normalised pump power at threshold. Using equation (A1.5):

$$\Lambda R_{th} + \frac{R_{th}}{\Lambda y} = \Lambda + Q$$

$$\text{Thus } R_{Th} = \frac{\Lambda^2 + Q}{\Lambda^2 + 1/y} \doteq \frac{y\Lambda^2}{y\Lambda^2 + 1} \qquad \text{(A1.16)}$$

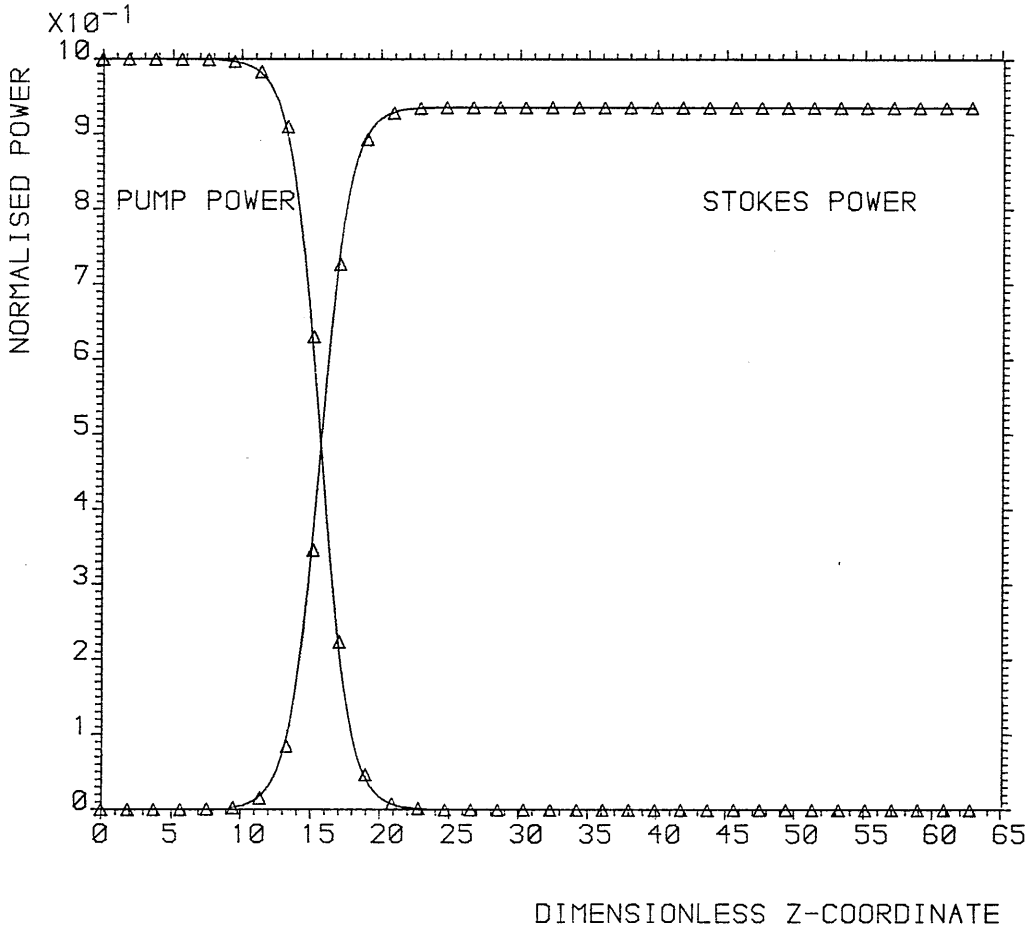

FIG. A1-1 VARIATION OF THE PUMP AND STOKES POWER WITH RESPECT TO LENGTH IN THE ZERO LOSS LIMIT. SOLID LINES: ANALYTICAL SOLUTION; TRIANGLES: NUMERICAL SOLUTIONS.
SEE TABLE 3-1 FOR DATA USED IN COMPUTATIONS.

Now substitute (A1.12) into (A1.16):

$$y\Lambda^2 + 1 = y\Lambda^2[1 + \frac{2Q}{\Lambda} \exp(\Lambda Z^{(1)}_{th})]$$

Thus

$$Z^{(1)}_{th} = \frac{1}{\Lambda} \text{Ln}[\frac{1}{2Q\Lambda y}] \qquad \text{(A1.17)}$$

Equation (A1.18) is the equivalent equation to (A1.17) in physical coordinates:

$$Z^{(1)}_{th} = \frac{\lambda_s}{\lambda_\ell} \frac{A}{P_o g_o} \text{Ln}[\frac{\lambda_s}{\lambda_\ell} \frac{P_o}{2qy}] \qquad \text{(A1.18)}$$

A1.2.2 Zero second derivative of the pump wave:

By the use of equations (3.9) and (3.12) it is a simple matter to show that:

$$\frac{d^2P_\ell}{dZ^2} = 0 \quad \text{and} \quad \frac{d^2R_\ell}{dZ^2} = 0$$

are equivalent conditions.

Differentiate equation (A1.1) with respect to Z to give:

$$\frac{d^2R_\ell}{dZ^2} = -\frac{dR_\ell}{dZ}(R_s + Q) - R_\ell \frac{dR_s}{dZ}$$

$$= R_\ell(R_s + Q)[R_s - \Lambda R_\ell + Q] \qquad \text{(A1.19)}$$

Now R_ℓ, R_s and Q must at all times be positive. So the second derivative can only be zero if

$$R_s - \Lambda R_\ell + Q = 0$$

For the second derivative criterion to be a useful one, one would expect the Stokes wave to have grown several orders of magnitude greater than Q, consequently the condition becomes

$$R_s = \Lambda R_\ell \qquad \text{(A1.20)}$$

Again by the use of equations of (A1.13) and (A1.14) it can be shown that:

$$Z_{th}^{(2)} = (\frac{1}{\Lambda}) \text{Ln} [\frac{1}{2Q\Lambda}] \qquad \text{(A1.21)}$$

Equation (A1.21) is the same as equation (A1.17) in the case where $y = 1$. In the zero loss limit the second derivative of the pump power is zero, at the same fibre length when the Stokes wave has been amplified to such a level that it is equal to the pump wave.

A1.2.3 The derivative of the pump power is m times its initial value:

At $Z = 0$ $$\frac{dR_\ell}{dZ} = mQ$$

so $$- R_\ell (R_s + Q) = mQ$$

so $$R_\ell = \frac{mQ}{R_s + Q}$$

Now from equations (A1.12) and (A1.13):

$$Q + \Lambda[1 - \{1 + (\frac{2Q}{\Lambda}) \exp(\Lambda Z_{th}^{(3)})\}^{-1}] = mQ[1 + (\frac{2Q}{\Lambda}) \exp(\Lambda Z_{th}^{(3)})]$$

Thus $$\frac{mQ + \Lambda}{2Q + \Lambda} = 1 + (\frac{2Q}{\Lambda}) \exp(\Lambda Z)$$

and so $$Z_{th}^{(3)} \doteq \frac{1}{\Lambda} \text{Ln} [\frac{m}{2} - 1] \qquad \text{(A1.22)}$$

If $m = 2$ $Z_{th}^{(3)}$ becomes infinite.

A1.2.4 Optimal conversion:

Optimal conversion to Stokes power occurs when $\frac{dR_s}{dZ} = 0$, that is when the Stokes power has reached its maximum value. From equation (A1.2)

$$\Lambda R_\ell (R_s + Q) = 0$$

which can only occur when $R_\ell = 0$, or $R_s = -Q$. Neither condition is possible at finite fibre lengths. In the zero loss limit the optimal conversion length is infinite. It can be seen from Fig. A1.1 that as Z approaches infinity R_s asymptotically approaches Λ.

Reference

A1.1 Davis, H.T., Introduction to nonlinear differential and integral equations. Dover, New York, 1962. Chapter 2 section 7 and chapter 3.

APPENDIX TWO: MATHEMATICAL DERIVATIONS ARISING FROM CHAPTER THREE

A2.1 Mathematical details of the derivation of the power evolution equations of section 3.3

Equations (3.21) and (3.22) are nonlinear with only one dependent variable each. The coefficients of the linear terms in R_ℓ and R_s, respectively are non-constant. Compare with equations (A1.7) and (A1.8). Equation (3.21) is a so called Bernoulli equation and (3.22) is a so called Riccatti equation[A1]. Given the choice, the solution of a Bernoulli equation is in general simpler. One wants to linearise equation (3.21) by substituting $R_\ell = 1/x$.

$$\frac{dx}{dZ} - x(\beta + Q + \Lambda\exp(-\beta Z)) = -\Lambda \qquad \text{(A2.1)}$$

Equation (A2.1) is now a first order inhomogeneous linear differential equation with one non-constant coefficient. By the use of the integrating factor:

$$\exp\{-\int(\beta + Q + \Lambda\exp(-\beta Z))dZ\}$$

giving:

$$x = \exp[(\beta + Q)Z - (\frac{\Lambda}{\beta})\exp(-\beta Z)][C + x_1] \qquad \text{(A2.3)}$$

where

$$x_1 = -\Lambda\int[\exp(-(\beta + Q)Z + (\frac{\Lambda}{\beta})\exp(-\beta Z))]dZ \qquad \text{(A2.4)}$$

The derivation to this point has followed that of Au Yeung and Yariv[A2], but has been re-stated in dimensionless coordinates. Their method of integrating (A2.4) by parts is not followed. Instead use substitution(A2.5) straight away.

$$u = (\frac{\Lambda}{\beta})\exp(-\beta Z) \qquad \text{(A2.5)}$$

so that:

$$x_1 = \int (\frac{\beta u}{\Lambda})^{Q/\beta} \cdot \exp(u)du \qquad \text{(A2.6)}$$

Now expand exp(u) as a Maclauren series and integrate to give:

$$x_1 = (\frac{\beta}{\Lambda})^{Q/\beta} \sum_{\ell=0}^{\infty} \frac{u^{Q/\beta + \ell + 1}}{\ell![Q/\beta + \ell + 1]}$$

$$= (\frac{\beta u}{\Lambda})^{Q/\beta} \{x_2 + x_3\} \qquad \text{(A2.7)}$$

where $$x_2 = \sum_{\ell=0}^{\infty} \frac{u^{\ell + 1}}{(\ell + 1)!} = \exp(u) - 1 \qquad \text{(A2.8)}$$

and $$x_3 = u[\frac{1}{1 + Q/\beta} - 1] + \frac{u^2}{1!}[\frac{1}{2 + Q/\beta} - \frac{1}{2}]$$

$$+ \frac{u^3}{2!}[\frac{1}{3 + Q/\beta} - \frac{1}{3}] + \ldots\ldots$$

$$\doteq -(\frac{Q}{\beta}) \sum_{\ell=0}^{\infty} \frac{u^{\ell + 1}}{(\ell + 1)!(\ell + 1)}, \qquad \text{(A2.9)}$$

since $Q/\beta << 1$.

Now substitute into equations (A2.7) and (A2.3):

$$x = \exp[(\beta + Q)Z - (\frac{\Lambda}{\beta})\exp(-\beta Z)][C + \exp(u) - 1$$

$$-(\frac{Q}{\beta}) \sum_{\ell=0}^{\infty} \frac{u^{\ell + 1}}{(\ell + 1)(\ell + 1)!}](\frac{\beta u}{\Lambda})^{Q/\beta} \qquad \text{(A2.10)}$$

The term $(\frac{\beta u}{\Lambda})^{Q/\beta} \doteq 1$ for all u since $Q/\beta << 1$.

Using (A2.5) as well as the initial condition, (3.17) it can be seen that when Z = 0:

$$x = 1 = \exp(-\frac{\Lambda}{\beta})[C + \exp(\frac{\Lambda}{\beta}) - 1 - (\frac{Q}{\beta}) \sum_{\ell=0}^{\infty} \frac{(\Lambda/\beta)^{\ell+1}}{(\ell + 1).(\ell + 1)!}]$$

Thus the integration constant, C becomes:

$$C = 1 + (\frac{Q}{\beta}) \sum_{\ell=0}^{\infty} \frac{(\Lambda/\beta)^{\ell+1}}{(\ell + 1)(\ell + 1)!}$$

So using (A2.5):

$$x = \exp(\beta Z)[1 + (\frac{Q}{\beta})\exp[-(\frac{\Lambda}{\beta})\exp(-\beta Z)]$$

$$\sum_{\ell=0}^{\infty} \frac{(\Lambda/\beta)^{\ell+1}[1 - \exp\{-(\ell + 1)\beta Z\}]}{(\ell + 1).(\ell + 1)!}] \qquad \text{(A2.11)}$$

Consider the series in (A2.9): this series arises from the integration;

$$\text{Mei}(u) = \int_{-\phi}^{u} (\frac{e^{v} - 1}{v})\, dv. \quad \text{(using a Maclauren expansion)}$$

Mei(u) is designated here as the "modified exponential integral". Mei(u) converges for all u and does so more rapidly than the series (A2.8). The magnitude of the terms in x_3 are considerably smaller than their counterparts in x_2 (see Abramowitz and Stegun[A3]). (A2.9) cannot be expressed in terms of simple analytic functions. By the use of the ratio test[A4] it can be seen that, like the exponential function, there is no restriction upon the values of u required for convergence. It can easily be seen that for all positive u:

$$\sum_{\ell=0}^{\infty} \frac{u^{\ell+1}}{(\ell + 1)!} > \sum_{\ell=0}^{\infty} \frac{u^{\ell+1}}{(\ell + 1).(\ell + 1)!} > \frac{1}{u} \sum_{\ell=0}^{\infty} \frac{u^{\ell+2}}{(\ell + 2)!}$$

That is:

$$e^{u} - 1 > \text{Mei}(u) > \frac{e^{u}-1}{u} - 1$$

when u is small $Mei(u) \doteq e^u - 1$

$Mei(0) = 0$

When u is large $Mei(u) \doteq \frac{e^u - 1}{u} - 1 = \frac{e^u}{u}$

For u = 5, 10, 15 and 20 Mei(u) differs from $(e^u)/u$ by 40.6%, 13.0%, 7.8% and 5.5%, respectively.

Thus from (A2.11):

$$x = \exp(\beta Z)\left[1+\left(\frac{Q}{\beta}\right)\exp\left[-\left(\frac{\Lambda}{\beta}\right)\exp(-\beta Z)\right]\right]\left\{Mei\left(\frac{\Lambda}{\beta}\right)-Mei\left(\frac{\Lambda}{\beta}\exp(-\beta Z)\right)\right\}$$

When β is small the arguments of the modified exponential integrals are large. In that case for all except low Z-values $Mei(\Lambda/\beta) >> Mei((\Lambda/\beta)\exp(-\beta Z))$ and using the fact that $Mei(\Lambda/\beta) \doteq \exp(\Lambda/\beta)/(\Lambda/\beta)$:

$$x \doteq \exp(-\beta Z)\left[1 + \left(\frac{Q}{\beta}\right)\exp\left[\left(\frac{\Lambda}{\beta}\right)(1-\exp(-\beta Z))\right]\right]$$

By using the fact that $R_\ell = 1/x$:

$$R_\ell(Z) = \frac{\exp(-\beta Z)}{1 + \eta(Z)} \qquad \text{(A2.12)}$$

where $$\eta(Z) = \frac{Q}{\beta}\exp\left[-\frac{\Lambda}{\beta}\exp(-\beta Z)\right]\left\{Mei\left(\frac{\Lambda}{\beta}\right)-Mei\left(\frac{\Lambda}{\beta}\exp(-\beta Z)\right)\right\} \qquad \text{(A2.13)}$$

Which in the small β approximation becomes:

$$\eta(Z) \doteq \left(\frac{Q}{\Lambda}\right)\exp\left[\frac{\Lambda}{\beta}(1-\exp(-\beta Z))\right] \qquad \text{(A2.14)}$$

The solution for $R_s(Z)$, the Stokes power, can be found easily by the use of equation (3.20):

$$R_s(Z) = \frac{\Lambda\eta\exp(-\beta Z)}{1 + \eta} \qquad \text{(A2.15)}$$

A2.2 Calculations of effective bandwidths for Raman gain profiles

In all calculations one commences by performing the integration in equation (3.34) and dividing the result by R_{si} (see equation (3.30).

Triangular gain profile:

The specification of the right angle triangle function is given by (2.12). Integrate between the pump and cut-off frequencies:

$$R_s(Z) = \frac{h}{\Lambda P_o} \exp(-\beta Z) \int_{\nu_\ell}^{\nu_s} \nu \exp\left(\frac{\Lambda(\nu-\nu_\ell)}{\beta\Delta\nu}\right) d\nu \qquad \text{(A2.16)}$$

substitute $u = \frac{\Lambda(\nu-\nu_\ell)}{\beta\Delta\nu}$:

$$R_s(Z) = h\beta\Delta\nu \exp(-\beta Z) \int_0^{\Lambda/\beta} \left(\frac{u\beta\Delta\nu}{\Lambda} + \nu_\ell\right) \exp(u)\, du$$

By using simple approximations arising from the fact that $\beta \ll 1$ and $\Delta\nu < \nu_\ell$ it can be shown that:

$$R_s(Z) \doteq \frac{h\nu_s}{\Lambda^2 P_o} \beta\Delta\nu \exp(-\beta Z + \Lambda/\beta) \qquad \text{(A2.17)}$$

Then compare (A2.17) with (3.30) and identify:

$$B_{eff} = \frac{\beta\Delta\nu}{\Lambda} \qquad \text{(A2.18)}$$

for a triangular gain profile.

Parabolic gain profile:

The parabolic gain function is given by (2.11). It is evaluated between the points where the parabola intersects the frequency axis, $\nu_s \pm \delta\nu/2$.

$$R_s(Z) = \frac{h}{\Lambda P_o} \exp(-\beta Z + \frac{\Lambda}{\beta}) \int_{\nu_s-\delta\nu/2}^{\nu_s+\delta\nu/2} \nu \exp\left[-\frac{\Lambda}{\beta}\left(\frac{\nu-\nu_s}{\delta\nu/2}\right)^2\right] d\nu \qquad \text{(A2.19)}$$

Substitute $u = \sqrt{\frac{\Lambda}{\beta}}\left(\frac{\nu-\nu_s}{\delta\nu/2}\right)$ to give:

$$R_s(Z) = \frac{2h}{\Lambda P_o}\left(\frac{\delta\nu}{2}\right)\exp\left(-\beta Z + \frac{\Lambda}{\beta}\right)\int_0^{\sqrt{(\Lambda/\beta)}} \left(\sqrt{(\Lambda/\beta)}.(\delta\nu/2)u+\nu_s\right).\exp(-u^2)du$$

$$= \frac{2h}{\Lambda P_o}\sqrt{\frac{\Lambda}{\beta}}.\left(\frac{\delta\nu}{2}\right)\exp\left(-\beta Z + \frac{\Lambda}{\beta}\right)\left[\nu_s\frac{\sqrt{\pi}}{2}\,\mathrm{erf}\left(\sqrt{(\Lambda/\beta)}\right)-\sqrt{(\beta/\Lambda)}\left(\frac{\delta\nu}{2}\right)+\sqrt{(\beta/\Lambda)}\left(\frac{\delta\nu}{2}\right)\exp\left(-\frac{\Lambda}{\beta}\right)\right],$$

where erf is the error function. For numbers greater than 3 the error function is unity to better than 4 decimal places. In many cases of interest $\sqrt{(\Lambda/\beta)} > 3$. In all cases $(\delta\nu/2) < \nu_s$.

Thus to a good approximation:

$$R_s(Z) = \frac{h}{\Lambda P_o}\,\nu_s\left(\frac{\pi\beta}{4\Lambda}\right)^{\frac{1}{2}}\delta\nu\exp(-\beta Z + \Lambda/\beta)$$

And so identify the effective bandwidth:

$$B_{eff} = \left(\frac{\pi\beta}{4\Lambda}\right)^{\frac{1}{2}}\delta\nu \qquad \text{(A2.20)}$$

References

A1 Davis, H.T. "Introduction to nonlinear differential and integral equations". Dover, New York 1962.

A2 Au Yeung, J. and Yariv, A., "Spontaneous and stimulated Raman scattering in long low loss fibres", IEEE J. Quantum Electron, QE-14, 347 (1978).

A3 Abramowitz, M and Stegun, I. "Handbook of mathematical functions", National Bureau of Standards.

APPENDIX THREE: ATTEMPTED ANALYTICAL SOLUTIONS TO THE TWO WAVELENGTH MODEL WITH UNEQUAL LOSSES

A3.1 Attempted solution by further use of $\varepsilon(Z)$

The first method considered for solving equations (4.5) and (4.6) was to de-couple using the normalised coupling parameter, $\varepsilon(Z)$. From equation (4.8) it can be seen that:

$$R_s = \Lambda R_\ell \left(\frac{\gamma - \beta_\ell}{\beta_s - \gamma}\right) \tag{A3.1}$$

From the definition of $\varepsilon(Z)$, equation (4.16):

$$R_s = \Lambda R_\ell \left(\frac{1-\varepsilon}{\varepsilon}\right) \tag{A3.2}$$

It should be noted that ε is an undetermined function of Z.

Substitute equation (A3.2) into (4.5) to give

$$\frac{dR_\ell}{dZ} + (\beta_\ell + Q)R_\ell = \Lambda\left(1 - \frac{1}{\varepsilon}\right)R_\ell^{\,2} \tag{A3.3}$$

(A3.3) is a Bernouilli equation (see section 3.3). Substitute:

$$R_\ell = 1/x$$

to give:

$$\frac{dx}{dZ} - (\beta_\ell + Q)x + \Lambda\left(1 - \frac{1}{\varepsilon}\right) = 0 \tag{A3.4}$$

By use of an integrating factor to give:

$$x = \exp[+(\beta_\ell + Q)Z]\{C + \Lambda \int \left(1 - \frac{1}{\varepsilon}\right)\exp[-(\beta_\ell + Q)Z]\,dZ\} \tag{A3.5}$$

C is a constant to be determined from the initial conditions.

If the integration in (A3.5) could be performed for an ε which is a known function of Z then x and hence R_ℓ could be determined for Z. Various attempts at finding exact and approximate functional

representations of $\varepsilon(Z)$ have been made; all unsuccessful.

The graphical representation of ε gives no obvious clue to its algebraic form. ε can be regarded as a function of three variables, namely Z, Q and the ratio β_s/β_ℓ. In principle one could perform a 3-dimensional curve fitting procedure to find, for example, the best polynomial in the three coordinates. Then by the use of (4.10) the power, $\Lambda R_\ell + R_s$ could be calculated in terms of Z, which would permit the re-expression of (A3-7) so that Z is the only dependent variable on the right hand side. Equations (4.5) and (4.6) would thus be decoupled. In this way one could obtain semi-empirical solutions for $R_\ell(Z)$ and $R_s(Z)$.

The procedure outlined above is not carried out for the following reasons. One would require a high-order polynomial (or other function) in Z so as to avoid the propagation of errors throughout the remaining mathematical steps. The problems with a high order polynomial are two-fold. Firstly, the optimisation procedure required to obtain a high order polynomial in three variables, Z, Q and β_s/β_ℓ would be non-trivial. Secondly, assuming that the optimisation converges to a stable solution, the integration in equation (A3.7) could be difficult to perform without resorting to further approximations.

Assuming that the semi-empirical solution for $R_\ell(Z)$ and $R_s(Z)$ yielded algebraic functions in Z, $R_\ell(Z)$ and $R_s(Z)$ would be expressions which were sufficiently complicated to require a computer to calculate and plot them. As many modern computers have access to mathematical libraries, including Runge-Kutta routines, such as those described in appendix 4, the whole procedure would appear to be self-defeating. The accuracy of the semi-empirical solution will never be as great as that of the Runge-Kutta routines upon which it is ultimately based. Finally,

it is felt that little physical information about the nature of stimulated Raman scattering with unequal losses would be acquired from a semi-empirical solution.

A3.2 The use of the zero loss limit as an approximation

An alternative method for finding a functional form for $\varepsilon(Z)$ is to substitute one of the expressions already obtained for $R_\ell(Z)$ and $R_s(Z)$, subject to one of the approximations. $\varepsilon(Z)$ could be calculated by using the results of the equal loss approximation (equations (3.23) and (3.24)). However the equal loss analysis requires some single value of β for the evaluation of equations (3.23) and (3.24). It is not clear which to use. An alternative would be to substitute the result of a small signal approximation. The problem here is that R_ℓ is approximated to be $\exp(-\beta_\ell Z)$, which is a very much less realistic expression than the corresponding one for R_s. R_ℓ and R_s under this scheme would differ greatly in their 'goodness' of fit to the real answer.

The most realistic scheme would appear to be to use the results of the zero loss analysis in conjunction with the expression for $\gamma(Z)$. Substitute (A1.12) and (A1.13) into (4.8) to give

$$\gamma(Z) = \frac{\beta_\ell + \eta' \beta_s}{1 + \eta'} \qquad \text{(A3.6)}$$

where $\eta' = (\frac{2Q}{\Lambda})\exp(\Lambda Z)$

Thus from (4.16):

$$\varepsilon(Z) = \frac{\beta_s - \beta_\ell}{(1+\beta_\ell) + \eta'(1+\beta_s)} \qquad \text{(A3.7)}$$

Equations (A3.6) and (A3.7) are now substituted into the expressions for R_ℓ and R_s in terms of γ and ε; see equations (4.5) and (4.6). It is

found that the solutions obtained are not realistic approximations to those obtained by the Runge-Kutta-Merson routine described in appendix 4.

A3.3 Decouple by taking the second derivative

Take the second derivative of equation (4.5) and substitute from equations (4.5) and (4.6) to obtain a second order equation in $R_\ell(Z)$:

$$\frac{d^2R_\ell}{dZ^2} - \frac{1}{R_\ell}\left(\frac{dR_\ell}{dZ}\right)^2 - R_\ell\frac{dR_\ell}{dZ} + \beta_s\frac{dR_\ell}{dZ} + \Lambda\beta_\ell R_\ell^2 + \beta_s(\beta_\ell + Q)R_\ell = 0 \quad \text{(A3.8)}$$

There is a similar nonlinear second order equation in R_s. In neither case is there an obvious solution.

APPENDIX FOUR: THE METHODS OF NUMERICAL SOLUTIONS

When the constants β_ℓ, β_s Λ and Q are known, the two wavelength model in the form of (3.15) and (3.16) or (4.5) and (4.6), as appropriate, subject to the initial conditions (3.17) and (3.18) are specified sufficiently well to yield numerical solutions. The equations are solved by a Runge-Kutta-Merson method. The integration is over the range Z = 0 to Z = L and fifth order hermite polynomials are used to interpolate for intermediate points[A1]. The computer routine was D02BBF[A2]. The accuracy of computation could be adjusted by using "TOL", one of the arguments required in the call to the routine. The computing time was not an important constraint here and thus TOL was set to a low value, 10^{-7}, giving high computational accuracy. The pump power, Stokes power and fibre length were all stored in 100-element one-dimensional arrays.

The multiwavelength model, as specified by equations (5.5) and (5.6), with q replaced by m = 91, subject to the initial conditions (5.7) and (5.8) is readily treated by the above method. The Stokes power evolution had to be stored in a 91 x 100 element two-dimensional array.

The solution of the differential equations for the power input-output relationships (section 4.6) was carried out so that the initial condition for the pump power is a variable and the fibre length is a constant. Routine D02BAF[A2] uses a Runge-Kutta-Merson method to integrate over the fixed range Z = 0 to Z = L 100 times. Intermediate Z values are of no particular interest and are not supplied. The tolerance, "TOL" was again set to 10^{-7} to give a high accuracy, but at the expense of computing time. See Hall and Watt[A1].

It is necessary to numerically integrate to calculate the parameter $\gamma(Z)$ in section 4.5, the effective Stokes loss in section 5.6 and effective core area in sections 6.4 and 6.5. The routine D01GAF[A2] was used. Third order finite difference formulae are used to calculate the definite integrals between lower and upper bounds Z(1) to Z(100) in sections 4.5 and 5.6 and lower and upper bounds $\gamma(1)$ to $\gamma(100)$ in sections 6.4 and 6.5. See Gill and Miller[A3].

In sections 6.4 and 6.5 it is necessary to compute the effective core areas from Bessel and Hankel function solutions to weakly guiding fibres, the Bessel and Hankel functions are computed from routines S17AEF[A2] and S18ACF[A2], respectively.

The locus of β,Z coordinates which satisfy a given threshold condition for chapter 7 is obtained by solving equations (4.5) and (4.6) until a specified relationship between $R_s(Z)$ and $R_\ell(Z)$ is satisfied. Routine D02BHF[A2] was used. In order to obtain smooth curves it is found to be necessary to increase the degree of segmentation and decrease the tolerance as β increases. In this way discontinuities were avoided when the gradient tends to infinity at $\beta = \beta_{\ell max}$. The highest value of TOL used was 10^{-7}, decreasing to about 10^{-10} at $\beta = \beta_{\ell max}$.

References

A1 Hall, G. and Watt, J.M. (Eds.) "Modern numerical methods for ordinary differential equations", p59, Clarendon Press, Oxford (1976).

A2 Numerical Algorithms Group (NAG): Fortran Library; Mark 10 implementation (1983), routines D02BBF, D02BAF, S17AEF, S18ACF and D02BHF. (NAG Central Office, Mayfield House, 256, Banbury Road, Oxford OY2 7DE).

A3 Gill, P.E. and Miller, G.F., "An algorithm for the integration of unequally spaced data". Comp. Journal 15, pp80-83 (1972).